Lost and Transferred Information by Changing Spatial and Temporal Resolution in Hydrological Modeling

A Dissertation

Presented in Partial Fulfillment of the Requirements for the

Degree of Doctorate of Philosophy

with a

Major in Biological and Agricultural Engineering

in the

College of Graduate Studies

University of Idaho

by

Mohammad M. Sohrabi

Major Professor: Daniele Tonina, Ph.D.
Committee Members: Daniel Isaak, Ph.D.; Jae Ryu, Ph.D.; Eloywn Yager, Ph.D.; Rohan Benjankar, Ph.D.
Department Administrator: Ching-An Peng, Ph.D.

December 2016

Authorization to Submit Dissertation

This dissertation of Mohammad M. Sohrabi, submitted for the degree of Doctorate of Philosophy with a Major in Biological and Agricultural Engineering and titled "Lost and Transferred Information by Changing Spatial and Temporal Resolution in Hydrological Modeling," has been reviewed in final form. Permission, as indicated by the signatures and dates below, is now granted to submit final copies to the College of Graduate Studies for approval.

Major Professor: _____ Date:_____
Daniele Tonina, Ph.D.

Committee Members: _____ Date:_____
Daniel Isaak, Ph.D.

_____ Date:_____
Jae Ryu, Ph.D.

_____ Date:_____
Eloywn Yager, Ph.D.

_____ Date:_____
Rohan Benjankar, Ph.D.

Department Administrator: _____ Date:_____
Ching-An Peng, Ph.D.

Abstract

Water management, from energy production to aquatic habitat quality assessment, uses hydrological modeling to predict water quantity, temperature and timing. Due to the strong effect of snow on the hydrology of mountainous regions, an integrated hydrologic modeling framework of snow, streamflow and stream temperature models is required for accurate predictions of hydrological processes. The prediction accuracy of such frameworks is reliant on meteorological input spatial and temporal resolutions. The main objectives of this work are (a) to find appropriate inputs spatial and temporal resolutions for the integrated hydrologic modeling for a range of climatic conditions and topographic elevations; and (b) understand the effects of these resolutions on snow properties, streamflow and stream temperature estimations. To address these objectives, a statistical stream temperature model, SWTM, was first developed to estimate mean daily stream temperatures at a point. Then, a process-based snow model, iSnobal, was run using 1-, 3- and 6-hourly inputs for wet, average and dry years over Boise River Basin (6,963 km^2), which spans rain-dominated ($\leq$1,400m), rain-snow transition (>1,400 and $\leq$1,900m), snow-dominated below treeline (>1,900 and $\leq$2,400m) and above treeline (>2,400m) elevations. ISnobal was run with inputs distributed at 50m – the benchmark for comparisons – and 100m resolutions and with aggregated inputs from the 50m model to 100m, 250m, 500m and 750m resolutions. Surface water input (SWI) estimations from these scenarios were used to run the process-based Penn State Integrated Hydrology model (PIHM) over upstream of the Anderson Ranch Dam (2,490 km^2). The mean daily streamflow estimations from the scenarios were then used along with mean daily air temperatures to run SWTM.

Comparison of estimated and observed stream temperatures indicated robust performance of SWTM across a range of climate and hydrologic conditions. SWTM showed better performance than the widely-used Mohseni model in terms of accuracy of fit and model errors. The analyses indicated that the inclusion of the autoregressive structure is critical in large streams and stream discharge is an important hydrologic driver during the spring-summer period for unregulated streams in snow-dominated basins. SWTM can be used to either reconstruct historical daily stream temperatures or to project daily stream temperatures under different climate change scenarios.

Using longer than hourly time steps of meteorological inputs led to inaccurate estimation of precipitation amount that is in form of rain or snow, and energy input to the snowpack. The magnitude of errors in snow cover area (SCA) and snow water equivalent (SWE) generally decreased as elevation increased, from rain-dominated to snow-dominated above treeline. However, the errors in SCA and SWE increased as annual precipitation decreased, toward the dry year. The results of this chapter (a) suggest hourly measurements of meteorological variables; (b) can be applied as a guide to decide on optimal observation/reanalysis time steps in different settings; and (c) can inform modelers of the errors in their simulations due to the temporal resolution of their inputs, and how the errors may vary depending on elevation ranges and wet/dry years.

Differences between the simulated SCA and SWE from the 50 m model and that of the aggregated scenarios were generally negligible, because the topographic feature effects on meteorological input distribution was transferred through aggregation. However, errors in the simulated SCA and SWE from the distributed 100 m scenario were large, particularly in the wet year and at the highest elevation band when and where snow mass was large. The large errors were because of losing the effect of small scale variability in topographic features on meteorological inputs distribution. Homogenization of topographic features due to coarsening the DEM from 50 m to 100m caused net radiation overestimation, wind-induced snow drifting moderation and precipitation phase mischaracterization.

The effect of inputs spatial resolution of on streamflow estimations was more pronounced than that of temporal resolution. Coarser resolution generated from aggregated inputs from 50 m resolution had negligible effects on streamflow as the effect of topographic features was transferred by aggregation. In contrast, the distributed 100 m scenario had the largest inaccuracy, which was reduced as the watershed area increased due to the buffering effect of the groundwater. In large watersheds (>800 km^2), the SWI estimations from all resolution scenarios led to similar streamflow estimations. However, in small watersheds (<300 km^2), using coarse spatial and temporal resolutions of the inputs caused inaccurate streamflow estimations, whose magnitude was strongly reliant on climate conditions and the watershed surface cover, which affect the groundwater buffering effect. The results show that only fine temporal hourly and spatial (50m) resolutions provide consistent streamflow modeling

performance among climatic conditions. All the inputs spatial and temporal resolutions investigated in this work were sufficient input scales to provide streamflow estimations for stream temperature modeling. Groundwater level and soil moisture measurements should be added to constrain process-based hydrological modeling, as streamflow may not be adequate for validating hydrological modeling.

Acknowledgements

I would like to thank my supervisor Daniele Tonina for making this research possible and for his advice. Without his passion in this field and his help in supporting the project, this work could not have been possible.

I would like to mention my committee members, Jae Ryu, Daniel Isaak, Elowyn Yager and Rohan Benjankar. Special thanks go to Jae Ryu who was my supervisor for the first two years of my PhD program and his advice and help led to three publications.

I would like to thank Dona Horan for her help and for providing stream water temperature data. I would like to thank Seth Wenger, Daniel Isaak and Rohan Benjankar for their help on developing the stream temperature model. I would like to thank Mukesh Kumar for helping me on the calibration and running the Penn State Integrated Hydrological Model. I would like to thank Mukesh Kumar, Danny Marks, Charles Luce and Patrick Kormos for helping me on the calibration, running and coupling iSnobal and the Penn State Integrated Hydrological Model.

I would like to mention the grants, which funded the research. This study has been supported by the Bureau of Reclamation grant number Rl2APJ 1025. The simulations referenced in this work were executed on the BIG-STEM computing platform at the University of Idaho, which is supported in part by NSF Grant CNS-1229766, the Murdock Charitable Trust and the state of Idaho's IGEM program. I would like to thank Ray Anderson, director of IT at college of engineering of the University of Idaho, for his help on preparing the framework.

Dedications

Mom

(Azam Taslimi)

Dad

(Heshmat Sohrabi)

Table of Contents

List of Figures

List of Tables

Chapter 1. Introduction

Understanding and prediction of hydrological variables such as snow accumulation and ablation, streamflow and stream temperature are critical for water resource planning and management, ecological and aquatic habitat studies (Piccolroaz et al. 2016; Smith et al. 2014). Snow is particularly important in mountainous watersheds, because it controls microbial activity during winter (Schimel et al. 2004), energy exchanges of environment (Molotch and Bales 2005) and growing season length (Darmody et al. 2004; Sensoy et al. 2006; Torp 2010; Trujillo et al. 2012). Distribution, timing and magnitude of snow melts also control soil moisture dynamics, groundwater recharge and streamflow generation, which are necessary for flood forecasting, reservoir operation and river restoration (Kormos et al. 2014; Kumar et al. 2013; Reba et al. 2011; Wang et al. 2013; Weill et al. 2013). In addition, availability of streamflow estimations improves prediction accuracy of stream temperature (Piccolroaz et al. 2016; Vliet et al. 2011), which plays a major role in water quality and aquatic ecosystems (Isaak et al. 2012; Isaak et al. 2015). These studies indicate the value of accurate snow accumulation and ablation, streamflow and stream temperature estimations for dam and water resource managers, ecologist and decision makers.

Due to advances in numerical modeling and computational power of computers, application of integrated hydrologic modeling of snow, streamflow and stream temperature models has increased (Merenlender and Matella 2013; Null et al. 2010). Integrated hydrologic modeling frameworks predict changes in response of hydrological processes with regard to changes in meteorological variables. Such frameworks require fine spatial and temporal resolutions of meteorological inputs to reflect changes of these variables on hydrological processes responses. Application of fine spatial and temporal resolutions of meteorological inputs considerably increases modeling costs such as runtime and storage space, whereas coarse inputs decreases modeling costs in expense of prediction accuracy. Reduction in prediction accuracy due to using coarse resolution inputs is not well known, particularly (a) in large mountainous watersheds, where hydrological characteristics vary from rain dominated to snow dominated (Winstral et al. 2014); (b) under different climate condition such as wet,

average and dry years, when catchments respond differently to a melt event (Rosenberg et al. 2013); and (c) in watersheds with different drainage area and geology (surface cover), where contribution of hydrological processes such as runoff and groundwater to streamflow generation varies (Frisbee et al. 2011; Miller et al. 2016; Orlova and Branfireun 2014) and this may change dependency of streamflow estimations to surface water input accuracy.

Thus, this work addresses these knowledge gaps with the following specific objectives: (a) quantifying the effect of spatial and temporal resolutions of meteorological inputs on estimations of snow cover area and mass with regard to elevation and climate conditions; (b) identifying the importance of detailed spatial information of energy fluxes and snow drifting on estimations of snow cover area and mass with regard to elevation range, climate condition and vegetation cover; and (c) quantifying the effect of inaccurate predictions of surface water input on streamflow, groundwater level and stream temperature estimations with regard to climate condition and watershed size and surface cover. The main hypotheses of this work are: (a) using longer than hourly time step of inputs results in mischaracterization of precipitation phase, particularly in rain dominated and rain-snow transition regions, due to misestimating of dew point temperatures; (b) coarsening spatial resolution of inputs affects energy balance and wind-induced snow drifting and consequently snow accumulation and ablation as it smoothens topographical complexity; (c) groundwater dominated systems are less affected by inaccuracy in surface water input (SWI) because of transient storage of water in the ground; and (d) the larger the system the less depends on SWI due to groundwater buffering and (e) the buffering effect of groundwater is a function of climate conditions and watershed surface cover.

To address the objectives and hypotheses of this work, 8 different spatial and temporal resolutions of meteorological inputs were used to run an integrated hydrologic modeling framework. To prepare this modeling framework, SWI estimated from a process-based snow model, iSnobal, was used instead of precipitation in a process-based streamflow model, PIHM. Estimated streamflow were, then, used to predict stream temperature using a statistical stream temperature model, SWTM. Using different resolutions of inputs to force the integrated hydrologic modeling framework helps to understand: (a) to what extent resolution of inputs affects estimation of snow properties such as snow cover area and snow mass; and

(b) how much changes in snow properties estimations caused by inputs resolution, which are reflected on SWI estimation, can impact streamflow, groundwater level and stream temperature estimations with regard to climate condition and watershed size and surface cover. To achieve these objectives, we develop a new statistical stream temperature models to overcome some of the limitations in the widely-used statistical stream temperature model in chapter 2; in chapter 3, we investigates the effects of temporal resolution of meteorological inputs on estimation of snow accumulation and ablation in different climate conditions and topographic elevations; in chapter 4 we address the effects of disregarding topography-induced heterogeneity of meteorological inputs on estimation of snow accumulation and ablation in different climate conditions and topographic elevations; finally in chapter 5, we demonstrate the effects of errors in estimation of snow accumulation and ablation caused by meteorological inputs resolution on estimation of streamflow, groundwater level and stream temperature given climate condition and watershed size and surface cover. The following is brief description of these chapters:

Chapter 2. Stream temperature plays an important role in aquatic ecosystems (Isaak et al. 2015; Mesa et al. 2013). Statistical stream temperature models, which rely on covariates that indirectly represent physical processes such as air temperature and streamflow, are beneficial tools to predict stream temperatures at a point (Ahmadi-Nedushan et al. 2007; Neumann et al. 2003). Available statistical models have been rarely tested under a wide range of climate conditions. Most statistical models were tested at one watershed and within one climate zone (Caissie et al. 2001; Caldwell et al. 2013; Webb et al. 2003). Conversely, the Mohseni (1998) model was tested for regulated and unregulated streams under a wide range of climate and hydrologic conditions. The Mohseni model that predicts stream temperatures at a site from air temperatures is widely used in riverine studies because of its simplicity and good performance. The Mohseni model performs poorly at shorter than weekly time steps and in snow dominated watersheds, where the snowmelt has a pronounced effect on spring and early summer stream temperatures (Benyahya et al. 2007; Isaak et al. 2012; Luce et al. 2014). The model performance is also sensitive to the difference between maximum and minimum values of weekly averaged stream temperatures and it performs poorly in regions where this difference is low (Benyahya et al. 2007; Mohseni et al. 1998). The main objective of this chapter is to develop a statistical model that overcomes these limitations of the Mohseni

model. The model developed in this chapter can be used as a reliable tool to either reconstruct historical daily stream temperatures or to project daily stream temperatures.

To overcome these limitations, a statistical stream water temperature model, SWTM, which uses mean daily air temperatures and discharge to estimate stream temperatures at a daily time step, is presented in Chapter 2. SWTM tracks changes in independent variables rather than depending on the difference between the maximum and minimum values of stream temperature. The model has an autoregressive structure to consider thermal inertia and prevent fluctuations in daily air temperatures from overly influencing daily stream temperature estimations. SWTM was tested against observed stream temperatures at 34 sites over Boise River Basin (BRB) and at 8 climatically different basins of the USA. Comparison of the estimated stream temperatures to those of the observed indicated robust performance of SWTM across a range of climate and hydrologic conditions. In addition, SWTM showed better performance than the Mohseni model in terms of accuracy of fit and model errors.

Chapter 3. Accurate estimation of snow accumulation and ablation requires a fine temporal resolution data to capture diurnal changes in meteorological variables (Beniston 1997; Garen and Marks 2005). The diurnal variability of meteorological variables in mountainous regions indicates high temporal gradients due to the low atmosphere mass (Little and Hanna 1978), which causes large incoming short-waves during the daytime and outgoing long-waves in the nighttime (Aguado and Burt 2013). Due to the fast diurnal variations of meteorological variables, using coarse temporal resolutions may cause errors in: (a) the precipitation phase characterization because hourly changes in dew point temperatures are neglected (Beniston 2012; Marks et al. 2013); and (b) net radiation and turbulent energy estimations, which are responsible for a large portion of the energy balance (Mazurkiewicz et al. 2008). These errors affect estimation of timing and magnitude of snow accumulation and ablation, whose magnitude is likely to vary across topographic elevations and between years with characteristically different climatology (Beniston 2012; Howat and Tulaczyk 2005; Keller et al. 2005; Marks et al. 2013; Martin et al. 1994; Scherrer and Appenzeller 2004). Therefore, the main objective of this chapter is to evaluate impact of temporal resolution of meteorological inputs on snow accumulation and ablation estimation for a range of climatic conditions and topographic elevations.

To address the main objective of this chapter, iSnobal was run using 1-, 3- and 6-hourly inputs for wet, average and dry years over Boise River Basin (6,963 km^2), which spans rain dominated, rain-snow transition, snow dominated below and above treeline regions. This helps to: (a) quantify the impact of temporal resolution of meteorological inputs on modeled SCA and SWE; (b) evaluating the role of annual precipitation on aforementioned impacts; and (c) identifying the elevation ranges wherein snow models are most sensitive to temporal resolution of meteorological inputs. The results indicated that using longer than hourly time steps of meteorological inputs leads to substantial inaccuracy in SCA and SWE estimations, particularly in years with low snow mass and in rain dominated and rain-snow transition regions. The results of this chapter can be applied as a guide to decide on optimal observation/reanalysis time steps in different settings

Chapter 4. Accurate estimation of snow distribution requires an appropriate model resolution to consider heterogeneity in snow accumulation and ablation (Bloschl 1999; Luce et al. 1998; Pohl et al. 2006). In mountainous settings, the interaction among rugged terrain and vegetation causes spatial disparities in meteorological variables (Marks et al. 1999; Trujillo et al. 2007) and consequently results in heterogeneity in snow accumulation and ablation (Elder et al. 1991). Therefore, a coarse spatial resolution, which causes neglecting small scale variability in slopes and aspects, may cause errors in the precipitation phase characterization, the net radiation estimation and the wind-induced snow drifting estimation. The degree of these errors may vary across topographic elevations and years with characteristically different climatology (Bloschl 1999; Luce et al. 1998; Winstral et al. 2014). Therefore, the main objective of this chapter is to understand transferred and lost information in snow accumulation and ablation estimation over a watershed due to the model spatial resolution for a range of climatic and topographic conditions.

To address this objective, iSnobal was run with inputs distributed at 50 – the benchmark for comparison – and with aggregated inputs from the 50 m model to 100 m, 250 m, 500 m and 750 m resolution for wet, average and dry years over the BRB. ISnobal was also run with inputs distributed at 100 m to understand how much the prediction accuracy vary given changes in topographic features due to coarsening the DEM from 50 m to 100 m resolution. The simulations using different spatial resolutions of inputs help: (a) quantify the effect of

inputs spatial resolution on estimation of SCA and SWE; (b) assess the role of annual climatology on the sensitivity of predictions accuracy to inputs spatial resolution; and (c) identify the elevation range where the prediction accuracy is most sensitive to inputs spatial resolution. Differences between the simulated SCA and SWE from the distributed 50 m scenario and those of the distributed 100 m scenario were large due to disregarding the small scale variability in topography, particularly in the wet year and at the highest elevation band. The results of this chapter can be used as a guide for selecting an appropriate inputs spatial resolution in different topographic settings and climate conditions.

Chapter 5. Accurate snow accumulation and ablation estimation is required for hydrologic modeling in addition to hydro-meteorological and geological processes that are calculated for rain dominated watersheds (Piccolroaz et al. 2016; Winstral et al. 2014). The results of the previous chapters showed the dependence of SCA and SWE estimations accuracy on spatial and temporal resolutions of meteorological inputs. Errors in estimation of SCA and SWE caused by different spatial and temporal scenarios are reflected on the distribution, timing and magnitude of SWI, which is the source of water for streamflow. Comparing estimated streamflow and stream temperatures generated from estimated SWI from these scenarios to those of the observed is a reliable quantitative metric to evaluate accuracy of the estimated SWI (Luce et al. 1998). This helps to understand appropriate inputs resolution in an integrated hydrologic modeling framework. Simulating streamflow and stream temperatures using the estimated SWI from these scenarios also help to quantify the effect of inaccuracy in the estimated SWI on estimation of peak flows and summer's high stream temperatures in various climate conditions. Therefore, this chapter's main objective is to quantify dependency of the prediction accuracy in an integrated hydrologic modeling to accuracy of SWI given climate conditions and the watershed size in mountainous watersheds.

To reach the main objective of this chapter, iSnobal, PIHM and SWTM were coupled and run over upstream of the Anderson Ranch Dam watershed (2,490 km^2), which varies from rain dominated to snow dominated above treeline. Differences between the estimated streamflow from the spatial and temporal scenarios were merely due to differences between the estimated SWI from the scenarios as other inputs of PIHM were the same for all the scenarios. PIHM and SWTM were calibrated for the distributed 50 m scenario, benchmark for comparison, for

the wet year and were validated for the dry and average years. The results indicated that the effects of spatial and temporal resolution of meteorological inputs on integrated hydrologic modeling depend on the watershed size and climate conditions. The effect of inputs spatial and temporal resolutions on stream temperature estimations was negligible. This chapter can be used as a guide for selecting appropriate spatial and temporal resolutions of inputs given climate conditions and the watershed size for integrated hydrologic modeling in mountainous watersheds.

1.1. References

Aguado, E., and Burt, J. E. (2013). *Understanding Weather and Climate*, Pearson.

Ahmadi-Nedushan, B., St-Hilaire, A., Ouarda, T. B. M. J., Bilodeau, L., Robichaud, E., Thiemonge, N., and Bobee, B. (2007). "Predicting river water temperatures using stochastic models: case study of the Moisie River (Qu´ebec, Canada)." *Hydrological Processes*, 21, 21–34.

Beniston, M. (1997). "Variation of snow depth and duration in the Swiss Alps over the last 50 years: Links to changes in large-scale climatic forcing." *Climate Change*, 36, 281–300.

Beniston, M. (2012). "Is snow in the Alps receding or disappearing?" *WIREs Climate Change (Wiley Interdisciplinary Reviews / Climate Change)*, DOI:10.1002/wcc.179.

Benyahya, L., Caissie, D., St-Hilaire, A., Ouarda, T. B. M. J., and Bobée, B. (2007). "A Review of Statistical Water Temperature Models." *Canadian Water Resources Journal*, 32(3), 179–19.

Bloschl, G. (1999). "Scaling issues in snow hydrology." *Hydrological Processes*, 13, 2149-2175.

Caissie, D., El-Jabi, N., and Satish, M. G. (2001). "Modelling of maximum daily water temperatures in a small stream using air temperatures." *Journal of Hydrology*, 251, 14-28.

Caldwell, R. J., Gangopadhyay, S., Bountry, J., Lai, Y., and Elsner, M. M. (2013). "Statistical modeling of daily and subdaily stream temperatures: Application to the Methow River Basin, Washington." *Water Resources Research*, 49, 4346–4361.

Darmody, R. G., Thorn, C. E., Shlyter, P., and Dixon, J. C. (2004). "Relationship of vegetation distribution to soil properties in Karkevagge, swedish lapland." *Arctic, Antarctic and Alpine Research*, 36(1), 21-32.

Elder, K., Dozier, J., and Michaelse, J. (1991). "Snow Accumulation and Distribution in an Alpine Watershed." *Water Resources Research*, 27(7), 1541-155.

Frisbee, M. D., Phillips, F. M., Campbell, A. R., Liu, F., and Sanchez, S. A. (2011). "Streamflow generation in a large, alpine watershed in the southern Rocky Mountains of Colorado: Is streamflow generation simply the aggregation of hillslope runoff responses?" *Water Resources Research*, 47, W06512.

Garen, D. C., and Marks, D. (2005). "Spatially distributed energy balance snowmelt modelling in a mountainous river basin: estimation of meteorological inputs and verification of model results." *Journal of Hydrology*, 315, 126-153.

Howat, I. M., and Tulaczyk, S. (2005). "Climate sensitivity of spring snowpack in the Sierra Nevada." *Journal of Geophysical Research*, 110, F04021.

Isaak, D. J., Wollrab, S., Horan, D., and Chandler, G. (2012). "Climate change effects on stream and river temperatures across the northwest U.S. from 1980–2009 and implications for salmonid fishes." *Climate Change*, 113(2), 499-524.

Isaak, D. J., Young, M. K., Nagel, D. E., Horan, D. L., and Groce, M. C. (2015). "The cold-water climate shield: Delineating refugia for preserving salmonoid fishes through the 21st century." *Global Change Biology*, 21, 2540–2553.

Keller, F., Goyette, S., and Beniston, M. (2005). "Sensitivity analysis of snow cover to climate change scenarios and their impact on plant habitats in alpine terrain." *Climate Change*, 72, 299–319.

Kormos, P. R., Marks, D., McNamara, J. P., Marshall, H. P., Winstral, A., and Flores, A. N. (2014). "Snow distribution, melt and surface water inputs to the soil in the mountain rain–snow transition zone." *Journal of Hydrology*, 519, 190-204.

Kumar, M., Marks, D., Dozier, J., Reba, M., and Winstral, A. (2013). "Evaluation of distributed hydrologic impacts of temperature-index and energy-based snow models." *Advances in Water Resources*, 56, 77-89.

Little, M. A., and Hanna, J. M. (1978). "Climate characteristics of high-altitude zones." The Biology of High-Altitude Peoples, P. T. Baker, ed., Cambridge University Press.

Luce, C., Staab, B., Kramer, M., Wenger, S., Isaak, D., and McConnell, C. (2014). "Sensitivity of summer stream temperatures to climate variability in the Pacific Northwest." *Water Resources Research*, 50(4), 3428–3443.

Luce, C. H., Tarboton, D. G., and Cooley, K. R. (1998). "The influence of the spatial distribution of snow on basin-averaged snowmelt." *Hdrological Processes*, 12, 1671-1683.

Marks, D., Domingo, J., Susong, D., Link, T., and D.Garen. (1999). "A spatially distributed energy balance snowmelt model for application in mountain basins." *Hydrological Process* 13, 1935-1959.

Marks, D., Winstral, A., Reba, M., Pomeroy, J., and Kumar, M. (2013). "An evaluation of methods for determining during-storm precipitation phase and the rain/snow transition elevation at the surface in a mountain basin." *Journal of Advances in Water Resources*, 55, 98-110.

Martin, E., Brun, E., and Durand, Y. (1994). "Sensitivity of the French Alps snow cover to the variation of climatic variables." *Annales Geophysicae*, 12(5), 469-477.

Mazurkiewicz, A. B., Callery, D. G., and McDonnell, J. J. (2008). "Assessing the controls of the snow energy balance and water available for runoff in a rain-on-snow environment." *Journal of Hydrology*, 354, 1-14.

Merenlender, A. M., and Matella, M. K. (2013). "Maintaining and restoring hydrologic habitat connectivity in mediterranean streams: an integrated modeling framework." *Hydrobiologia*, 719(1), 509-525.

Mesa, M. G., Weiland, L. K., Christiansen, H. E., and Sauter, S. T. (2013). "Development and Evaluation of a Bioenergetics Model for Bull Trout." *Transactions Of The American Fisheries Society*, 142, 41-49.

Miller, M. P., Tesoriero, A. J., Capel, P. D., Pellerin, B. A., Hyer, K. E., and Burns, D. A. (2016). "Quantifying watershed-scale groundwater loading and instream fate of nitrate using high-frequency water quality data." *Water Resources Research*, 52, 330–347.

Mohseni, O., Stefan, H. G., and Erickson, T. R. (1998). "A nonlinear regression model for weekly stream temperatures." *Water Resources Research*, 34(10), 2685–2692.

Molotch, N. P., and Bales, R. C. (2005). "Scaling snow observations from the point to the grid element: Implications for observation network design." *Water Resources Research*, 41, W11421.

Neumann, D. W., Rajagopalan, B., and Zagona, E. A. (2003). "Regression Model for Daily Maximum Stream Temperature." *Journal of Environmental Engineering*, 129(7), 667-674.

Null, S. E., Deas, M. L., and Lund, J. R. (2010). "Flow and water temperature simulation for habitat restoration in the Shasta River, California." *River Research and Applications*, 26, 663-681.

Orlova, J., and Branfireun, B. A. (2014). "Surface Water and Groundwater Contributions to Streamflow in the James Bay Lowland, Canada." *Arctic, Antarctic, and Alpine Research*, 46(1), 236-250.

Piccolroaz, S., Calamita, E., Majone, B., Gallice, A., Siviglia, A., and Toffolon, M. (2016). "Prediction of river water temperature: a comparison between a new family of hybrid models and statistical approaches." *Hydrological Processes*, DOI: 10.1002/hyp.10913.

Pohl, S., Marsh, P., and Liston, G. E. (2006). "Spatial-Temporal Variability in Turbulent Fluxes during Spring Snomelt." *Arctic, Antarctic and Alpine Research*, 38(1), 136-146.

Reba, M. L., Marks, D., Winstral, A., Link, T. E., and Kumar, M. (2011). "Sensitivity of the snowcover energetics in a mountain basin to variations in climate." *Hydrological Processes*, 25(21), 3312-3321.

Rosenberg, E. A., Clark, E. A., Steinemann, A. C., and Lettenmaier, D. P. (2013). "On the contribution of groundwater storage to interannual streamflow anomalies in the Colorado River basin." *Hydrol. Earth Syst. Sci.*, 17, 1475-1491.

Scherrer, S. C., and Appenzeller, C. (2004). "Trends in Swiss Alpine snow days: The role of local- and large-scale climate variability." *Geophysical Research Letters*, 31, L13215.

Schimel, J. P., Bilbrough, C., and Welker, J. M. (2004). "Increased snow depth affects microbial activity and nitrogen mineralization in two Arctic tundra communities." *Soil Biology & Biochemistry*, 36, 217-227.

Sensoy, A., Sorman, A. A., Tekeli, A. E., Sorman, A. U., and Garen, D. C. (2006). "Point-scale energy and mass balance snowpack simulations in the upper Karasu basin, Turkey." *Hydrological Processes*, 20, 899–922.

Smith, T., Marshall, L., and McGlynn, B. (2014). "Calibrating hydrologic models in flow-corrected time." *Water Resources Research*, 50, 748–753.

Torp, M. (2010). "The effect of snow on plants and their interactions with herbivores," PhD, Umeå University, Umeå

Trujillo, E., Molotch, N. P., Goulden, M. L., Kelly, A. E., and Bales, R. C. (2012). "Elevation-dependent influence of snow accumulation on forest greening." *Nature Geoscience*, 5(10), 705-709.

Trujillo, E., Ramı´rez, J. A., and Elder, K. J. (2007). "Topographic, meteorologic, and canopy controls on the scaling characteristics of the spatial distribution of snow depth fields." *Water Resources Research*, 43, W07409.

Vliet, M. T. H. V., Ludwig, F., Zwolsman, J. J. G., Weedon, G. P., and Kabat, P. (2011). "Global river temperatures and sensitivity to atmospheric warming and changes in river flow." *Water Resources Research*, 47, W02544.

Wang, R., Kumar, M., and Marks, D. (2013). "Anomalous trend in soil evaporation in a semi-arid, snow-dominated watershed." *Advances in Water Resources*, 57, 32-40.

Webb, B. W., Clack, P. D., and Walling, D. E. (2003). "Water–air temperature relationships in a Devon river system and the role of flow." *Hydrological Processes*, 17, 3069–3084.

Weill, S., Altissimo, M., Cassiani, G., Deiana, R., Marani, M., and Putti, M. (2013). "Saturated area dynamics and streamflow generation from coupled surface–subsurface simulations and field observations." *Advances in Water Resources*, 59, 196-208.

Winstral, A., Marks, D., and Gurney, R. (2013). "Simulating wind-affected snow accumulations at catchment to basin scales." *Advances in Water Resources*, 55, 64-79.

Winstral, A., Marks, D., and Gurney, R. (2014). "Assessing the Sensitivities of a Distributed Snow Model to Forcing Data Resolution." *Journal of Hydrometeorology*, 15, 1366–1383.

Chapter 2. Estimation of Daily Stream Water Temperatures with a Bayesian Regression Approach

2.1. Abstract

Stream water temperature plays a significant role in aquatic ecosystems where it controls many important biological and physical processes. Reliable estimates of water temperature at the daily time step are critical in managing water resources. We develop a parsimonious piecewise Bayesian model for estimating daily stream water temperatures that accounts for temporal autocorrelation and both linear and non-linear relationships with air temperature and discharge. The model was tested at 8 climatically different basins of the USA and at 34 sites within the mountainous Boise River Basin (Idaho, USA). The results show that the proposed model is robust with an average root mean square error of 1.25 $^{\circ}$C and Nash-Sutcliffe coefficient of 0.92 over a 2-year period. Our approach can be used to predict historic daily stream water temperatures or make projections of stream temperatures under climate change in any location using observed daily stream temperature and regional air temperature data.

Keywords: *Daily stream water temperature, Bayesian approach, Air temperature, Stream temperature prediction, Discharge*

2.2. Introduction

Stream water temperature plays an important role in aquatic ecosystems and is an important cue for organism behavior (Isaak et al. 2012; Jobling 1997; Rice et al. 1983; Rieman et al. 2007), fish metabolism (Forseth and Jonsson 1994; Isaak et al. 2015; Mesa et al. 2013; Railsback and Rose 1999) and growth rates (Brett 1979; Crozier et al. 2010; Xu et al. 2010). Stream water temperature controls dissolved oxygen concentrations, which may affect water quality and biogeochemically reactive solutes (Marzadri et al. 2011; Marzadri et al. 2012; Tonina et al. 2015; Webb et al. 2008) while high stream water temperatures may negatively

affect industrial activity (Boogert and Dupont 2005; Null et al. 2012; Vliet et al. 2013; Vliet et al. 2012b). These studies indicate the value of accurate estimates of daily stream water temperatures for dam and water resource managers, ecologists, economists and decision makers.

Many stream temperature models have been developed. These can be divided into mechanistic models that use physical processes (Carron and Rajaram 2001; Ficklin et al. 2012; Vliet et al. 2012a) and statistical models that rely on covariates that indirectly represent physical processes (Ahmadi-Nedushan et al. 2007; Bogan et al. 2003; Gu et al. 1999; Hockey et al. 1982; Mohseni et al. 1998; Neumann et al. 2003). Process-based models require a large number of input variables (e.g., wind speed, net radiation, relative humidity, stream hydraulic cross sections), which may not be available in many locations, limiting opportunities for prediction. Process models may also be more computationally intensive because they solve a large number of equations to quantify energy balance and heat transport within the watershed.

Conversely, statistical models are simpler to apply and have lower data requirements (Benyahya et al. 2007) but sacrifice interpretability. Regression approaches rely on correlations between stream water temperature and environmental covariates that vary spatially or temporally. When used with air temperature data series measured contemporaneously with stream temperature, predictions can be made at various times-steps (e.g., daily, weekly, monthly). However, air-water temperature relationships become weaker at finer temporal resolutions (Ahmadi-Nedushan et al. 2007; Webb et al. 2003), due to the large heat capacity of water, which does not respond to heat exchanges as quickly as air temperature. At short time-steps, temporal autocorrelation may also cause parameter estimation bias because measurements are not independent (Webb et al. 2003). Statistical autoregressive (AR) models account for the autocorrelation structure within stream water temperature time series by considering stream water temperatures of previous time steps and the correlation with meteorological variables of interest (e.g., air temperature). Stochastic models have two components, (1) the long-term annual component (seasonal variation) and (2) the departure from annual component (short-term variation; residual). In these models, a fixed function, e.g. a sinusoidal function, is fitted to stream water temperature time series, which in turn may cause non-stationary in the residual from year to year (Benyahya et al.

2007; Caissie et al. 2001). Non-parametric approaches, such as artificial neural networks (ANN) train the models with relatively long time series of input data, which prevent their applicability in locations with short time series. These models capture complex non-linear relationship between independent and dependent variables solely based on data and without assuming *a priori* statistical distributions and relationships among variables (Bélanger et al. 2005; Benyahya et al. 2007). Their lack of a general theoretical framework and dependence on the training data makes them less reliable in predicting stream water temperatures outside the range of their training conditions (i.e. dry or wet) (Benyahya et al. 2007; Risley et al. 2003).

One of the most widely used stream water temperature model in riverine studies is the Mohseni et al. (1998) model because of its simplicity and good performance (reported average RMSE of 1.64 mm). It is a statistical model that predicts stream temperatures at a site from air temperatures at a remote climate station. It is often fit at a weekly time-step but can be run at any interval resolvable within the temperature time-series. A non-linear regression function captures hysteresis effects associated with differential stream-atmosphere heat transfer rates that vary seasonally (Mohseni et al. 1998). The model was initially developed using only air temperature as a covariate but stream discharge is now routinely incorporated. However the model has a low performance in snow dominated watersheds, where contribution of snowmelt to discharge has a pronounced effect on spring and early summer stream water temperatures (Isaak et al. 2012; Luce et al. 2014; Vliet et al. 2011). Its performance is sensitive to the difference between maximum and minimum values of weekly averaged stream temperatures and it performs poorly in regions where this difference is low (Benyahya et al. 2007; Mohseni et al. 1998). Consequently, it is not adequate for snow-dominated mountain regions, where these limitations are exacerbated.

Thus the main objective of this work was to develop and test a new parsimonious statistical model to predict stream water temperature at the daily temporal resolution under a wide range of climatic conditions in both regulated and unregulated streams and for current, historical and future conditions. The model was designed to overcome one of the limitations of existing statistical models by including the effect of discharge on stream water temperature. However, it can be parameterized solely with air temperature data when discharge data are unavailable.

It is based on a piecewise Bayesian approach and accounts for the autocorrelation structure within the stream water temperature time series. We tested model performance in different climatic regions and compared it to that of the widely-used Mohseni et al. (1998) model in a mountain river basin and selected locations throughout the U.S. with different climatic regimes.

2.3. Study Area and Data

Model development was done in the Boise River Basin of central Idaho, USA (Figure 2.1) because of the availability of extensive stream temperature datasets (http://www.fs.fed.us/rm/boise/AWAE/projects/NorWeST.html); and climate monitoring stations. The terrain of the basin is mountainous ranging from about 1,000 to 3,000 m, which creates complex meteorological conditions with strong temporal and spatial variability and provides a challenging test for water temperature model performance. The Boise River Basin also has strongly seasonal weather patterns, with large snowpack accumulations occurring during winter and annual floods occurring during late spring when snow melts.

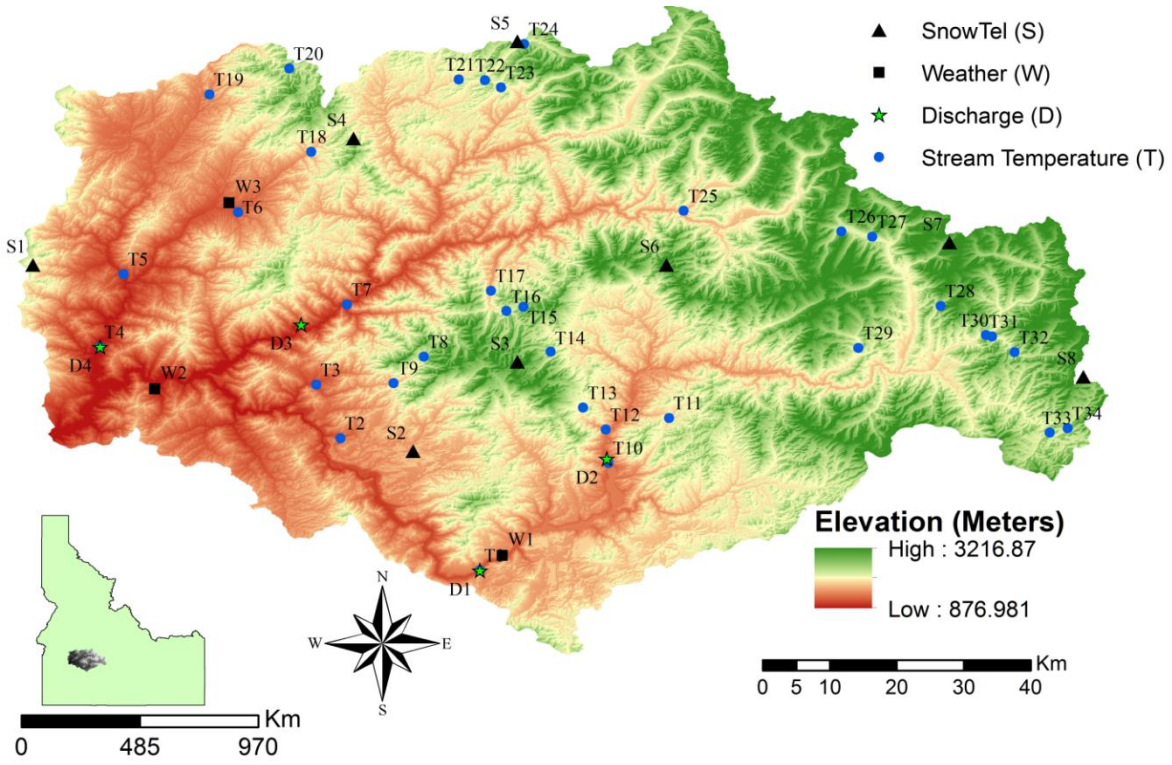

Figure 2.1. Study area and spatial distribution of the metrological, hydrological and temperature gage stations.

Eight additional stream temperature stations were selected in different portions of the U.S. to test and validate the generality of the model (Figure 2.2). Those climate regions include (Sohrabi et al. 2015): Semi-Arid Steppe (CT1), Marine West Coast (also known as Oceanic Climate) which is also the predominant climate across most parts of Europe (CT2), Mediterranean (CT3), Mid-Latitude Desert (CT4), Highland or Alpine (CT5), Humid Continental with cool summer (CT6), Humid Continental with warm summer (CT7) and Humid Subtropical (CT8). These eight stations are distributed over a wide range of elevations, from 29 to 2,700 meters above mean see level (See Table 2.1). Each station recorded mean daily stream temperature and discharge.

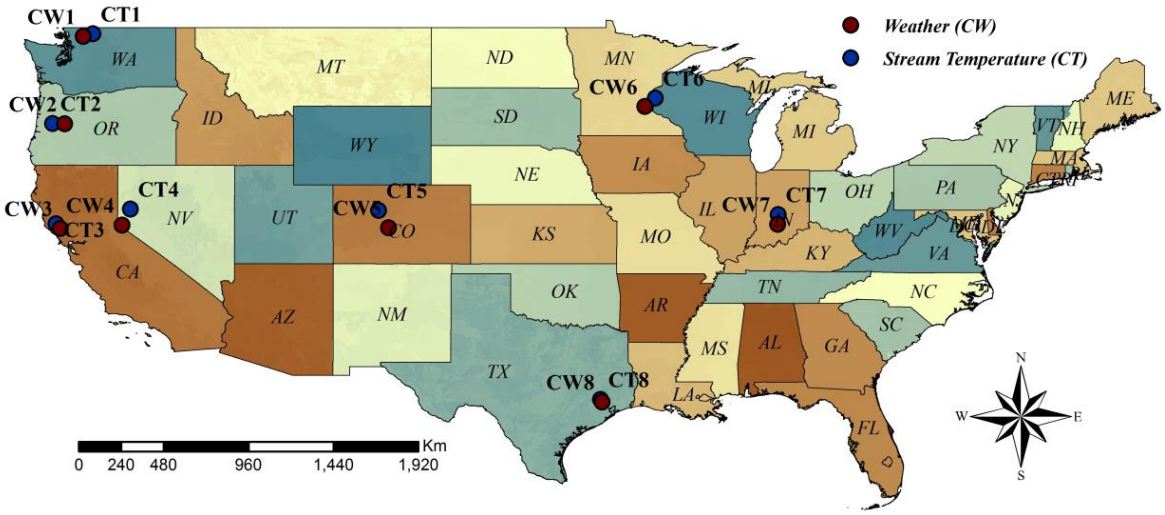

Figure 2.2. Location of weather and stream temperature stations at eight different climate regions in United States.

Table 2.1**.** Detailed information of stream temperature stations

Station NO.	Stream	Latitude	Longitude	T*	Elevation (m)
CT1	Skagit River at Newhalem, WA	48.67	-121.25	CW1	59
CT2	Long Tom River near Alvadore, OR	44.12	-123.30	CW2	205
CT3	Russian River near Hopland, CA	39.03	-123.13	CW3	609
CT4	Truckee River near Nixon, NV	39.78	-119.34	CW4	1435
CT5	Eagle River near Wolcott, CO	39.70	-106.73	CW5	2682
CT6	ST. Croix River at ST. Coix Falls, WI	45.41	-92.65	CW6	295
CT7	White River near Centerton, IN	39.50	-86.40	CW7	228
CT8	Spring Creek near Spring, TX	30.11	-95.44	CW8	29
T1	Dixie creek	43.34	-115.48	W1	1171
T2	Smith Creek	43.52	-115.67	S2	1171
T3	Little Rattlesnake Creek	43.59	-115.70	W3	1134
T4	Mores Creek	43.64	-115.48	W3	1134
T5	Grimes Creek	43.74	-115.96	W4	1032
T6	Bannock Cr	43.82	-115.80	W4	1216
T7	MF Boise River	43.70	-115.66	W4	1048
T8	Rattlesnake Creek	43.63	-115.56	S3	2000
T9	Rattlesnake Creek	43.59	-115.60	S2	1527
T10	SF Boise River	43.48	-115.31	S3	1281
T11	Grouse Creek	43.54	-115.23	S3	1660
T12	Dog	43.53	-115.31	S3	1371
T13	Dog Creek	43.56	-115.34	S3	1838
T14	Trinity Creek	43.63	-115.39	S3	2034
T15	Scotch Creek	43.69	-115.42	S3	2063
T16	EF Roaring River	43.69	-115.44	S3	1831
T17	Roaring River	43.72	-115.47	S3	1547
T18	Mores Creek	43.90	-115.71	S4	1499
T19	GRIMES CR	43.98	-115.84	W4	1362
T20	Grimes Creek	44.01	-115.74	S4	2002
T21	Pikes Fork	44.00	-115.51	S5	1701
T22	Crooked River	44.00	-115.47	S5	1806
T23	Bear Creek	43.99	-115.45	S5	1790
T24	Crooked River	44.05	-115.42	S5	1942
T25	Queens River	43.82	-115.21	S7	1507
T26	SF Ross Fork	43.79	-115.00	S8	2025
T27	Gold Run Cr	43.79	-114.95	S8	1997
T28	Paradise Ck	43.69	-114.86	S8	2056
T29	Skeleton Cr	43.64	-114.97	S8	1853
T30	BIG SMOKY	43.66	-114.80	S9	1799
T31	Big Peak Creek	43.65	-114.79	S9	1854
T32	Big Peak Creek	43.63	-114.76	S9	1959
T33	Little Smoky Creek	43.52	-114.72	S9	1945
T34	Little Smoky Creek	43.53	-114.69	S9	2015

T* shows weather or Snowtel stations which were used to estimate stream water temperature for each stream water temperature station. Letter C, T, S and W stand for Climate Region, Stream Water Temperature station, SNOTEL and Weather stations, respectively, for example CW1 indicates the weather station located at first climate region.

2.4. Methods

2.4.1. Data Collection

We obtained mean daily water temperature data in the Boise River Basin at 34 stations for the period of August 2010 to August 2012. Miniature digital temperature sensors were placed in solar shields and epoxied to the downstream side of large boulders below the low-flow summer water surface as described in Isaak et al. (2013). One additional water temperature record was obtained at T4 station, which had data from November 1969 to July 1972 at a USGS flow gage. The water temperature records were matched with contemporaneous meteorological and hydrological data from 3 weather stations, 8 SNOTEL stations and 4 stream discharge gaging stations (Figure 2.1). Table 2.1, Table A. 2.1, Table A. 2.2 and Table A. 2.3 report detailed information of stream water temperature, weather, SNOTEL (www.wcc.nrcs.usda.gov) and discharge stations (USGS website: www.usgs.gov), respectively. Because there was not a weather or SNOTEL station for each reach with a temperature sensor, we matched the nearest weather or SNOTEL station to each stream water temperature gage (therefore, recorded mean daily air temperature of some weather and SNOTEL stations were matched with multiple water temperature sensors). The observed mean daily discharges at D1, D3 and D4 gages were used for estimation of stream water temperature at T1, T7 and T4, respectively. Station D2 had discharge and stream water temperature measurements from April 1963 to September 1965 and from April 1978 to October 1979 (Table A.3). We used the observed data for these two periods at D2 to test the capability of our model to reconstruct historical stream water temperatures in periods with different hydrological conditions from those of the calibration period (see section 2.4.6). After October 1979, only discharge was recorded at D2. At this gage the observed discharge was used for estimation of stream water temperature at T10, which is close to D2, for the period of August 2010 to August 2012.

At the eight stations selected to test the performance of the model in different climates, daily discharge measurements with less than 4% missing values were available for all stations except CT2. The discharges in this station (CT2) were influenced by upstream irrigation diversions and were not used. The stations CT1, CT2, CT3 and CT6 located downstream of a dam were used to test the model at regulated streams.

2.4.2. Model Development

We developed a piecewise model, called the Stream Water Temperature Model (SWTM), which accounts for both linear and non-linear relationships between dependent and independent variables. The model uses mean daily air temperature (T_a) as meteorological driver and discharge (Q) as hydrological driver to estimate mean daily stream water temperature (T_s). It accounts for antecedent conditions by considering the stream water temperature of the previous time step (day). We fit the model using Bayesian methods (Gelman and Hill 2007; Lunn et al. 2000a).

Stream water temperature is correlated with air temperature and discharge (Luce et al. 2014; Mohseni et al. 1998). Air temperature is commonly used as a surrogate for heat flux exchanges in stream water temperature models. The linear relationship between air temperature and steam water temperature becomes non-linear as air temperature approaches freezing (0°C) (Figure 2.3) (Mohseni et al. 1998; Neumann et al. 2003; Webb et al. 2003). Discharge is a proper proxy for snowmelt and rain, which have notable influences on stream water temperature (Gu et al. 1999; Hockey et al. 1982; Webb et al. 2003). Webb et al. (2003) identified a linear relationship between discharge and stream water temperature at any time scale (e.g. daily or weekly).

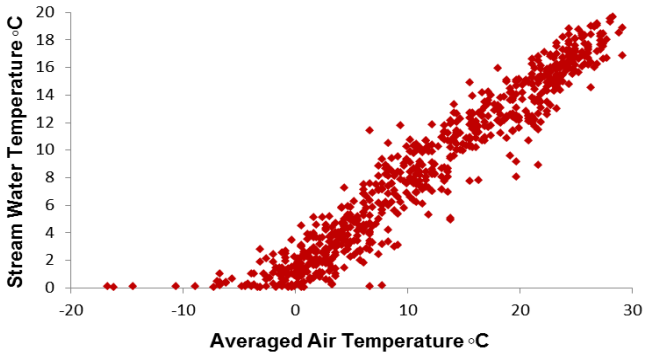

Figure 2.3. Linear and non-linear relationship between daily stream water and air temperatures at station T10.

Heat capacity of a system is the amount of heat required to increase the temperature by 1°C (IUPAC 2014). Because heat capacity of water is large and larger than that of the air, stream

water temperature does not respond to heat exchanges as quickly as air temperature. Consequently, stream water temperature changes slowly unless there are sources of water of a different temperature from that of the stream or changes in canopy cover. The correlation distance increases with discharge, as more heat or heat loss is required to warm or cool the water. This spatial longitudinal correlation is particularly true at fine temporal resolution i.e. hourly and daily (Ahmadi-Nedushan et al. 2007; Webb et al. 2003). The SWTM model considers the thermal inertia with an autoregressive component. We tested lag times varying between 0 and 7 days. We found that the highest autocorrelation was associated with a one-day lag (Figure 2.4) and therefore specified a 1-day lag in the model.

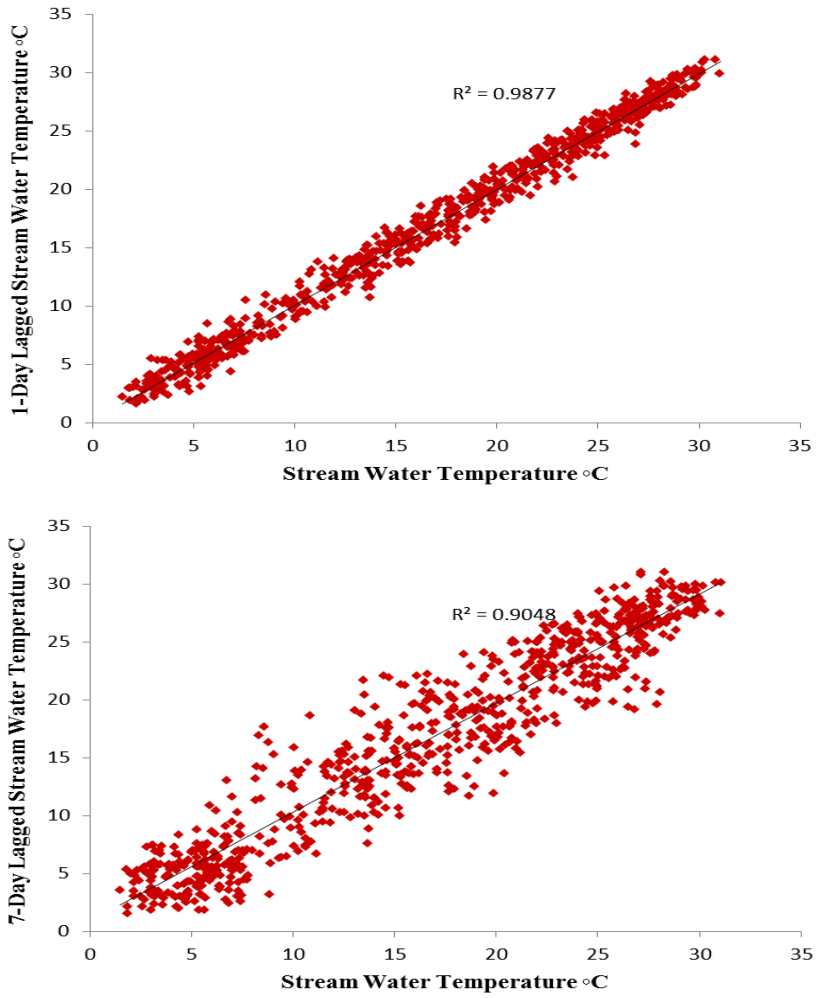

Figure 2.4. One-day and seven-day lagged autocorrelation of daily stream water temperature at station CT7.

A robust stream temperature model at a daily resolution should account for two important properties: non-linearity near the freezing point and the thermal inertia of the water. To account for this, we divided the data series temporally into three parts: days T_a <1°C (group 1), days in the October to May period that T_a >1°C (group 2), and the June-September period (group 3). A linear model is applied for data in group 2 and 3, whereas a non-linear model is used for data in group 1. In both the linear and non-linear models, it is assumed that stream water temperature has a Gaussian (normal) distribution (Eq. 2.1), because daily T_s and T_a are strongly correlated and daily T_a follows a Gaussian distribution (Robeson 2002).

$$T_s = Normal\,(\mu(t), \tau) \quad \text{(Eq. 2.1)}$$

Where μ (mean) and τ (standard deviation) are location and scale parameters, respectively. The standard deviation τ is time independent, whereas μ is time dependent and defined in two different ways for the linear (Eq. 2.2) and non-linear (Eq. 2.3) models:

$$\mu(t) = a_1 \times T_a(t) + a_2 \times \mu(t-1) + a_3 \times Q(t) + b \quad \text{(Eq. 2.2)}$$

$$\mu(t) = \exp\,[a_1 \times T_a(t)] + |a_2| \times \mu(t-1) + a_3 \times Q(t) + |b| \quad \text{(Eq. 2.3)}$$

where a_1, a_2 and a_3 are coefficients related to air temperature, stream water temperature at the previous time step and discharge, respectively, *t* is time and *b* is intercept in both linear and non-linear models. For streams that have temperatures near the freezing point, a negative value could be estimated for a_2 or *b*; we prevent this by using absolute values of a_2 and *b* in the model (Eq. 2.3), to result in posterior distributions with a positive mean for these parameters. The second variable ($\mu(t-1)$) in Eq. 4.2 and 4.3 carries over the estimated stream water temperature from the prior time step.

With a large sample size the choice of prior distribution has a negligible impact on posterior inference (Gelman 2002). We used minimally informative prior distributions. It is assumed that coefficients and intercepts in Eq. 4.2 and 4.3 followed a Gaussian distribution (Gelman 2006; Kwon et al. 2008):

$$a_1, a_2, a_3 \text{ and } b \approx Normal\,(0, 10^{-4}) \quad \text{(Eq. 2.4)}$$

The scale parameter τ must have positive values. We assumed the scale parameter followed a Gamma distribution to constrain the scale parameter to positive values (Spiegelhalter et al. 2003).

$$\tau \approx Gamma\,(10^{-3}, 10^{-3}) \quad \text{(Eq. 2.5)}$$

We fit these parameters using WinBUGS software, called from R with the R2WinBUGS package (Sturtz et al. 2005). WinBugs (Lunn et al. 2000b) applies Markov Chain Monte Carlo (MCMC), using Gibbs sampling and the Metropolis–Hastings algorithm to infer posterior distributions. MCMC is a numerical method that generates dependent samples that follow a given probability distribution. The role of MCMC is to generate large enough dependent samples that the characteristics of a posterior distribution can be precisely summarized (Campbell et al. 1999; Tierney 1994). At each iteration, a parameter is updated by sampling from its full conditional distribution, which depends on the data, the prior and on the current values of the other parameters (Gilks et al. 1995). The R2WinBUGS package is used to call WinBUGS from R to facilitate the preparation and manipulation of the data in WinBUGS (Sturtz et al. 2005). We ran three chains for 2,000 iterations each, following a 1,000 iteration burn-in period. We evaluated convergence using the Gelman-Rubin statistic.

2.4.3. Model Evaluation

The model was calibrated with the first two thirds of the data and validated with the remaining one third. Accuracy of fit and error of the model were evaluated with the Nash-Sutcliffe coefficient (NSC) and root mean square error (RMSE), respectively. NSC is calculated as follows (Nash and Sutcliffe 1970):

$$NSC = 1 - \left[\sum_{i=1}^{n} (T_{s_{sim,i}} - T_{s_{obs,i}})^2 \Big/ \sum_{i=1}^{n} (T_{s_{obs,i}} - \overline{T_{s_{obs}}})^2 \right] \quad \text{(Eq. 2.6)}$$

where $T_{s_{sim,i}}$ and $T_{s_{obs,i}}$ are the simulated and observed stream water temperatures, $\overline{T_{s_{obs}}}$ is the mean observed stream water temperature, *n* is number of observations (time step). RMSE is computed based on the below equation:

$$RMSE = \sqrt{\sum_{i=1}^{n} (T_{s_{sim,i}} - T_{s_{obs,i}})^2 \Big/ n - m} \quad \text{(Eq. 2.7)}$$

where *m* is the number of parameters in the model. The effect of *m* (Eq. 2.7) is negligible when *n* is large as in this study; thus *m* is ignored. We calculated also RMSE for each month and averaged it over the study sites. To have an accurate comparison of model performance at all the stations, mean daily stream water temperatures were estimated using only mean daily air temperatures (Ta model).

2.4.4. Role of Discharge

Discharge measurements were available only at 11 (T1, T4, T7, T10, CT1, CT3, CT4, CT5, CT6, CT7 and CT8) of the 42 stations. At these stations, mean daily stream water temperatures were estimated using both air temperature and discharge as inputs (Ta-Q model) and also using Ta model. Comparison between Ta-Q and Ta models allowed us to quantify the effect of discharge on model performance. Out of these 11 stations, 3 stations are regulated (CT1, CT3 and CT6), 2 stations (CT7 and CT8) are located at rain-dominated basins and 6 stations (T1, T4, T7, T10, CT4 and CT5) are located at snow-dominated basins.

2.4.5. Effect of Inclusion of the Autoregressive Component

The most important effect of the autoregressive component is to prevent unrealistically rapid changes in the estimated stream water temperatures due to sudden changes in air temperatures. The effect of the autoregressive component was evaluated by comparing estimated stream water temperatures from Ta model with and without the autoregressive component.

2.4.6. Historical Reconstruction

We tested the capability of the model to predict historical stream water temperatures for periods that may also have different hydrological conditions (e.g. dry or wet) from those of the calibration period. We performed this analysis using data from station D2, because at this station stream water temperature and discharge were available for two different hydrological conditions. The April 1963- September 1965 period coincides with an exceptionally wet period, whereas the April 1978- October 1979 period is representative of an averaged year with precipitation close to the long-term mean (Sohrabi et al. 2015; Sohrabi et al. 2013). We calibrated the Ta-Q model for the 1978-1979 period and compared its predictions with the 1963-1965 temperature records.

2.4.7. Comparison to the Modified Mohseni Model

SWTM performance for both Ta and Ta-Q versions was compared to that of the Mohseni model. We used the modified Mohseni model (2011) that uses mean daily air temperature and discharge to estimate mean daily stream temperature. Ta-Q model was used at the 11 sites that recorded discharge, and Ta model was used for the remaining sites with only air temperature measurements.

2.5. Results

2.5.1. Model Evaluation

The NSC and RMSE values indicated that the Ta model performed well at unregulated streams but substantially worse at regulated streams. The 2-year RMSE and 2-year NSC, including both calibration and validation periods, ranged from 0.87 $^{\circ}$C (at T15) to 2.5 $^{\circ}$C (at CT5) and from 0.63 (at CT1 and CT3) to 0.97 (at CT6, CT7 and CT8; Figure 2.5), respectively. The largest RMSE was related to site CT5, which was located in a snow-dominated basin. Large errors were observed from May through August, the period when the contribution of snow melt to discharge substantially affects stream water temperatures. Across all sites the highest errors occurred in May (Figure 2.7), the month during which snowmelt makes the largest contribution to stream discharge (unlike the Ta-Q model, the Ta model does not account for the effect of discharge). The second highest RMSE (2.1 $^{\circ}$C) was related to CT2 (Figure 2.5 and Figure 2.6 a), which is 0.32 km downstream from a dam. Site CT6, located 0.48 km downstream from a dam, had the highest NSC and a RMSE of 1.59 $^{\circ}$C (Figure 2.5 and Figure 2.6 b). The RMSE was relatively low (1.1- 1.19 $^{\circ}$C) during July and August (Figure 2.7), indicating good model performance during the warmest part of the year, which is particularly important for many aquatic habitat and water quality applications.

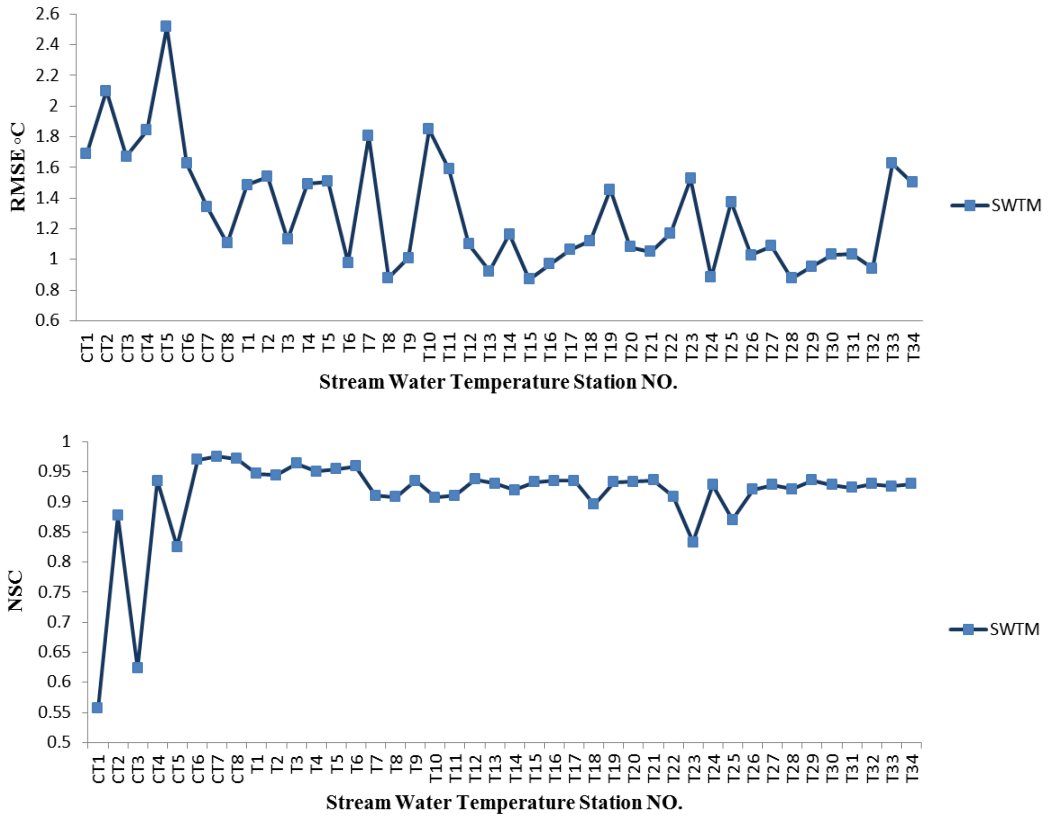

Figure 2.5. 2-year RMSE and NSC, including both calibration and validation periods, of Ta model.

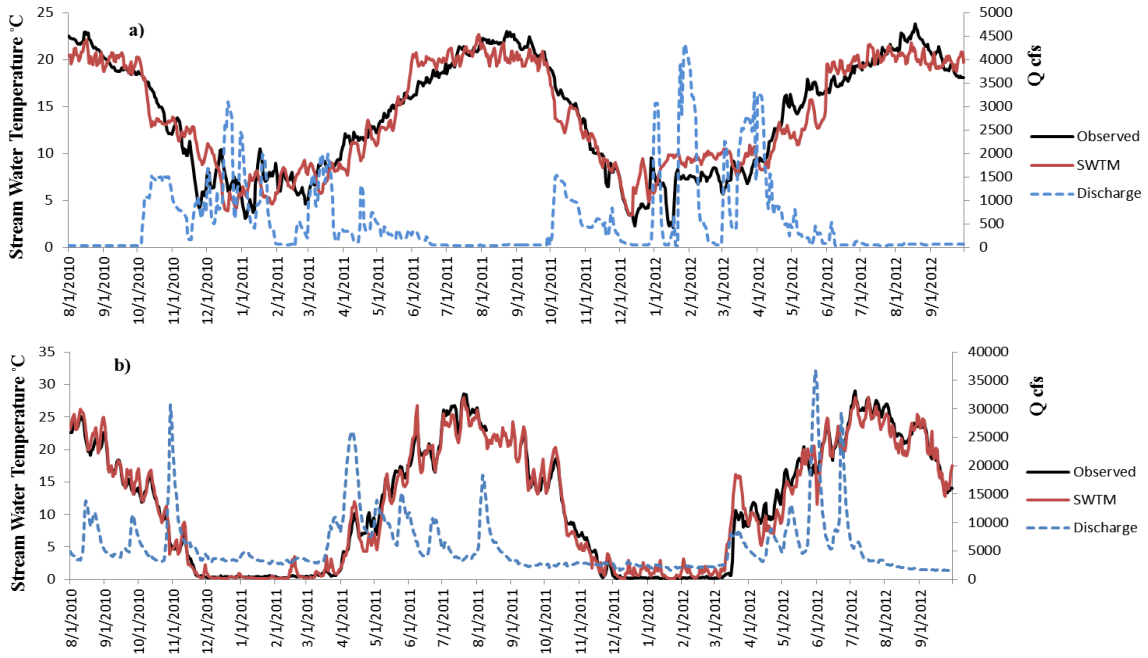

Figure 2.6. Simulated and observed daily stream water temperatures and discharge at CT2 (a) and CT6 (b) stations.

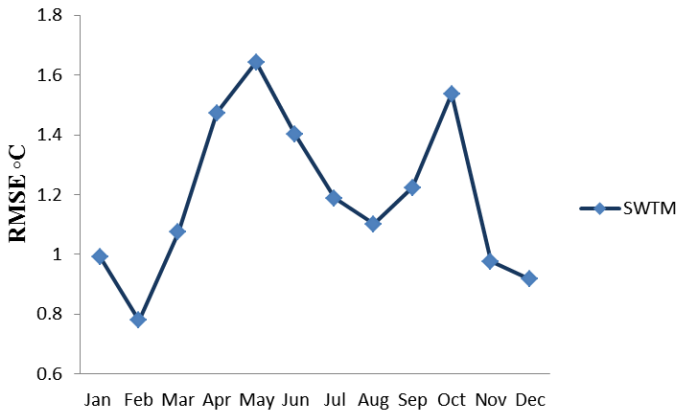

Figure 2.7. Average RMSE of Ta model for each month.

2.5.2. Role of Discharge

Stream discharge as an additional input variable had negligible influence on model performance for streams in rain-dominated basins and those with regulated flows. However, it significantly enhanced model performance for most snow-dominated streams (except T1; Figure 2.8) for the months between April through August, the period when discharge is dominated by snowmelt (Figure 2.9). The largest difference (RMSE) in performance between Ta and Ta-Q models was in June (1.5˚C), when snowmelt had the highest contribution to discharge (Figure 2.10). Performance of the Ta model was slightly better than that of Ta-Q model in March. For other months beside outside of the April to August period, the Ta-Q model was only modestly better (< 0.1˚C in RMSE) than the Ta model.

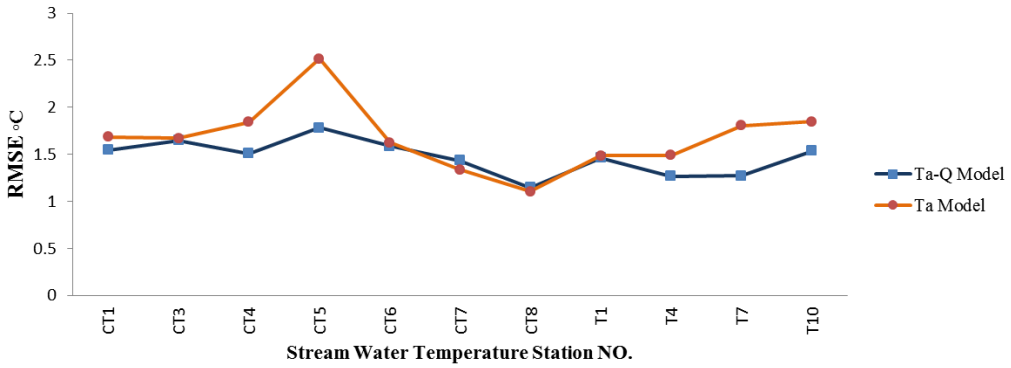

Figure 2.8. Changes in the RMSE of SWTM by adding discharge.

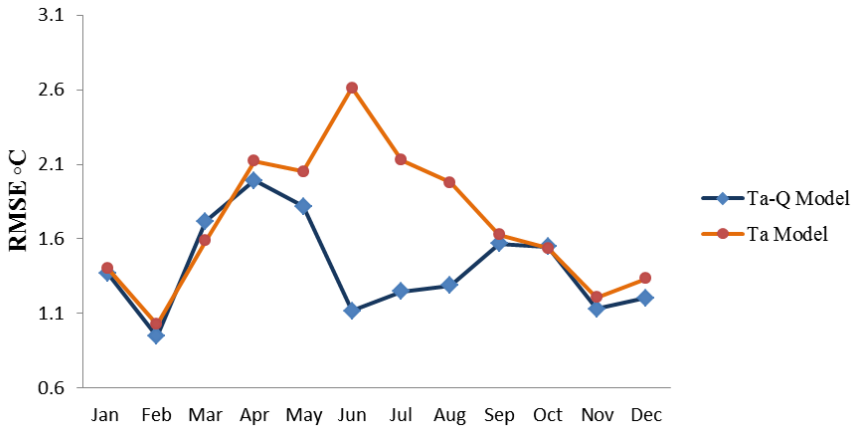

Figure 2.9. Changes in the RMSE of SWTM by adding discharge as a predictor at monthly scale.

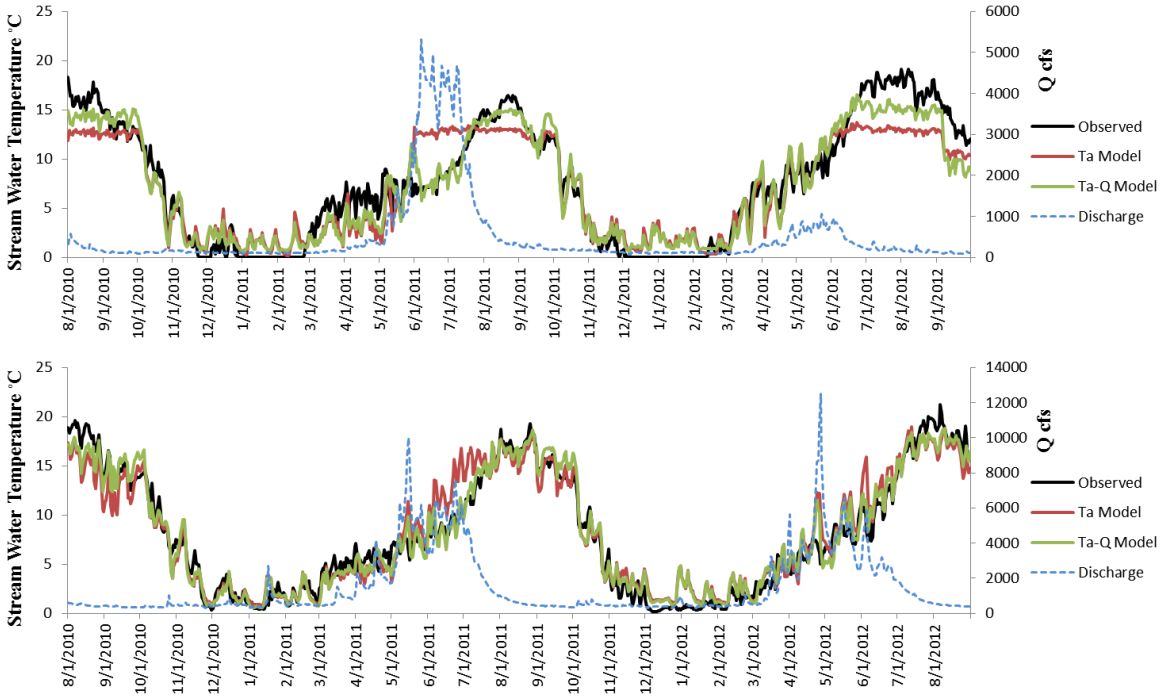

Figure 2.10. Time series of simulated and observed daily stream water temperatures at CT5 (the top figure) and T7 (the bottom figure) stations, respectively.

2.5.3. Effect of Inclusion of the Autoregressive Component

Our analysis shows that the autoregressive component may have different effects on model performance when daily stream water temperatures are modeled at short (weekly) or long (yearly) time scale analysis. The autoregressive component has an important effect on predicting daily stream water temperatures within short temporal windows (weekly time scale analysis) as shown from fall to spring when sudden changes in temperature occur on a single day (Figure 2.11; the top figure) regardless of watershed size. However, at large time scales (monthly or yearly time scale) the autoregressive component increases model performance only in streams with a drainage area >100 km^2; its effect is negligible in streams <50 km^2 drainage area. On average RMSE was increased by 0.21°C in large streams due to neglecting the autoregressive component, whereas on average only a 0.06°C increase in RMSE was observed in small streams. The largest increase in RMSE (increase of 1.14°C) was observed at CT7 site, which was the largest unregulated stream among the study sites (Figure 2.11; the bottom figure).

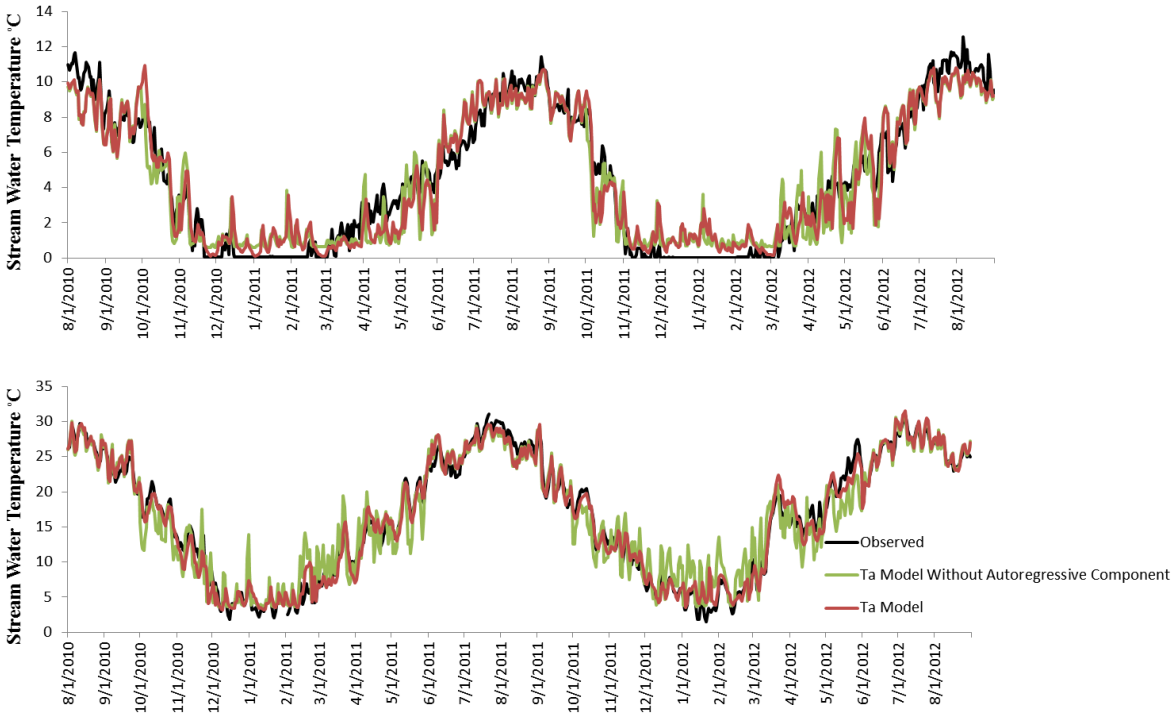

Figure 2.11. Effect of disregarding autoregressive component at T22 (the top figure) and CT7 (the bottom figure). Red line indicates estimated stream water temperatures from Ta model. Green line shows estimated stream water temperatures from Ta model without autoregressive component.

2.5.4. Historical Reconstruction

SWTM predicted stream water temperature reasonably well (RMSE of 1.55˚C) for the 2-year validation period at station D2, in spite of different climatic and hydrological conditions between the calibration and validation periods (Figure 2.12). SWTM extensively underestimated stream water temperature for only five days (mid-June 1965) (Figure 2.12). During those five days, air temperatures dropped from 21.5˚C to 11.5˚C and discharges increased significantly due to an exceptional summer rainfall event (40 mm in 5 days).

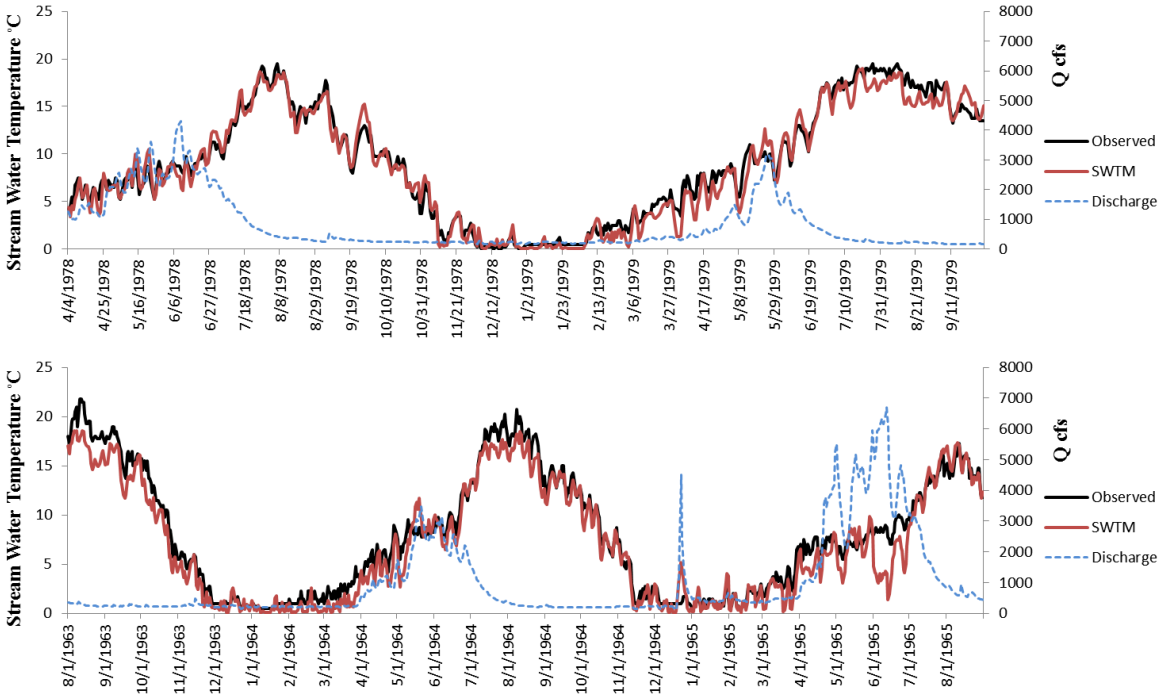

Figure 2.12. Hindcast of daily stream water temperature (Ta-Q model) for the period with different hydrological conditions from the calibration period at station D2. The top figure indicates calibration period (average year) and the bottom figure shows validation period (wet year).

2.5.5. Comparison to the Modified Mohseni Model

Performance of SWTM exceeded that of the modified Mohseni model (Figure 2.13). Average RMSE and NSC of SWTM were 1.25 ˚C and 0.91, respectively, whereas average RMSE and NSC of the modified Mohseni model were 1.68 ˚C and 0.86, respectively. Performance differences were most pronounced at stations with discharge measurements (T1, T4, T7, T10, CT4, CT5, CT7 and CT8). For these stations, SWTM had an average RMSE of 1.43 ˚C, compared to 2.24 ˚C, for the modified Mohseni model. The largest difference was observed at CT5 (Figure 2.14), in which RMSE and NSC of SWTM was 1.43 ˚C lower and 0.2 larger, respectively, than that of the modified Mohseni model. SWTM also performed better than the Mohseni model on regulated streams (Figure 2.13), with RMSE of 1.72 ˚C compare to 2.31 ˚C for the modified Mohseni model.

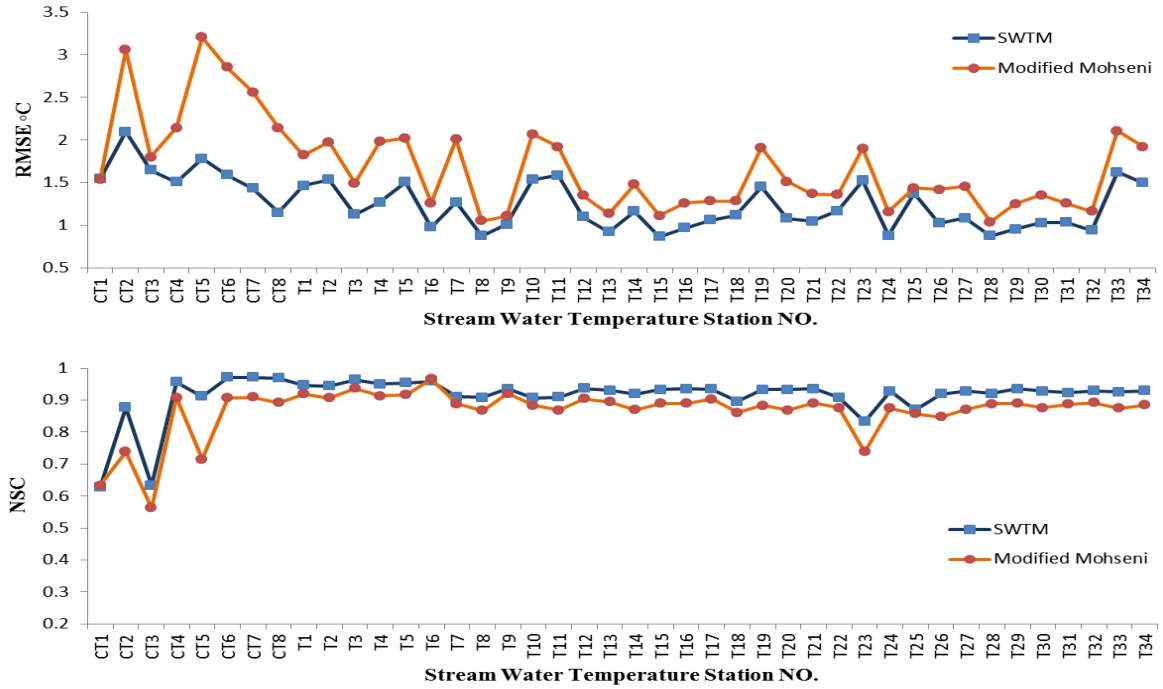

Figure 2.13. Comparison of daily stream water temperature predicted with the modified Mohseni and SWTM.

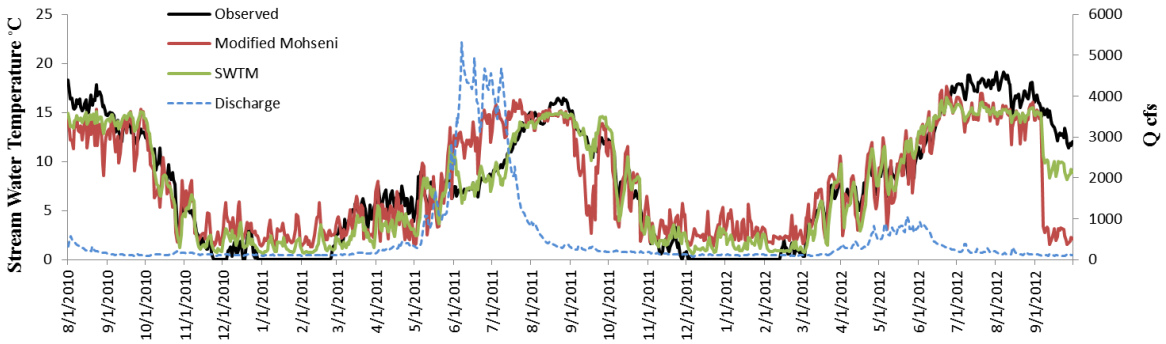

Figure 2.14. Comparison between generated daily stream temperatures from SWTM and the modified Mohseni model at CT5, a snow dominated basin.

2.6. Discussion

The performance of SWTM was good with average RMSE and NSC of 1.25°C and 0.91, respectively, over the study sites. Comparing these RMSE and NSC values to those of reported in the literature indicates robust performance of SWTM. Ficklin et al. (2012) reported average NSC of 0.82 and mean error of 0.66°C, and Vliet et al. (2011) reported

average RMSE and NSC of 2.26°C and 0.85, respectively, for estimation of mean daily stream temperatures. Mohseni et al. (1998) demonstrated average RMSE and NSC of 1.64°C and 0.93, respectively, for estimation of weekly stream temperature.

Available statistical stream temperature models have been rarely tested under a wide range of climate conditions. Most statistical models, such as those presented in the works of Caissie et al. (2001), Webb et al. (2003), Ahmadi-Nedushan et al. (2007) and Caldwell et al. (2013), were tested at one watershed and within one climate zone. Conversely, the Mohseni model was tested for regulated and unregulated streams under a wide range of climate and hydrologic conditions. However, it performed poorly in regions where the difference between maximum and minimum weekly averaged stream water temperature was low (Benyahya et al. 2007; Mohseni et al. 1998), as for instance our study site CT3, where the Mohseni model had a NSC value of 0.56, compared to SWTM with NSC of 0.63. Its performance was also low in snow dominated watersheds, where discharge variation had a pronounced effect on summer stream water temperature (Luce et al. 2014).

The results indicate robust performance of SWTM across a range of climate and hydrologic conditions. Because SWTM tracks changes in the independent variables rather than depending on the difference between maximum and minimum values of stream water temperature, its performance is similar in different climate and hydrologic conditions. On the other hand, seasonality influences the hysteresis between air-water temperature (Benyahya et al. 2007; Langan et al. 2001; Webb and Nobilis 1997). Our model is separately fitted for cold and warm seasons to minimize the effect of seasonality. The autoregressive structure is another important feature of SWTM, because it prevents fluctuations in daily air temperatures from overly influencing daily stream water temperature estimations. Similar to Webb et al. (2003), our results indicated that inclusion of the autoregressive component is critical in large streams. These streams can absorb large amounts of heat with negligible change in their temperature because their large water volume provides high thermal capacity inertia. This causes hysteresis in the air-water temperature relationship and lowers the correlation between air and water temperatures.

Similarly to previous studies (Ahmadi-Nedushan et al. 2007; Bogan et al. 2003; Neumann et al. 2003; Webb et al. 2003), the analyses show that air temperature is the primary predictor for

estimating stream water temperature for most hydrological settings. Consistent with the findings of Webb et al. (2003), our model shows that discharge is a secondary factor in predicting stream water temperatures in rain-dominated basins and those with regulated flows. Ahmadi-Nedushan et al. (2007) reported that discharge has a secondary impact in snow-dominated streams as well. However, our analyses indicate that stream discharge is a major hydrologic driver for unregulated streams in snow-dominated basins with a large drainage area, particularly during the spring-summer period from April through August. Ahmadi-Nedushan et al. (2007) used flow-derived variables, i.e. minimum and maximum flow of 3-, 5- and 7-day periods, rather than discharge measurements as independent variables. The disagreement between results of this work and those of Ahmadi-Nedushan et al. (2007) might be due to the difference in accounting for flow information. Our results indicate that the largest difference between the performance of Ta and Ta-Q models occurs in June. In this month, air temperature substantially increases but stream discharge also increases due to snow melt. The latter contribution prevents stream water temperatures from increasing rapidly following the air temperature trend, which causes the Ta model to over-predict stream water temperature. An increase in a stream discharge increases thermal capacity and decreases travel time which in turn leads to less sensitivity of water temperature to air temperature, which is a surrogate for net heat exchanges at the air-water interface (Webb et al. 2003). In addition, when the source of discharge is cold water from snow melt, it causes hysteresis in the air-water temperature relationship (Mantua et al. 2010; Mohseni et al. 1998). The results suggest that the performance of Ta-Q over Ta decreases with smaller contributing drainage area, because discharge typically decreases with drainage area.

Statistical stream water temperature models such as SWTM may have some limitations when applied to time series far from the calibration period. For example, SWTM does not consider impacts of possible changes in vegetation on stream water temperatures. Shading influences sensible and latent heat fluxes, particularly in summer (Bogan et al. 2003). Furthermore, in groundwater dominated streams, particularly when there is considerable hyporheic exchange close to a stream temperature sensor, differences in hydrological conditions of calibration and validation periods, i.e. dry or wet conditions, may results in large errors due to changes in magnitude of the interactions between surface and subsurface waters (Bogan et al. 2003). These two limitations can be solved by using equilibrium temperature as a predictor instead of

air temperature. Equilibrium temperature is defined as the temperature that a water body can have when the integral of the heat fluxes across the air-water interface is zero (Bogan et al. 2003). Equilibrium temperature can be calculated using weather data including air temperature, dew point temperature, precipitation, solar radiation, sky cover, and wind speed. Bogan et al. (2003) found a linear relationship between equilibrium temperature above 0°C and stream water temperature. In streams where stream water temperatures follow heat exchanges at the air-water interface and are minimally affected by shading and groundwater exchanges, stream water temperature should be approximately equal to equilibrium temperature (roughly a 1:1 relationship (Bogan et al. 2003)). However, in streams where water temperatures are substantially influenced by groundwater exchanges or shading, for example, equilibrium temperatures are considerably lower or higher than stream water temperatures during winter and summer, respectively. In these streams, the relationship between equilibrium temperature and stream water temperature substantially deviates from the 1:1 relationship, but equilibrium temperatures can be adjusted to consider impact of shading and groundwater. To account for effect of shading and groundwater, which are not considered in equilibrium temperature calculation, on stream water temperature, a slope and intercept are calculated for the linear relationship between equilibrium temperature and stream water temperature to minimize their difference. (Bogan et al. 2003).

Model accuracy decreases in predicting stream water temperatures downstream of large reservoirs. The lower performance is mostly due to the reservoir releases, particularly from the hypolimnion, rather than variations in heat flux at air-water interface (Lowney 2000; Null et al. 2013; Risley et al. 2010; Sinokrot et al. 1995). The downstream distance at which the influence of the reservoir becomes negligible depends on reservoir depth and size, outlet vertical location and discharge (Mohseni et al. 1998; Sinokrot et al. 1995). Sinokrot et al. (1995) reported that the impact of reservoir releases from the hypolimnion can persist as far as 48 km downstream from the dam depending on the magnitude of releases. However, water releases may also form a consistent temporally-gradually varying stream temperature pattern (Lowney 2000), which SWTM proved capable of capturing at CT6. Dam releases are high between mid-spring to mid-summer (Figure 6b) at CT6, mimicking the effect of high discharge of unregulated streams due to snow melt in snow dominated regions during the period of mid-spring to mid-summer on stream water temperature.

The geostatistical models such those presented in the work of Isaak et al. (2010) interpolate and extrapolate stream water temperature throughout the river network from point measured stream water temperature. Our model could provide point temperatures in locations where measurements are no longer available or were not available in the past with reasonable estimates of uncertainty. This may allow coupling of the two models to provide more reliable forecasts of stream water temperature from climate change air temperature than available models. This will allow prediction of stream water temperature at the daily scale, which is an important variable for aquatic habitat quality, and of spatially distributed stream water temperature changes avoiding the uniform spatial change adopted in the work of Isaak et al. (2010).

Stream water temperatures at the daily time scale are important for estimating fish habitat quality during the low summer flows when stream water tends to reach the highest temperatures, or quantifying the days with stream water temperatures exceeding certain thresholds (Crozier et al. 2010; Mesa et al. 2013; Xu et al. 2010). It could be particularly useful in projecting the effects of climate change on riverine environments and forecasting potential effects on fish population dynamics (Ficklin et al. 2012).

2.7. Conclusions

We found that the SWTM model provided daily stream water temperature predictions of good accuracy, with average RMSE and NSC of 1.25°C and 0.92, respectively. Monthly RMSE of SWTM and time series of simulated daily stream water temperatures indicate that SWTM is capable of predicting well during the warmest periods, which are critical for aquatic habitats (RMSE of August is 1.1°C). Our results indicate that discharge improves model performance in snow-dominated basins with large drainage areas.

SWTM can be a useful tool to either reconstruct historical daily stream water temperatures or to project daily stream water temperatures under different climate change scenarios. Similar to other statistical models, performance of SWTM may be influenced by regulated discharges. However, even at regulated streams SWTM performed notably better than the commonly-used Mohseni model. It assumes static influence of both riparian vegetation shading and

groundwater contribution. In situations where riparian vegetation or/and groundwater influence is expected to change, air temperature should be replaced with equilibrium temperature.

2.8. References

Ahmadi-Nedushan B, St-Hilaire A, Ouarda TBMJ, Bilodeau L, Robichaud E, Thiemonge N, Bobee B. 2007. Predicting river water temperatures using stochastic models: case study of the Moisie River (Qu´ebec, Canada). Hydrological Processes, **21**: 21–34.

Bélanger M, El-Jabi N, Caissie D, Ashkar F, Ribi JM. 2005. Estimation de la température de l'eau en rivière en utilisant les réseaux de neurones et la régression linéaire multiple. Journal of Water Science, **18**: 403-421.

Benyahya L, Caissie D, St-Hilaire A, Ouarda TBMJ, Bobée B. 2007. A Review of Statistical Water Temperature Models. Canadian Water Resources Journal, **32**: 179–119.

Bogan T, Mohseni O, Stefan HG. 2003. Stream temperature-equilibrium temperature relationship. Water Resources Research, **39**: 1245 - 1257.

Boogert A, Dupont D. 2005. The nature of supply side effects on electricity prices: The impact of water temperature. Economics Letters, **88**: 121-125.

Brett JR. 1979. Environmental factors and growth. Fish Physiology, **VIII**: 599-675.

Caissie D, El-Jabi N, Satish MG. 2001. Modelling of maximum daily water temperatures in a small stream using air temperatures. Journal of Hydrology, **251**: 14-28.

Caldwell RJ, Gangopadhyay S, Bountry J, Lai Y, Elsner MM. 2013. Statistical modeling of daily and subdaily stream temperatures: Application to the Methow River Basin, Washington. Water Resources Research, **49**: 4346–4361.

Campbell EP, Fox DR, Bates BC. 1999. A Bayesian approach to parameter estimation and pooling in nonlinear flood event models Water Resources Research, **35**: 211-220.

Carron JC, Rajaram H. 2001. Impact of variable reservoir releases on management of downstream temperatures. Water Resources Research, **37**: 1733-1743.

Crozier LG, Zabel RW, Hockersmith EE, Achord S. 2010. Interacting effects of density and temperature on body size in multiple populations of Chinook salmon. Journal of Animal Ecology, **79**: 342-349.

Ficklin DL, Luo Y, Stewart IT, Maurer EP. 2012. Development and application of a hydroclimatological stream temperature model within the Soil and Water Assessment Tool. Water Resources Research, **48** W01511.

Forseth T, Jonsson B. 1994. The growth and food ration of piscivorous brown trout. Functional Ecology, **8**: 171-177.

Gelman A. 2002. Prior Distribution. In: Encyclopedia of Environmetrics, pp: 1634 – 1637.

Gelman A. 2006. Prior distributions for variance parameters in hierarchical models. Bayesian Anal., **1**: 515–533.

Gelman A, Hill J. 2007. Data Analysis Using Regression and Multilevel/Hierarchical Models. Cambridge University Press.

Gilks WR, Best NG, Tan KKC. 1995. Adaptive rejection metropolis sampling within Gibbs sampling. Appl. Statist, **44**: 455–472.

Gu R, McCutcheon S, Chen C-J. 1999. Development of weather-dependent flow requirements for river temperature control. Environmental Management, **24**: 529-540.

Hockey JB, Owens IF, Tapper NJ. 1982. Empirical and theoretical models to isolate the effect of discharge on summer water temperature in the Hurunui River. Journal of Hydrology, **21**: 1-12.

Isaak DJ, Horan DL, Wollrab SP. 2013. A simple protocol using underwater epoxy to install annual temperature monitoring sites in rivers and streams. Department of Agriculture, Forest Service, Rocky Mountain Research Station, pp: 21.

Isaak DJ, Luce CH, Rieman BE, Nagel DE, Peterson EE, Horan DL, Parkes S, Chandler GL. 2010. Effects Of Climate Change And Wildfire On Stream Temperatures And

Salmonid Thermal Habitat In A Mountain River Network. Ecological Applications, **20**: 1350–1371.

Isaak DJ, Wollrab S, Horan D, Chandler G. 2012. Climate change effects on stream and river temperatures across the northwest U.S. from 1980–2009 and implications for salmonid fishes. Climate Change, **113**: 499-524.

Isaak DJ, Young MK, Nagel DE, Horan DL, Groce MC. 2015. The cold-water climate shield: Delineating refugia for preserving salmonoid fishes through the 21st century. Global Change Biology, **21**: 2540–2553.

IUPAC. 2014. The Gold Book. In: Compendium of Chemical Terminology version 2.3.3, pp: 610.

Jobling M. 1997. Temperature and growth: modulation of growth rate via temperature change. In: Global Warming: Implications for Freshwater and Marine Fish, Cambridge University Press, pp: 225-253.

Kwon H-H, Brown C, Lall U. 2008. Climate informed flood frequency analysis and prediction in Montana using hierarchical Bayesian modeling. Geophysical Research Letters, **35**: L05404.

Langan SJ, Johnston L, Donaghy MJ, Youngson AF, Hay DW, Soulsby C. 2001. Variation in river water temperatures in an upland stream over a 30-year period. Science of The Total Environment, **265**: 195-207.

Lowney CL. 2000. Stream temperature variation in regulated rivers: Evidence for a spatial pattern in daily minimum and maximum magnitudes. Water Resources Research, **36**: 2947 - 2955.

Luce C, Staab B, Kramer M, Wenger S, Isaak D, McConnell C. 2014. Sensitivity of summer stream temperatures to climate variability in the Pacific Northwest. Water Resources Research, **50**: 3428–3443.

Lunn DJ, Thomas A, Best N, Spiegelhalter D. 2000. WinBUGS-A Bayesian modelling framework: Concepts, structure, and extensibility. Statatistical Computation, **10**: 325–337.

Lunn DJ, Thomas A, Best N, Spiegelhalter D. 2000. WinBUGS -- a Bayesian modelling framework: concepts, structure, and extensibility. Statistics and Computing, **10**: 325--337.

Mantua N, Tohver I, Hamlet A. 2010. Climate change impacts on stream flow extremes and summertime stream temperature and their possible consequences for freshwater salmon habitat in Washington State. Climate Change, **102**: 187–223.

Marzadri A, Tonina D, Bellin A. 2011. A semianalytical three-dimensional process-based model for hyporheic nitrogen dynamics in gravel bed rivers. Water Resources Research, **47**: W11518.

Marzadri A, Tonina D, Bellin A. 2012. Morphodynamic controls on redox conditions and on nitrogen dynamics within the hyporheic zone: Application to gravel bed rivers with alternate-bar morphology. Journal of Geophysical Research, **117**.

Mesa MG, Weiland LK, Christiansen HE, Sauter ST. 2013. Development and Evaluation of a Bioenergetics Model for Bull Trout. Transactions Of The American Fisheries Society, **142**: 41-49.

Mohseni O, Stefan HG, Erickson TR. 1998. A nonlinear regression model for weekly stream temperatures. Water Resources Research, **34**: 2685–2692.

Nash JE, Sutcliffe JV. 1970. River flow forecasting through conceptual models part I- A discussion of principles. Journal of Hydrology, **10**: 282-290.

Neumann DW, Rajagopalan B, Zagona EA. 2003. Regression Model for Daily Maximum Stream Temperature. Journal of Environmental Engineering, **129**: 667-674.

Null SE, Ligare ST, Viers JH. 2013. A method to consider whether dams mitigate climate change effects on stream temperatures. American Water Resources Association, **49**: 1456 - 1473.

Null SE, Viers JH, Deas ML, Tanaka SK, Mount JF. 2012. Stream temperature sensitivity to climate warming in California's Sierra Nevada: Impacts to coldwater habitat. Climate Change, **116**: 149–170.

Railsback SF, Rose KA. 1999. Bioenergetics Modeling of Stream Trout Growth: Temperature and Food Consumption Effects. Transactions Of The American Fisheries Society, **128**: 241-256.

Rice JA, Breck JE, Bartell SM, Kitchell JF. 1983. Evaluating the constraints of temperature, activity, and consumption on growth of Largemouth Bass. Environmental Biology of Fishes, **9**: 263-275.

Rieman BE, Isaak DJ, Adams S, Horan D, Nagel D, Luce C, Myers D. 2007. Anticipated climate warming effects on bull trout habitats and populations across the Interior Columbia River Basin. Transactions of the American Fisheries Society, **136**: 1552–1565.

Risley JC, Constantz J, Essaid H, Rounds S. 2010. Effects of upstream dams versus groundwater pumping on stream temperature under varying climate conditions. WATER RESOURCES RESEARCH, **46**: W06517.

Risley JC, Roehl EA, Conrads PA. 2003. Estimating Water Temperatures in Small Steams in Western Oregon Using Neural Network Models. U.S. Geological Survey Report 02-4218.

Robeson SM. 2002. Relationships between mean and standard deviation of air temperature: implications for global warming. **22**: 205-213.

Sinokrot BA, Stefan HG, McCormick JH, Eaton JG. 1995. Modeling of climate change effects on stream temperatures and fish habitats below dams and near groundwater inputs. Climatic Change, **30**: 181-200.

Sohrabi M, Ryu J, Abatzoglou J, Tracy J. 2015. Development of Soil Moisture Drought Index to Characterize Droughts. J. Hydrol. Eng., **DOI: 10.1061/(ASCE)HE.1943-5584.0001213**.

Sohrabi MM, Ryu J, Abatzoglou J, Tracy J. 2013. Climate extreme and its linkage to regional drought over Idaho. Natural Hazards, **65**: 653-681.

Spiegelhalter DJ, Thomas A, Best NG, Gilks WR, Lunn D. 2003. BUGS: Bayesian inference using Gibbs sampling. Cambridge.

Sturtz S, Ligges U, Gelman A. 2005. R2WinBUGS: A Package for Running WinBUGS from R. Journal of Statistical Software, **12**: 16.

Tierney L. 1994. Markov Chains for exploring posterior distributions. The Annals Of Statistics, **22**: 1701-1728.

Tonina D, Marzadri A, Bellin A. 2015. Benthic uptake rate due to hyporheic exchange: The effects of streambed morphology for constant and sinusoidally varying nutrient loads. Water, **7 (2015)**: 398-419.

Vliet MTHV, Ludwig F, Zwolsman JJG, Weedon GP, Kabat P. 2011. Global river temperatures and sensitivity to atmospheric warming and changes in river flow. Water Resources Research, **47**: W02544.

Vliet MTHV, Vogele S, Rubbelke D. 2013. Water constraints on European power supply under climate change: impacts on electricity prices. Environmental Research Letters, **8**: 10.

Vliet MTHV, Yearsley JR, Franssen WHP, Ludwig F, Haddeland I, Lettenmaier DP, Kabat P. 2012a. Coupled daily streamflow and water temperature modelling in large river basins. Hydrology and Earth System Sciences, **9**: 8335–8374.

Vliet MTHV, Yearsley JR, Ludwig F, Vogele S, Lettenmaier DP, Kabat P. 2012b. Vulnerability of US and European electricity supply to climate change. Nature Climate Change, **2**: 676-681.

Webb BW, Clack PD, Walling DE. 2003. Water–air temperature relationships in a Devon river system and the role of flow. Hydrological Processes, **17**: 3069–3084.

Webb BW, Hannah DM, Moore RD, Brown LE, Nobilis F. 2008. Recent advances in stream and river temperature research. Hydrological Processes, **22**: 902–918.

Webb BW, Nobilis F. 1997. Long-term respective on the nature of the air-water temperature relationship: A case study. Hydrological Processes, **11**: 137-147.

Xu C, Letcher BH, Nislow KH. 2010. Context-specific influence of water temperature on brook trout growth rates in the field. Freshwater Biology, **55**: 2253-2264.

2.9. Appendix A: The Detailed Information of Weather, SNOTEL and Discharge Stations

Table A. 2.1. Detailed information of weather stations

Station NO.	COOP-ID	Station Name	Latitude	Longitude	Elevation (m)
CW1	-	Concrete PPL Fish Station, WA	48.54	-121.74	59
CW2	-	Leaburg 1 SW, OR	44.10	-122.68	205
CW3	-	Hawkeye, CA	38.78	-122.91	609
CW4	-	Minden, NV	38.95	-119.77	1435
CW5	-	Red Deer, CO	38.82	-106.21	2682
CW6	-	University of Minnesota ST Paul, MN	44.98	-93.17	295
CW7	-	Hardin Ridge, IN	39.00	-86.42	228
CW8	-	Houston Intercontinental Airport, TX	29.98	-95.36	29
W1	100282	Anderson Dam	43.36	-115.45	387
W2	100448	Arrowrock Dam	43.58	-115.92	986
W3	104442	Idaho City	43.83	-115.82	1209

Table A. 2.2. Detailed information of SNOTEL stations

Station NO.	Station Name	Hydrological_Unit	Latitude	Longitude	Elevation (m)
S1	Bogus Basin	Lower Boise	43.75	-116.08	1932
S2	Prairie	South Fork Boise	43.50	-115.57	1463
S3	Trinity MTN.	South Fork Boise	43.62	-115.43	2368
S4	Mores Creek Summit	North and Middle Fork Boise	43.92	-115.65	1859
S5	Jackson Peak	North and Middle Fork Boise	44.05	-115.43	2155
S6	Atlanta Summit	North and Middle Fork Boise	43.75	-115.23	2310
S7	Vienna Mine	Upper Salmon	43.78	-114.85	2731
S8	Dollarhide Summit	Big Wood	43.60	-114.67	2566

Table A. 2.3. Detailed information of discharge stations

Station NO.	Station Name	Latitude	Longitude	Drainage Area (km^2)
CT1	Skagit River at Newhalem, WA	48.67	-121.24	3008
CT2	Long Tom River near Alvadore, OR	44.12	-123.29	645
CT3	Russian River near Hopland, CA	39.02	-123.12	926
CT4	Truckee River near Nixon, NV	39.77	-119.33	4677
CT5	Eagle River near Wolcott, CO	39.70	-106.72	1536
CT6	ST. Croix River at ST. Coix Falls, WI	45.40	-92.64	15974
CT7	White River near Centerton, IN	39.49	-86.40	6256
CT8	Spring Creek near Spring, TX	30.11	-95.43	1047
D1	Dixie Creek	43.34	-115.48	10
D2	Featherville	43.49	-115.31	1641
D3	Twin Springs	43.67	-115.72	2130
D4	Mores Creek AB Robie Creek NR Arrowrock Dam	43.64	-115.99	1016

Chapter 3. Role of Temporal Resolution of Meteorological Inputs on Process-Based Snow Modeling

3.1. Abstract

Accurate snow accumulation and melt simulations are crucial for understanding and predicting hydrological dynamics in mountainous settings. As snow models require temporally varying meteorological inputs, time resolution of these inputs is likely to play an important role on the model accuracy. Since meteorological data at a fine temporal resolution (~1 hr) is generally not available in many snow dominated settings, it is important to evaluate the role of meteorological inputs temporal resolution on the performance of process-based snow models. The objective of this work is to assess the loss in model accuracy with temporal resolution of meteorological inputs, for a range of climatic conditions and topographic elevations. To this end, a process-based snow model was run using 1-, 3- and 6-hourly inputs for wet, average and dry years over Boise River Basin (6,963 km^2), which spans rain-dominated (≤1400m), rain-snow transition (>1400 and ≤1900m), snow-dominated below treeline (>1900 and ≤2400m) and above treeline (>2400m) elevations. The results show that sensitivity of the model accuracy to the inputs time step generally decreases with increasing elevation from rain-dominated to snow-dominated above treeline. Using longer than hourly inputs causes substantial underestimation of snow cover area (SCA) and snow water equivalent (SWE) in rain-dominated and rain-snow transition elevations, due to the precipitation phase mischaracterization. In snow-dominated elevations, the melt rate is underestimated due to errors in estimation of net snow cover energy input. In addition, the errors in SCA and SWE estimates generally decrease toward years with low snow mass, i.e. dry years. The results indicate significant increases in errors in estimates of SCA and SWE as the temporal resolution of meteorological inputs become coarser than an hour. However, use of 3-hourly inputs can provide accurate estimates at snow-dominated elevations. The study underscores the need to record meteorological variables at an hourly time step for accurate process-based snow modeling.

Keywords: *Temporal resolution, Physics-based snow modeling, Mountainous regions, Rain-snow transition, Alpine treeline, Model accuracy, Model evaluation*

3.2. Introduction

Snow strongly affects the hydrology and ecology of mountainous regions (Homan et al. 2010; Raleigh and Lundquist 2012). From a hydrologic perspective, snow is a critical water storage reservoir that delays hydrologic response to precipitation (Garen and Marks 2005). Snow cover stores water in winter and releases it during spring and early summer (Kormos et al. 2014a). Snow melt, rain on bare ground and their combination define the so called surface water input (SWI). The spatio-temporal distribution of SWI is of great importance for hydrological studies (Grünewald and Lehning 2011; Lee et al. 2005). Soil moisture dynamics, evapotranspiration, streamflow generation and groundwater recharge depend on the spatial distribution, timing and magnitude of SWI (Kormos et al. 2014a; Kumar et al. 2013; Reba et al. 2011; Wang et al. 2013; Weill et al. 2013). From an ecological perspective, snow cover, with its duration and depth, controls soil moisture and moderates spring and early summer air temperature by increasing albedo (Molotch and Bales 2005). Soil moisture and air temperature are fundamental controls on vegetation distribution and greening (Darmody et al. 2004; Sensoy et al. 2006; Torp 2010; Trujillo et al. 2012). Snow also insulates soil from very low air temperatures due to its low thermal conductivity (Flerchinger and Saxton 1989; Liston and Elder 2006; Torp 2010), resulting in continued microbial activity during winter (Schimel et al. 2004). Moreover, stream temperature that has a significant role in aquatic ecosystem sustainability is influenced by snow melt (Gu et al. 1999; Webb et al. 2003). The contribution of snow melt to streamflow moderates increase in stream temperature in late spring and early summer (Luce et al. 2014). Aforementioned influences indicate that accurate estimation of snow accumulation and ablation is critical to understand and predict both hydrological and ecological dynamics.

Accurate estimation of snow accumulation and melt requires a fine temporal resolution (at least 6 hourly) data in order to capture diurnal changes in meteorological variables (Beniston 1997; Garen and Marks 2005). The diurnal variation of meteorological variables in

mountainous regions shows high temporal gradients (Little and Hanna 1978), due to the low atmosphere density (mass) (Aguado and Burt 2013), which facilitates large incoming short-waves during the daytime and outgoing long-waves in the nighttime. Because of the fast variations of meteorological variables such as wind speed, air temperature and vapor pressure (Marks et al. 1998), which determine both energy and water fluxes across the air-snow cover interface, coarse temporal resolutions may cause errors in identification of the precipitation phase and estimation of timing and magnitude of snow accumulation and melt. In rain dominated and rain-snow transition bands, where precipitation may fall in form of snow or rain, fast variations in dew point or wet-bulb temperature may result in incorrect identification of precipitation phase (Beniston 2012). This in turn may lead to inaccurate estimation of snow mass and advected heat from precipitation to the snow cover (Hock and Holmgren 2005; Kormos et al. 2014a). In snow dominated bands, where turbulent energy is responsible for a large portion of the energy balance (Marks et al. 1998), particularly in winter and early spring, and radiation is the dominant contributor to energy balance from mid-spring to early summer; estimation of the energy exchange between snow and the atmosphere can be less reliable when coarse temporal resolution inputs are used. These examples suggest that the impact of input data resolution on estimation accuracy is likely to vary across elevation bands.

The impact of temporal resolution of meteorological inputs on snow accumulation and ablation can be quantified by evaluating changes in variables such as snow cover area (SCA) and snow water equivalent (SWE). Expectedly, the impacts are expected to vary with snow variable. For example, SCA strongly depends on changes in heat fluxes (Keller et al. 2005; Martin et al. 1994; Scherrer and Appenzeller 2004), while SWE is also sensitive to precipitation mass (Beniston 2012; Howat and Tulaczyk 2005). Impacts are also likely to vary between years with characteristically different climatology. For example, in a wet year, daily temporal gradient of heat fluxes is on an average less significant due to high humidity and large number of cloudy days (Rohli and Vega 2008). In contrast, in a dry year, heat fluxes temporal gradient is pronounced.

Despite the aforementioned sensitivity of snow processes to hourly variation of meteorological variables, the influence of temporal resolution of meteorological inputs on snow accumulation and ablation has not been assessed yet. This work addresses this

knowledge gap by: (1) quantifying the impact of time resolution of meteorological inputs on modeled SCA and SWE; (2) evaluating the role of annual precipitation on aforementioned impacts; and (3) identifying the elevation ranges wherein snow models are most sensitive to temporal resolution of meteorological inputs.

3.3. Study Area and Data

The study site is a portion of the Boise River basin (BRB) (Idaho, USA) upstream of the Lucky Peak Dam (Figure 3.1). BRB has a drainage area of 6,963 km^2 and it is mainly covered with coniferous forest (41%) and shrubland (35%). The remaining area is covered with bare rock, grass, deciduous forest, or burned/harvested forest. Basin elevations range from 841 m to 3,168 m. Lower elevations are rain dominated and receive approximately 500 mm of annual precipitation, and higher elevations are snow dominated and receive approximately 1,500mm of annual precipitation.

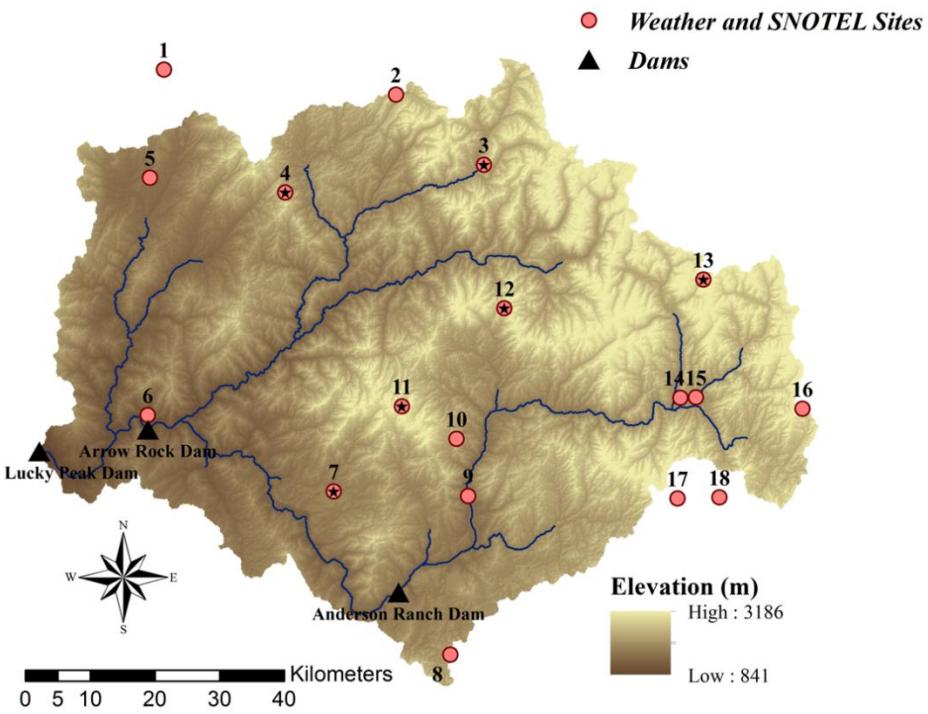

Figure 3.1. Boise River Basin and weather and SNOTEL sites. Black stars indicate SNOTEL sites with SWE measurements, which were used in the evaluation of model performance.

There are 18 weather and SNOTEL stations in or near BRB that measure meteorological variables on hourly basis (Figure 3.1 and Table 3.1). Ten of these stations are operated by Natural Resources Conservation Service (NRCS; SNOTEL sites). The rest of the stations are either operated by Bureau of Land Management (BLM) and U.S. Department of Agriculture (USDA) Forrest Service (FS; 5 stations) or Bureau of Reclamation (BR; 3 stations). Hourly precipitation (p) and temperature (t) are available at all the stations. Relative humidity (rh), solar radiation (sr) and wind (w) are measured at 5, 6 and 9 of these stations, respectively (Table 3.1).

Table 3.1. Detailed information of the stations.

NO.	Station Name	Latitude (Decimal ◦)	Longitude (Decimal ◦)	Elevat-ion (m)	Variables Measured	Operated by
1	Little Anderson	44.09	-115.88	1389	p, t, rh, sr, w	BLM & FS
2	Jackson Peak	44.05	-115.44	2155	p, t, w, SWE	NRCS
3	Graham Guard STA.	43.95	-115.27	1734	p, t, w, SWE	NRCS
4	Mores Creek Summit	43.93	-115.67	1859	p, t, SWE	NRCS
5	Town Creek	43.94	-115.91	1415	p, t, rh, sr, w	BLM & FS
6	Arrowrock Dam	43.61	-115.92	998	p, t	BR
7	Prairie	43.50	-115.57	1463	p, t, SWE	NRCS
8	Camas Creek Divide	43.27	-115.35	1740	p, t, SWE	NRCS
9	South Fork Boise	43.49	-115.31	1286	p, t	BR
10	Wagontown	43.57	-115.33	1881	p, t, rh, sr, w	BLM & FS
11	Trinity Mountain	43.63	-115.44	2368	p, t, SWE	NRCS
12	Atlanta Summit	43.76	-115.24	2310	p, t, sr, w, SWE	NRCS
13	Vienna Mine	43.80	-114.85	2731	p, t, w, SWE	NRCS
14	Fleck Summit	43.62	-114.90	2164	p, t, rh, sr, w	BLM & FS
15	Big Smokey Ranger	43.62	-114.87	1706	p, t	BR
16	Dollarhide Summit	43.60	-114.67	2566	p, t, SWE	NRCS
17	Soldier Mountain Peak	43.48	-114.91	2904	p, t, rh, w	BLM & FS
18	Soldier R.S.	43.48	-114.83	1749	p, t, SWE	NRCS

Variable abbreviations: p, precipitation; t, air temperature; rh, relative humidity; sr, solar radiation; w, wind speed and direction; SWE, snow water equivalent.
Abbreviations for institutes operate the stations: BLM & FS, Bureau of Land Management and U.S. Department of Agriculture (USDA) Forrest Service, respectively; NRCS, Natural Resources Conservation Service; BR, Bureau of reclamation.

3.4. Methodology

3.4.1. Snow Model: iSnobal

Snobal was developed by Marks (1988) to calculate snow accumulation and ablation at a point. Spatial (image) version of Snobal, iSnobal, uses the same set of equations as Snobal to solve mass and energy flux exchanges at each DEM cell (Marks et al. 1999b). Both versions are part of the Image Processing Workbench (IPW) software system developed by Frew (1990) and improved by Marks et al. (1999a). ISnobal has been successfully applied to

simulate snow accumulation and melt distribution over several watersheds such as the Wasatch Range in Utah (Susong et al. 1999), the Emerald Lake basin in California (Marks et al. 1999b), the sub-Arctic and boreal forest (Link and Marks 1999), the Reynolds Creek Experimental Watershed (Chen et al. 2016; Kumar et al. 2013; Kumar et al. 2012; Seyfried et al. 2009; Wang et al. 2016) and the Boise River Basin (Garen and Marks 2005). The model uses a two-layer representation of the snowpack. The top layer has a fixed-thickness of 0.25 mm, while the lower layer's thickness is variable and consists of the remainder of the snowpack. Water exchanges such as evaporation, condensation and sublimation are calculated at the snow-air interface in the top layer. Heat and energy exchanges are computed for both layers at each time step for each grid cell using the energy balance equation (Eq. 3.1), (Garen and Marks 2005; Marks et al. 1999b):

$$\Delta Q = R_n + H + L_v E + G + M \qquad \text{(Eq. 3.1)}$$

where ΔQ (W m^{-2}) indicates changes in the snow cover energy and R_n, H, L_vE, G and M (all units of W m^{-2}) are energies that are added to and/or subtracted from the snow cover energy due to changes in net radiation, sensible and latent heat, conduction and advection, respectively. L_v (W m^{-2} kg^{-1}) and E (kg) represent specific latent heat for water and mass of water that has phase change, respectively. Increase in energy of the snow cover leads to decrease in the cold content. Cold content is the energy required to raise the snow cover temperature to 0 °C. When the cold content reaches 0°C, melt occurs. Melt is calculated in both layers. Notably, melt estimates in the model includes both melt and rain on snow. Once the total liquid water content in snowpack is higher than a specified threshold, water drains out and is terms has surface water input (SWI).

3.4.2. Spatial Distribution of Meteorological Data

ISnobal requires spatially distributed meteorological inputs, which are precipitation, air temperature, vapor pressure, solar and thermal radiation and wind speed. We distributed these

inputs at 50 m spatial resolution and, then, rescaled them to obtain 100 m resolution to reduce modeling costs such as runtime and data storage. Rescaling inputs from 50 to 100 m grid-cell has negligible effects on estimation of snow variables as shown by work of Winstral et al. (2014). Spatially distributed data was obtained by interpolation using detrended elevation (vertical) and distance (horizontal) Kriging method (Garen and Marks 2005). More details about the interpolation methodology for different meteorological variables are described below.

Air temperature-elevation trends were constrained to be zero or negative values, because air temperature decreases with increase in elevation. However, relative humidity-elevation trends were not constrained. The distributed relative humidity and air temperature were then used to compute dew point temperature and vapor pressure, which in turn was used to identify the precipitation phase and calculate latent heat flux exchanges from the snow cover, respectively (Garen and Marks 2005).

Wind speed and direction were distributed using a detrended elevation and distance based Kriging method. Wind speed of a grid cell, then, was adjusted based on a wind factor calculated from two terrain parameters, maximum upwind slope (s_x) and upwind slope break (s_b). Detailed description of the wind distribution approach can be found in the literature (Winstral et al. 2002; Winstral and Marks 2002; Winstral et al. 2009; Winstral et al. 2013), however, here the approach is explained in brief. Values of s_x and s_b were calculated for each cell, and for each wind direction. The s_x values are the maximum slope between the cell of interest and all cells in the upwind direction up to a user defined search distance (d_{max}). At topographically exposed cells, where s_x is negative, wind speed is increased due to vertical flow constriction (Winstral and Marks 2002). In contrast, at topographically sheltered grid cells, where s_x is positive, wind speed is decreased due to expansion of flow (Winstral and Marks 2002). The s_b parameter calculates upwind breaks in slope to identify flow separation zones, where there is no contact between airflow and the ground and downwind lee eddy is formed, which substantially reduces wind speed (Winstral et al. 2013). The value of s_b is the difference between two s_x values, the local s_x minus outlying s_x, which are calculated using two different search distances. Local s_x is calculated using d_{max}, whereas outlying s_x is calculated using a distance quite larger than d_{max}. 100 and 1,000 m were used for local s_x and

outlying s_x d_{max} values, respectively, which were suggested and used in the literature (Winstral et al. 2002; Winstral and Marks 2002; Winstral et al. 2009; Winstral et al. 2013).

Precipitation was distributed analogous to wind speeds. Precipitation was first distributed using a detrended elevation and distance based Kriging method with precipitation-elevation trends that were constrained to be zero or positive, because precipitation increases with elevation (Garen and Marks 2005). Next, at each grid cell, wind-induced snow redistribution was calculated using a snow drift factor that was computed based on s_b and wind speed (Winstral et al. 2002; Winstral et al. 2013; Winstral et al. 2014). Snow erosion occurred at cells where wind speed was high and s_b was negative. The transported snow particles from eroded cells were, then, deposited at cells where wind speed was substantially low, such as cells with large s_b. This precipitation distribution approach has been previously used in several studies (Winstral and Marks 2002; Winstral et al. 2013; Winstral et al. 2014).

Solar radiation was distributed and corrected to account for variations in solar angle, shading, vegetation, and albedo (Link and Marks 1999; Susong et al. 1999). Snow albedo was adjusted with snow age to consider the influence of dust and organic debris exposure (Garen and Marks 2005). Distributed thermal radiation was first calculated for clear sky based on temperature, vapor pressure, elevation and sky view factor. Calculated thermal radiation was then adjusted for cloud cover and vegetation (Link and Marks 1999).

3.4.3. Scenario Design

Three iSnobal scenario simulations were performed using hourly (scenario 1h), 3-hourly (scenario 3h) and 6-hourly (scenario 3h) meteorological inputs. Although, resolution of meteorological inputs are different across the three scenarios, iSnobal uses a one hour simulation time step (Marks et al. 1999b) to perform calculations. The model employs a simple linear interpolation to generate hourly values from inputs with longer than hourly temporal resolution. As at least 6-hourly time step of the inputs is required to capture diurnal variations in meteorological variables (Beniston 1997; Garen and Marks 2005), we did not consider longer than 6-hourly time step in this study. To generate the 3- and 6- hourly inputs, hourly air temperature, vapor pressure, wind speed, solar and thermal radiation were averaged

over 3- and 6-hour windows. However, hourly precipitation was summed to represent total precipitation for a given 3- or 6-hour.

Model runs were conducted for entire water years (wy), which start on October of the previous year and end in September of the current year. Each scenario was run for a wet (wy2006; top 20 percentile, 359mm), average (wy2010; 325mm), and dry year (wy2007; bottom 10 percentile,209mm) to identify the impact of forcing's time step on snow modeling for different climatic conditions (Sohrabi et al. 2015). These years were identified based on a 60 year data set (1950-2010) at the Boise Airport station.

3.4.4. Model Performance Evaluation and Analyses

The results were analyzed: 1) at point scale where observed and estimated snow water equivalent (SWE) from the three scenarios were compared; and 2) in a spatially distributed fashion by comparing SCA and SWE from 3h and 6h scenarios within four elevation bands.

Point scale comparisons of SWE were performed at six out of the ten SNOTEL sites located inside BRB: Prairie, Graham Guard, Mores Creek Summit, Atlanta Summit, Trinity Mountain and Vienna Mine (Figure). Performance of the model was quantified using Nash-Sutcliffe coefficient (NSC; (Eq. 3.2)) and the ratio of root mean square error (RMSE) and standard deviation ratio (RSR; (Eq. 3.3)). Goodness of fit and error between SWE_{1h}, estimated SWE generated from scenario 1h, and observed SWE was quantified using NSC and RSR, respectively. This assumes that simulation based on finest resolution data set i.e., the SWE_{1h} scenario, does a best job of representing the snow physics and is expected to result in the best model performance. We adopted a model performance scheme proposed by Moriasi et al. (2007), which classifies model performance into four categories based on NSC and RSR values. These model performance categories are very good ($NSC > 0.75$ and $RSR \leq 0.5$), good ($0.65 < NSC \leq 0.75$ and $0.5 < RSR \leq 0.6$), satisfactory ($0.5 < NSC \leq 0.65$ and $0.6 < RSR \leq 0.7$) and unsatisfactory ($NSC \leq 0.5$ and $RSR > 0.7$).

$$NSC = 1 - \left[\frac{\sum_{i=1}^{n} (SWE_{1h,i} - SWE_{obs,i})^2}{\sum_{i=1}^{n} (SWE_{obs,i} - \overline{SWE_{obs}})^2} \right] \quad \text{(Eq. 3.2)}$$

$$RSR = \frac{\sqrt{\sum_{i=1}^{n} (SWE_{1h,i} - SWE_{obs,i})^2 \Big/ n}}{STD_{obs}} \quad \text{(Eq. 3.3)}$$

where $SWE_{obs,i}$, $\overline{SWE_{obs}}$, STD_{obs} and n are observed SWE at time i, the mean and standard deviation of observations and number of observations, respectively.

Daily time series of SCA and SWE generated from the three scenarios were analyzed by classifying the simulated data into four elevation bands (Table 3.2). The rain-snow transition band (E2) is an elevation band in which precipitation generally falls either as rain or snow based on changes in dew point temperature (Marks et al. 2013). E2 is typically located from 1,500 to 1,800 m in the Pacific Northwestern of the USA (Kormos et al. 2014a; Kormos et al. 2014b). Here, E2 was set from 1,400 to 1,900 m. Bands below and above E2 are rain dominated (E1) and snow dominated (E3) bands, respectively. Snow dominated region above the treeline (E4) indicates elevation ranges where trees are not able to grow due to low temperatures and long snow cover durations. E4 is located above 2,400 m based on BRB latitude (Korner 1998). Simulated SWE was spatially averaged over each elevation band. SCA represents the percent of area covered with snow and was calculated for each band by summing the area of all cells with SWE greater than 0 and then dividing the aggregated area by the total area of each elevation band. Daily time series of spatially averaged SWE and aggregated SCA simulated from 3h and 6h scenarios for the wet, average and dry years were compared to those of scenario 1h. The spatially averaged snow water equivalent ($\overline{SWE}_{i,j}(t)$) and aggregated snow cover area ($SCA_{i,j}(t)$) for the i-th elevation band (E1, E2, E3 and E4) with area, A_i, and the j-th scenario (1h, 3h, 6h) are calculated as follows:

$$\overline{SWE}_{i,j}(t) = \frac{1}{A_i}\int_0^{A_i} SWE_{i,j}(t,a)\,da \quad with\ i = E1\ to\ E4\ and\ \ j = 1h, 3h, 6h \tag{Eq. 3.4}$$

$$SCA_{i,j}(t) = \frac{100}{A_i}\int_0^{A_i} SC_{i,j}(t,a)\,da \quad and \quad \begin{cases} SC_{i,j}(t,a) = 1 & SWE_{i,j}(t,a) > 0 \\ SC_{i,j}(t,a) = 0 & SWE_{i,j}(i,x) = 0 \end{cases} \tag{Eq. 3.5}$$

where $SWE_{i,j}(t,a)$ and $SC_{i,j}(t,a)$ are the snow water equivalent and snow cover index, respectively, for a cell of area a (100 m by 100 m) at time t. The spatially averaged residual or mean error of SWE is calculated as:

$$\mathrm{Res}_{i,j}(t) = \overline{SWE}_{i,j}(t) - \overline{SWE}_{i,1h}(t) \qquad with\ i = E1 - E4\ and\ \ j = 3h, 6h \tag{Eq. 3.6}$$

Table 3.2. Elevation Bands

Bands	***Elevation (m)***	***Description***	***% of Grid Cells***
E1	≤ 1400	Rain Dominated	16
E2	> 1400 and ≤ 1900	Rain-Snow Transition	44
E3	> 1900 and ≤ 2400	Snow Dominated	28
E4	> 2400	Alpine Treeline	12

To present residuals in SWE in percentage, the residuals were divided by the mean of the estimated SWE from the 50 m (d) for a given snow season. Results were quantified using mean absolute error (MAE). A large value of MAE indicates deviation of estimated snow variables generated from scenarios 2 and 3 from those of scenario 1. MAE is calculated as follows (Moriasi et al. 2007):

$$MAE_{i,j} = \frac{1}{T}\int^{T} \left| SV_{i,1h}(t) - SV_{i,j}(t) \right| dt \quad with\ i = E1 - E4\ and\ j = 3h, 6h \tag{Eq. 3.7}$$

where snow variable, $SV_{i,j}$, stands for $\overline{SWE}_{i,j}(t)$ and $SCA_{i,j}(t)$ for the *j*-th scenario and *T* represents the simulation period. MAE was computed for the entire snow season (total MAE), accumulation (Rising Limb; RL) and ablation (Falling Limb; FL) periods at each elevation band. RL starts as snow accumulation begins and ends when SWE reaches its maximum, FL starts after maximum SWE occurs and continues to the time snow disappears.

3.5. Results and Discussion

3.5.1. Model performance as Compared to Observed SWE

Simulated SWE_{1h} captures the measured SWE time series reasonably well with average NSC of 0.83 and RSR of 0.36, excluding the Prairie site (Table 3.3 and Figure 3.2). NSC of modeled SWE_{1h} at Prairie was 0.64/ 0.44/ 0.14, while the RSR was 0.59/ 0.78/ 0.79 for wet, average and dry years, respectively. Notably, the dry year exhibited low NSC and large RSR errors. At all the sites, the best model performance was observed in the wet year with averaged NSC of 0.88 and RSR of 0.29 over all the sites. Vienna Mine had the highest NSC (0.99) and lowest RSR (0.07) in the wet year. Model performance decreased substantially in the dry year with averaged NSC of 0.64 and RSR of 0.53 over all the sites. Excluding Paririe, the lowest NSC (0.54) and highest RSR (0.68) were observed at Trinity Mountain. Over the three years, the best model performance was observed at Mores Creek Summit with average NSC of 0.95 and RSR of 0.22. Snow accumulation started at the same time for both simulated and observed SWE regardless of the year, but melt-out date was estimated later or earlier due to overestimation or underestimation of SWE, respectively. SWE_{1h} and SWE_{3h} were very similar (Figure 3.2). However, in terms of magnitude, SWE_{6h} was generally smaller than SWE_{1h} at sites located in E2, such as Prairie, Graham Guard and Mores Creek Summit. In particular, in the wet and average years at Prairie site, scenario 6h did not estimate any snow accumulation, although scenario 1h and 3h registered accumulation. At sites, which were

located in E3 and E4, SWE_{6h} was generally larger and snow melt rate was smaller than that of SWE_{1h}.

Comparison between measured and predicted SWE was at par to previous studies (Marks et al. 1999b; Sultana et al. 2014). However, model performance at the Prairie site was ranked unsatisfactory. This station is at the lowest elevation and lies at the lower fringe of the snow transition zone. For instance, Sultana et al. (2014) reported unsatisfactory model performance with very low NSC (ranged from 0.1 to 0.9) and high RSR (ranged from 0.28 to 0.86).

Table 3.3. Calculated values of NSC and RSR at SNOTEL sites.

	NSC			RSR		
SNOTEL Sites	Wet	Average	Dry	Wet	Average	Dry
Prairie	0.64	0.44	0.14	0.59	0.78	0.79
Graham Guard	0.88	0.72	0.78	0.34	0.52	0.46
Mores Creek Summit	0.98	0.91	0.96	0.14	0.30	0.21
Atlanta Summit	0.85	0.55	0.79	0.39	0.67	0.46
Trinity Mountain	0.96	0.96	0.54	0.19	0.19	0.68
Vienna Mine	0.99	0.97	0.65	0.07	0.18	0.59

Mismatch between estimated and observed SWE is due to the following reasons. Observed SWE at SNOTEL sites are point measurements represent SWE for an area of approximately 7 m^2, whereas simulated SWE quantifies average of SWE over 10,000 m^2. Influence of topographic features on snow drifting and energy exchanges get modified with spatial scale (Luce et al. 1998; Luce et al. 1999; Winstral et al. 2014), thus influencing SWE estimates. Moreover, snow pillows are located in a flat area whereas relatively larger model grid cells have slope and aspect (Raleigh and Lundquist 2012), resulting in discrepancies that are common between simulated and measured SWE (Grünewald and Lehning 2011; Lee et al. 2005; Molotch and Bales 2005).

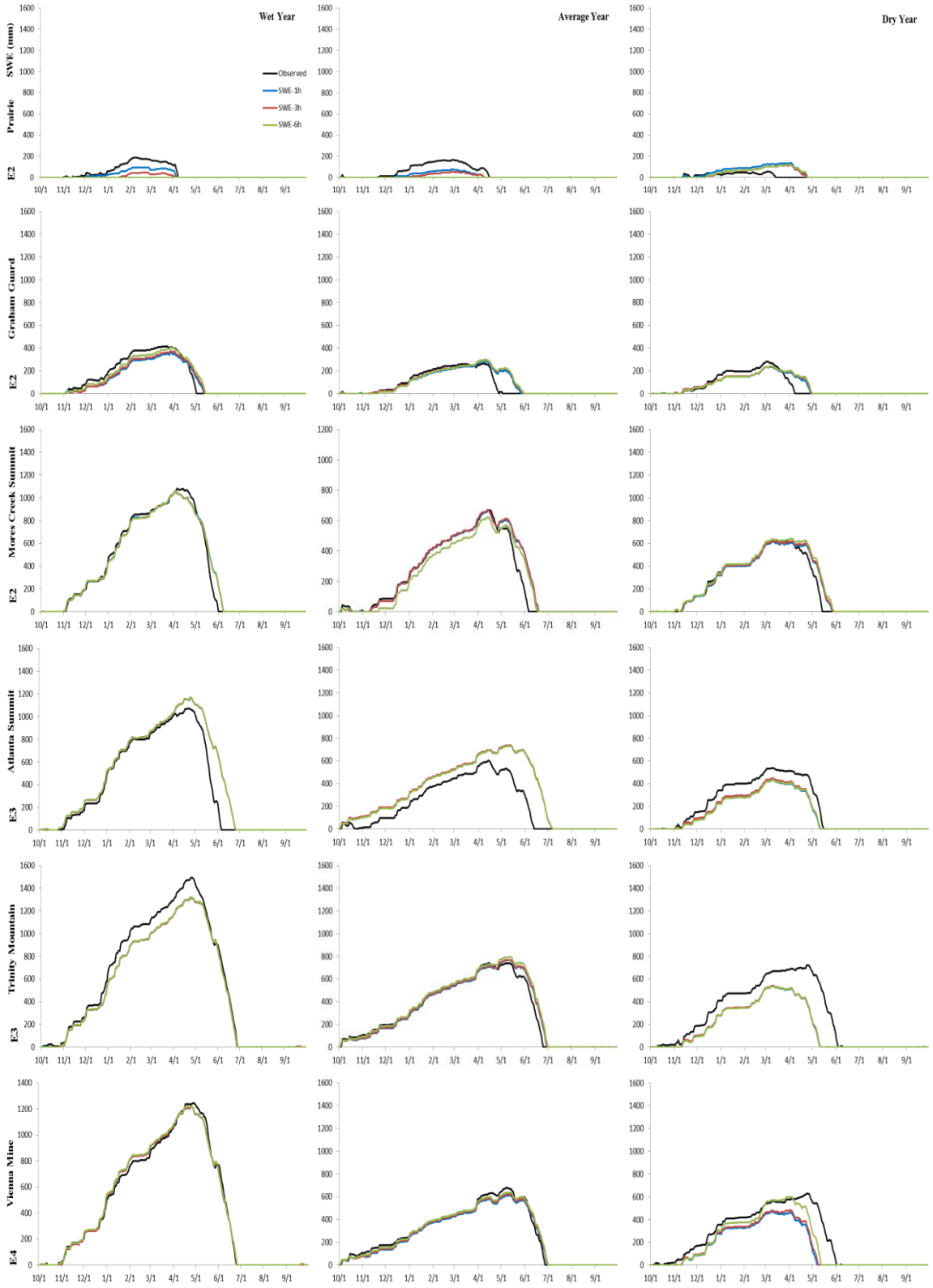

Figure 3.2. Comparison between simulated and observed SWE at Prairie, Graham Guard, Mores Creek Summit, Atlanta Summit, Trinity Mountain and Vienna Mine. Note that the SNOTEL sites were ordered from low (Prairie) to high (Vienna) elevation. SWE-1h indicates estimated SWE using hourly inputs.

3.5.2. Temporal Resolution Effects on Snow State

3.5.2.1. Snow Cover Area (SCA)

MAE_{6h} was considerably larger than MAE_{3h} in all the years and elevation bands. Total MAE_{3h} did not exceed 19.8%, whereas total MAE_{6h} was as high as 24.5% (Table 3.4). MAE_{3h} and MAE_{6h} for FL were less pronounced than those for RL. Meteorological inputs with temporal resolution longer than an hour led to underestimation of SCA during the snow accumulation (RL) period (Figure 3.3). The largest underestimation was observed for the coarsest input. Use of 3h and 6h inputs resulted in slow melting of snow during the snow ablation period (FL). The change in melt rate with regard to hourly inputs was larger for SCA_{6h} than for SCA_{3h}. Model results based on coarser resolution inputs missed rapid increases in SCA. For instance, SCA_{1h} increased by 11% (from 60% to 71%) on December 2nd in the wet year in E1, whereas estimated SCA from scenarios 3h and 6h did not change at all (Figure 3.3).

The underestimation of SCA in RL was large in rain dominated (E1) and rain-snow transition (E2) bands, but negligible at the snow dominated elevation bands (E3 and E4). However, the change in snow melt rate in FL was larger in E3 and E4 than in E1 and E2. Differences between SCA_{1h}, SCA_{3h} and SCA_{6h} were less pronounced in E3 and E4 than in E1 and E2 (Table 3.4). MAE_{3h} and MAE_{6h} in RL generally decreased from E1 to E4. In contrast, MAE_{3h} and MAE_{6h} in FL increased from E1 to E4. The dry year had the largest total MAE_{3h} (19.8%) and MAE_{6h} (24.5%). In addition, the largest MAE_{3h} (28.2%) and MAE_{6h} (34.5%) for RL were related to the dry year. MAE_{3h} and MAE_{6h} in E1 were substantially larger in the wet year than those of in the average year.

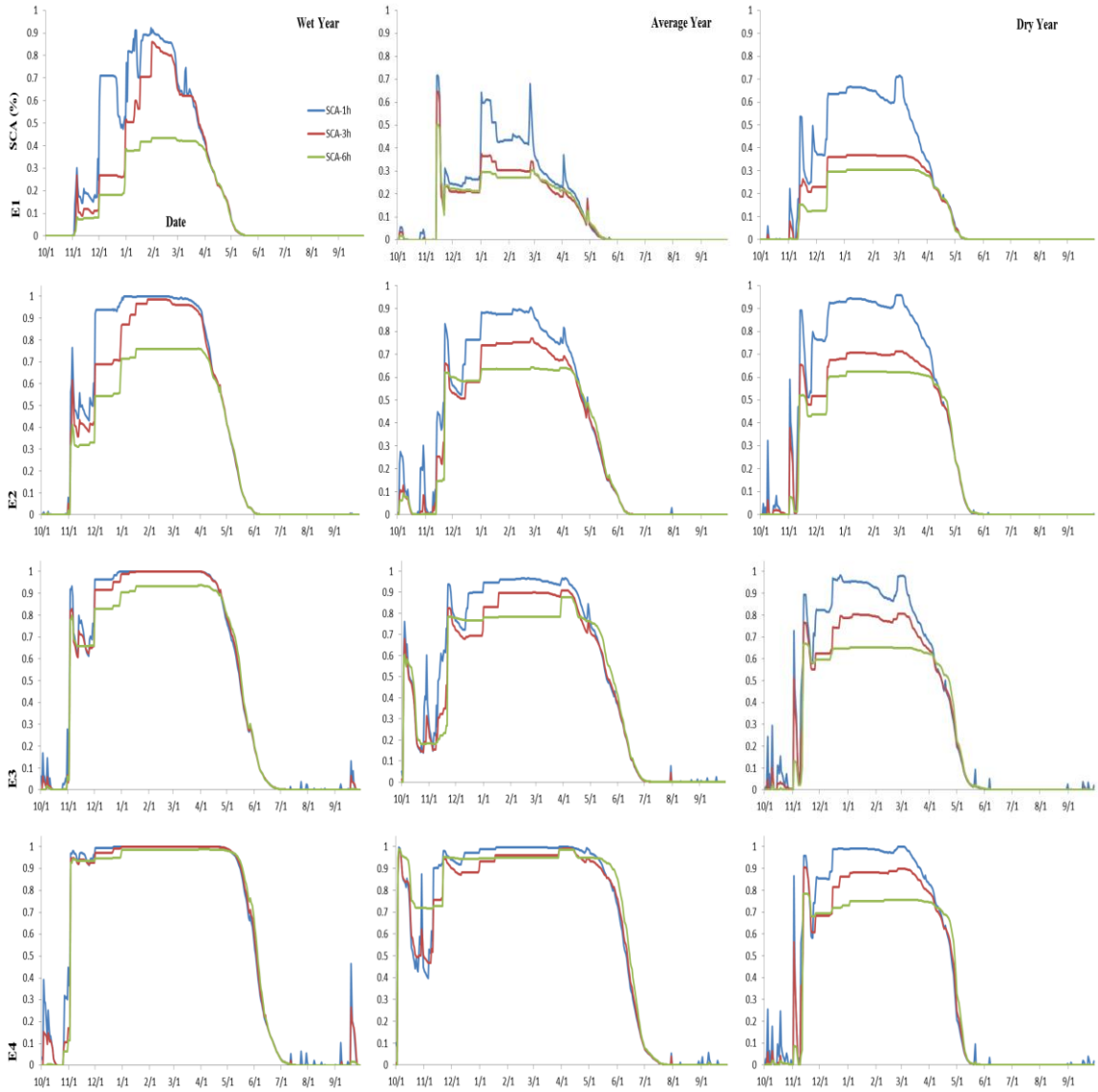

Figure 3.3. Aggregated SCA from 1h, 3h and 6h scenarios (SCA-1h, SCA-3h and SCA-6h) over 4 elevation bands.

Table 3.4. MAE_{3h} and MAE_{6h} for SCA (%) at each band.

	MAE_{3h} (Wet | Average | Dry)				MAE_{6h} (Wet | Average | Dry)			
	E1	E2	E3	E4	E1	E2	E3	E4
RL	16 | 11 | 28	9 | 12 | 21	2 | 9 | 14	2 | 5 | 10	33 | 13 | 34	26| 19 | 30	8 | 14 | 25	4 | 7 | 19
FL	1 | 3 | 7	1 | 2 | 8	1 | 2 | 3	1 | 2 | 3	2 | 2 | 9	4 | 4 | 11	3 | 4 | 7	3 | 5 | 10
Total	11 | 7 |20	7 | 9 | 16	2 | 7 | 10	2 | 4 | 8	24 | 8 | 24	20 | 15 | 23	7 | 11 | 19	4 | 7 | 16

3.5.2.2. Snow Water Equivalent (SWE)

Deviation of SWE_{3h} from SWE_{1h} was much smaller than between SWE_{1h} and SWE_{6h} in all the years and elevation bands (Figure 3.4 and Table 3.5). The 6h simulation indicated average residual and MAE of 11.1% and 9.7 mm, respectively, whereas the 3h simulation showed average residual and MAE of 6.9% and 5.2 mm, respectively, over all the years and elevation bands. Residuals and total MAE generally decreased with increasing elevation with average residual of 13.9%, 6.8%, 4.1% and 2.7% for the 3h simulation and 20.3%, 10.5%, 6% and 7.4% for the 6h simulation from E1 to E4, respectively, over all the years. For the entire snow season, residuals were negative in E1 but positive in E4. However, residuals were negative during the winter but positive in the spring in E2 and E3. Positive (negative) errors indicate that SWE_{1h} is smaller (larger) than SWE_{3h} or SWE_{6h}. Residuals decreased from E1 to E4 during RL, but they increased during FL. Residuals and MAE generally increased toward years with lower snow mass, from the wet year to the dry year. The wet, average and dry years indicated average residual of 3.2%, 7.6% and 9.8% for the 3h simulation and 8.4%, 9.4% and 15.3% for the 6h simulation over all the elevation bands, respectively. Notably, the average year had larger residuals than the dry year for the 6h simulation in E4.

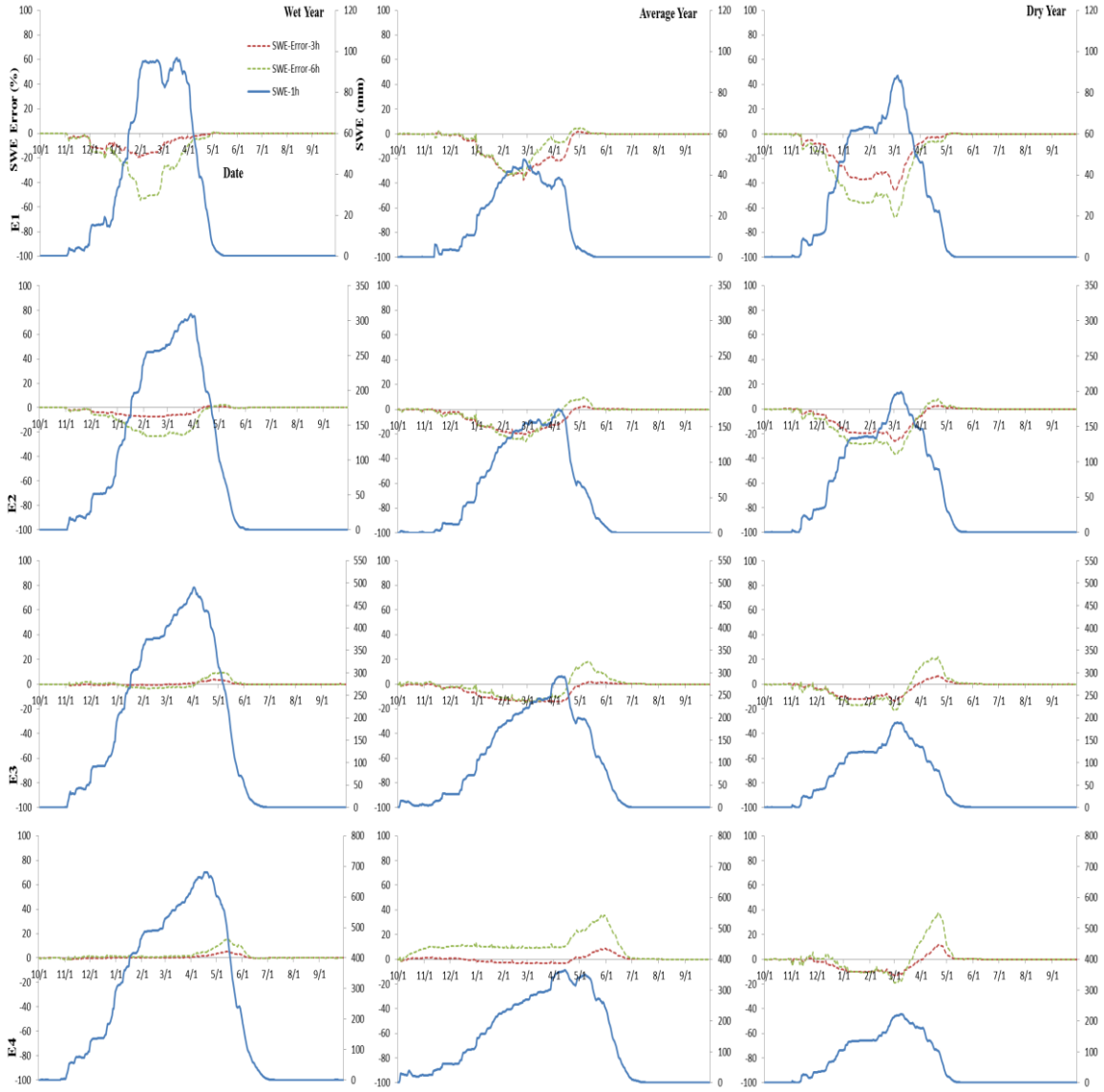

Figure 3.4. Spatially averaged SWE over 4 elevation bands. SWE-1h indicates estimated SWE using hourly inputs. SWE-Error-3h and SWE-Error-6h indicate the percent of the residuals in the estimated SWE using 3-hourly and 6-hourly inputs, respectively.

Table 3.5. MAE_{3h} and MAE_{6h} for SWE (mm) at each band.

	MAE_{3h} (Wet | Average | Dry)				MAE_{6h} (Wet | Average | Dry)			
	E1	E2	E3	E4	E1	E2	E3	E4
RL	5 | 3 | 13	7 | 8 | 11	1 | 9 | 6	1 | 3 | 5	11 | 3 | 21	17 | 9 | 16	4 | 7 | 8	3 | 15 | 5
FL	1 | 3 | 5	1 | 2 | 6	3 | 3 | 3	6 | 5 | 5	3 | 1 | 8	3 | 3 | 9	8 | 10 | 8	18 | 30 | 14
Total	3 | 3 | 10	5 | 7 | 9	2 | 7 | 5	2 | 4 | 5	8 | 2 | 16	13 | 7 | 14	5 | 8 | 8	8 | 20 | 8

3.5.2.3. Explanations for the differences in estimated SCA and SWE with temporal resolution of meteorological inputs

One of reasons for differences in estimates of SCA and SWE from the 1h, 3h and 6h scenarios was mischaracterization of precipitation phase, particularly in the early snow season (Figure 3.5). Coarser resolution inputs did not capture the hourly changes in dew point temperatures and precipitation, causing misidentification of precipitation phase in all the elevation bands. Notably, the mischaracterization of precipitation phase in E1 to E3 was very different than that observed in E4. In E1 to E3, several events that were characterized as snowfall in 1h scenario were misidentified as a rainfall or a mixed rain/snow event in the 6h scenario. In contrast, many events that were identified as mixed rain/snow or a rainfall in the 1h scenario in E4 were misidentified as snowfall in the 6h scenario. To explore the reasons of these mischaracterizations in precipitation phase, one grid cell each in E2, hereafter E2-cell, and E4, hereafter E4-cell, were selected for further analyses.

At the E2-cell, differences between the 1h simulation and those of the 3h and 6h were very small from October 1st until November 10th, 2009. During this period, dew point temperatures were far above the freezing point that neglecting hourly changes in dew point temperatures did not lead to misidentification of the precipitation phase. The pronounced difference between the 1h, 3h and 6h simulations started on November 10th, when the snow cover formed for the 1h and 3h simulations but all the precipitation turned into SWI in the 6h simulation. On this day, all the precipitation that occurred before noon was identified as snowfall in all the scenarios (Figure 3.5 a and b; see Marks et al. (2013) for detailed information about estimation of precipitation phase based on dew point temperature). At noon, the 1h scenario precipitation was identified as snow, but was identified as a mixed rain/snow event in the 3h and 6h scenarios. The rest of the precipitation on this day was estimated as a mixed rain/snow event that mainly consisted of 25% rain and 75% snow in 1h and 3h scenarios and 75% rain and 25% snow in the 6h scenario. As a result, SWI of 7, 7.4 and 20.9 mm was estimated in the 1h, 3h and 6h scenarios, respectively. Discrepancies in identification of precipitation phase affected snow cover accumulation start date. For example, on this day, the snow cover was formed in the 1h and 3h scenarios, but accumulation started 11 days later at the E2-cell in the 6h scenario. As a result, snow mass

and the timing of the snow cover formation were impacted by misidentification of precipitation phase. At E4-cell, estimation of snow mass was affected more than the timing of the snow cover formation due to the misidentification of precipitation phase. At this cell, the snow cover accumulation started on October 3rd, 2009 in all the three scenarios. A pronounced difference between the three scenarios was observed starting November 2nd, 2009, the day on which all precipitation was identified as snowfall in the 3h and 6h scenarios, but was identified as a mixed rain/snow event with 75% rain and 25% snow in the 1h scenario. On this day 0.9 mm out of 3.6 mm precipitation was estimated as snow and the rest was estimated as rain in 1h scenario. In addition, estimated precipitation temperature and density of snow for scenario the 1h and 6h were substantially different due to differences in dew point temperatures at the time of precipitation. As a result, snow ablation occurred in 1h scenario, while it accumulated in the 6h scenario.

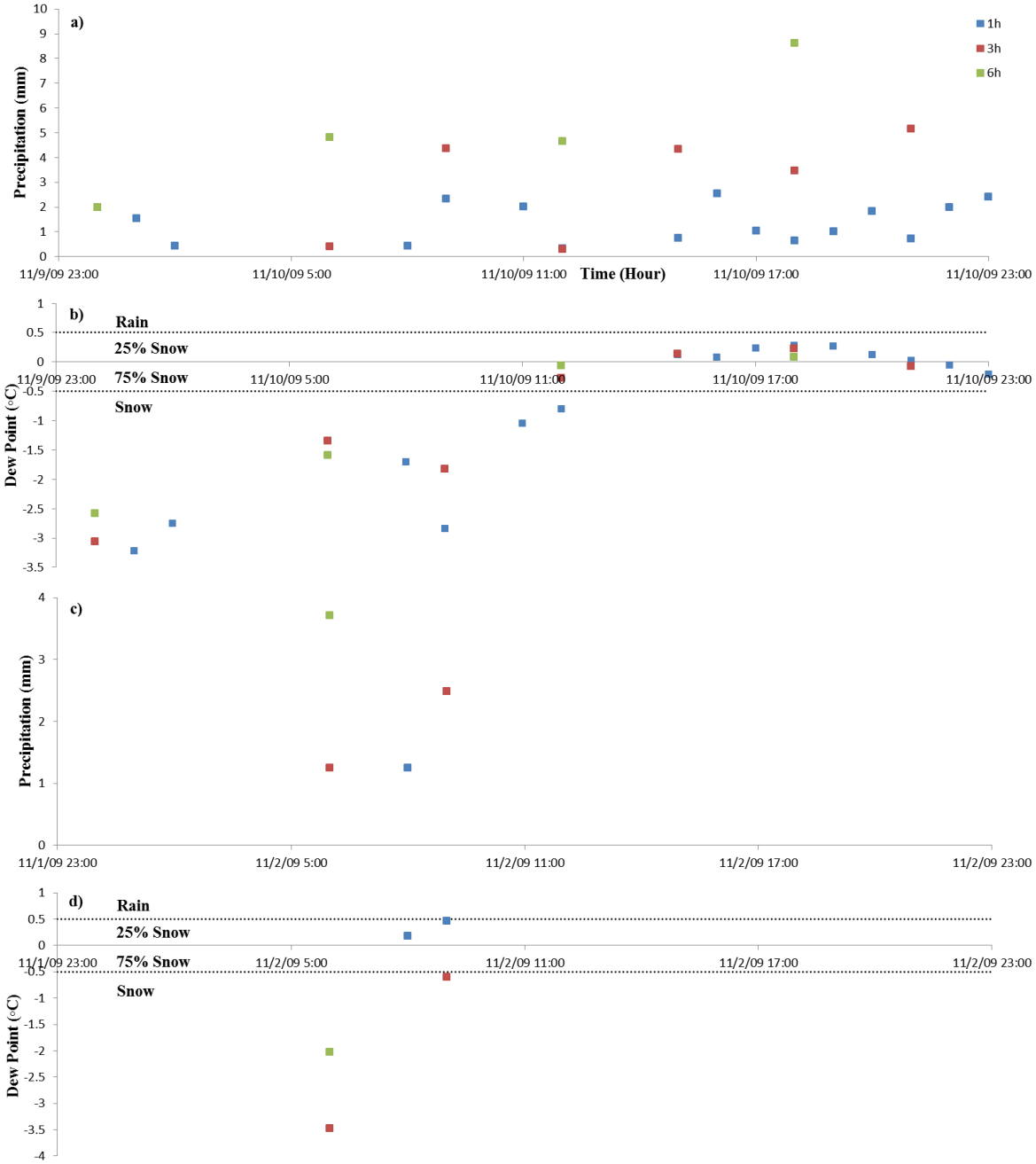

Figure 3.5. Mischaracterization of precipitation phase due to the use of coarser than hourly precipitation and dew point temperature data. Figures (a) and (b) indicate precipitation and dew point temperatures, respectively, at E2-cell. Figures (c) and (d) show precipitation and dew point temperatures, respectively, at E4-cell. Figures (b) and (d) indicate dew point temperatures at hours that precipitation occurred.

Another reason for the observed differences in SCA and SWE estimates between the three scenarios is net snow cover energy input (ΔQ). Coarser resolution of meteorological inputs generally resulted in underestimation of ΔQ. The 3h and 6h scenarios fail to capture the large

magnitudes of energy fluxes, particularly on sunny days (e.g., November 23rd, 2009) when hourly variation of solar radiation and air temperature is pronounced (Figure 3.6). For instance, at noon on this day, solar net radiation was 30 and 50 W/m^2 for the 1h scenario and was 8 and 20 W/m^2 for the 6h scenario at E2-cell and E4-cell, respectively. As a result, net radiation in the 6h scenario was estimated to be lower by 2.7 and 1.2 W/m^2 than in the 1h scenario at E2-cell and E4-cell, respectively. Turbulent energy was also underestimated for the 3h and 6h scenarios. The degree of this underestimation was related to the moderated variations in the magnitude of air temperature, vapor pressure and wind speed due to coarser than hourly inputs. For example, air temperature was well above freezing point for a few hours on November 23rd, 2009, whereas 6-hourly air temperature did not exceed 0.5 and 0 °C at E2-cell and E4-cell, respectively. For vapor pressure, not only the diurnal range narrowed, but the timing of its maximum also shifted. Diurnal range of wind speed also shortened, particularly at the E2-cell where wind speed had high variation during the day. Due to these changes, turbulent energy of the 6h scenario was estimated to be lower by 3.8 and 0.6 W/m^2 than in the 1h scenario at E2-cell and E4-cell, respectively.

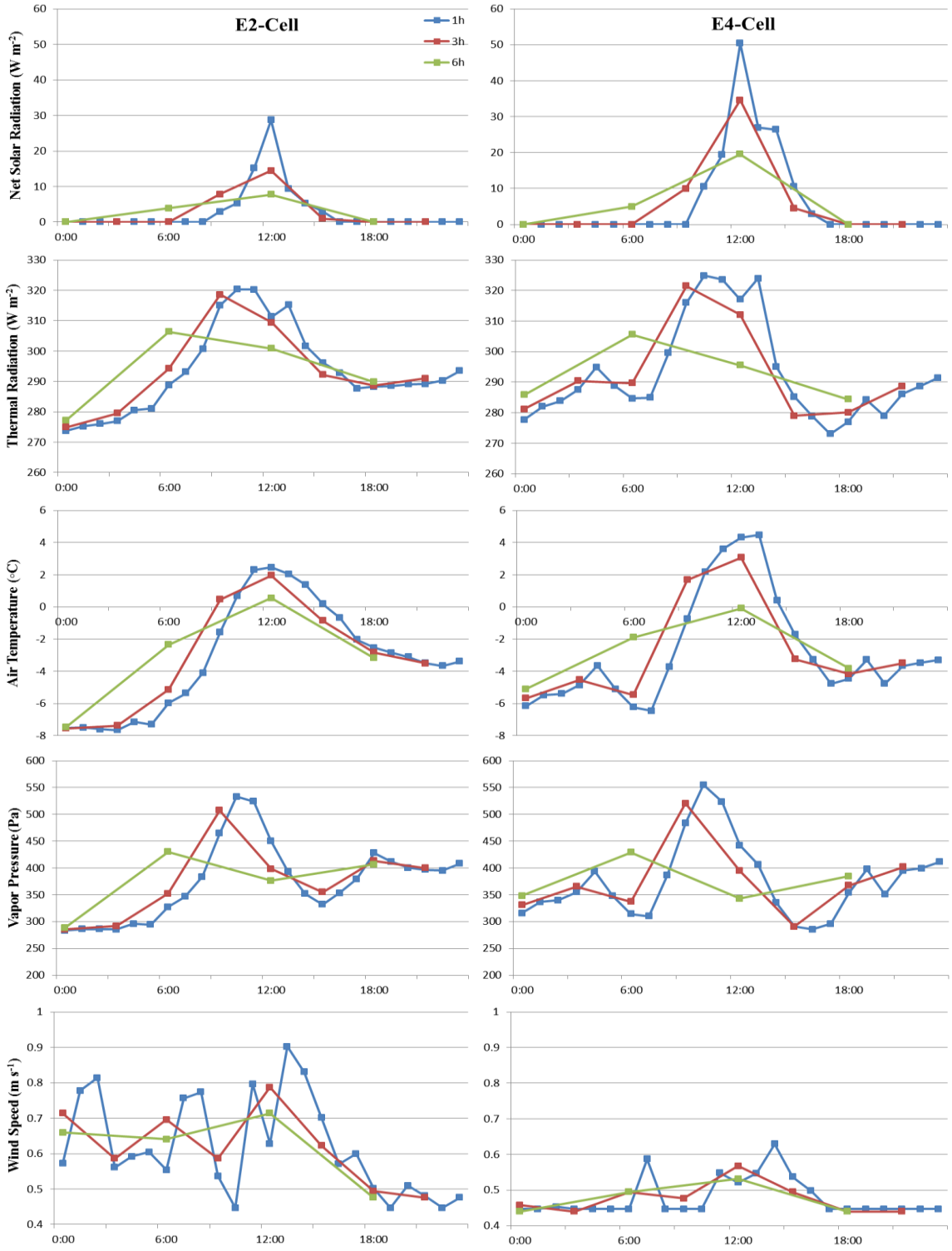

Figure 3.6. Changes in energy flux input due to coarse temporal resolution of inputs on a sunny day (November 23rd, 2009). The left column is for a grid cell located in E2 band, E2-cell, and the right column belongs to a grid cell located in E4 band, E4-cell.

The results indicate that MAE_{3h} and MAE_{6h} of SCA decreased during RL from E1 to E4. This was due to misidentification of several snowfall events as rain or mixed snow/rain events. The phase of precipitation is strongly dependent on dew point temperature (Hock and Holmgren 2005; Marks et al. 2013). In E1 and E2, if hourly dew point temperatures fluctuated around the freezing point during the snow accumulation (RL) period, coarser temporal resolutions missed dew point temperatures that were below the freezing point, particularly in the 6h scenario. In contrast, dew point temperatures were much below the freezing point during most of the snow season in snow dominated bands, particularly E4. As a result, temporal resolution of inputs had a small effect on the timing of snow cover formation (Morán-Tejeda et al. 2013). Coarser temporal resolutions also caused underestimation of snow melt rate (overestimation of SCA) during snow ablation period (FL), particularly in E3 and E4, as high diurnal values of the energy fluxes were considerably moderated. In particular, net radiation and turbulent energy, which are the main driver for snow ablation (Hock and Holmgren 2005; Mazurkiewicz et al. 2008), were underestimated.

Negative residuals of SWE were observed during RL in E1 to E3 and occasionally in E4, indicating underestimation of SWE generated from the 3h and 6h scenarios in comparison to that in 1h scenario. This was again due to limitation of the 3h and 6h scenarios to estimate the correct precipitation phase. Identification of a precipitation event as rainfall instead of snowfall resulted in underestimation of SWE, because of: (a) underestimation of snow mass; and (b) incorrect identification and/or overestimation of the magnitude of rain-on-snow events, which can contribute to snow ablation (Marks et al. 1998; Mazurkiewicz et al. 2008). The magnitude of these negative residuals decreased as elevation increased from E1 to E4. In E3 and E4, because of low air temperatures, misidentification of snowfall as rainfall or mixed/snow rain occurred seldom. Positive residuals of SWE were observed during RL in E4, because diurnal dew point temperatures exceeding 0 °C for a few hours in a day, particularly in the early snow seasons, were not captured due to averaging in coarser inputs. In addition, lower magnitudes of peak diurnal dew point temperatures caused underestimation of precipitation temperature and snow density. As a result, the estimated SWE in the 3h and 6h simulations was larger than that in the 1h simulation.

Positive residuals of SWE were also observed during FL in E1 to E4, indicating underestimation of snow ablation rate. As stated earlier, this was due to moderation of diurnal variations in energy fluxes. Radiation on sunny days (Elder et al. 1991; Keller et al. 2005) and turbulent energy on warm and cloudy days (Pohl and Marsh 2006) are mainly responsible for snow ablation. Therefore, reduction in the maximum diurnal magnitude of radiation and turbulent energy in coarser meteorological inputs led to underestimation of the snow cover energy and consequently snow ablation rate. The magnitude of these positive residuals increased from E1 to E4 because of increase in elevation and reduction in trees density. Higher elevations with a very sparse tree distribution, as in E4 (above treeline), have substantially large incoming short-wave during daytime, outgoing long-wave during nighttime and diurnal variation of wind speed (Aguado and Burt 2013; Pohl et al. 2006; Rohli and Vega 2008; Winstral et al. 2013), which result in substantial diurnal variation of energy fluxes. Another reason that caused large positive residuals of SWE during FL in E4 was the overestimation of SWE during RL.

Among the three selected years, the greatest residuals in the estimated SCA and SWE were observed in the dry year (Figure 3.3 and Figure 3.4). In this year, the number of precipitation events was substantially lower than in the wet and the average years. Thus, precipitation misidentification as rainfall instead of snowfall for the coarser input scenarios substantially impacted the estimated snow mass, timing of the snow cover formation and number of grid cells with accumulated snow. Large residuals in SWE were also observed in the average year in E4. This was because: (a) hourly variation of energy fluxes was larger in this year than the wet year due to lower humidity and fewer cloudy days (Aguado and Burt 2013; Rohli and Vega 2008); and (b) number of precipitation events that led to positive residuals of SWE due to misidentification of precipitation phase was substantially larger than in the dry year.

Further confidence in the results could be obtained by implementing the model in other snow dominated settings and by using different process-based models. It is to be noted that this work quantifies model errors vis-à-vis temporal resolution of inputs, but only for the case when all meteorological inputs have identical resolution. The work does not address the sensitivity of model results to temporal resolution of any individual meteorological variable. Before translating the results from this study to other regions the following points should be

taken into account. The elevation bands that indirectly define precipitation regimes in this work may be different in other regions depending on the latitude and regional climatology (Kormos et al. 2014b; Korner 1998). The results presented here were based on aggregation (of precipitation) and averaging (of other meterological inputs) of hourly data. This methodology may transfer additional statistical information to coarser meteorological inputs, which may not be inherent in a data set observed at coarse time steps. Also, in vicinity of large body of water, which may influence, diurnal meteorological variations and energetics (Aguado and Burt 2013; Rohli and Vega 2008), variation of model errors with input resolution and elevation may exhibit alternate relations.

3.6. Summary and Conclusions

This work explores how estimates of snow accumulation and ablation from a process-based snow model are affected by resolution of meteorological inputs. The results revealed that coarser than hourly temporal resolution may significantly affect the accuracy of simulated snow variables. Using longer than hourly time steps of meteorological inputs may lead to inaccurate estimation of mass i.e. precipitation amount that is in form of rain or snow, and energy input to the snowpack. In particular, in rain dominated and rain-snow transition elevation bands, precipitation phase is likely to be estimated as rainfall instead of snowfall, when longer than hourly inputs are used. As a result, rain-on-snow events are identified incorrectly or the magnitude of these events is overestimated. This model inaccuracy is reflected in substantial underestimation of SCA and SWE in rain-dominated and rain-snow transition bands (Table 3.6). The model accuracy is less dependent on the inputs temporal resolution during accumulation period in snow-dominated bands, both below and above the treeline, because precipitation phase is characterization of less concern. In these elevation bands, using coarse temporal resolution of inputs causes underestimation of the melt rate during ablation period due to neglecting diurnal hourly variation of energy fluxes. Estimation of SCA and SWE is considerably impacted at coarser resolutions in dry years because of large sensitivity to misidentification of precipitation phase, given that number of precipitation events is relatively low. In contrast, SCA and SWE estimations in wet years are less

dependent on the temporal resolution of inputs, due to a less pronounced diurnal variation of energy fluxes and dew point temperatures.

Table 3.6. The effect of inputs time steps on the model accuracy.

SCA	Wet	Average	Dry	SWE	Wet	Average	Dry
E1 (3h|6h)	++ | ++	++ | ++	++ | ++	E1 (3h|6h)	++ | ++	++ | ++	++ | ++
E2 (3h|6h)	++ | ++	++ | ++	++ | ++	E2 (3h|6h)	++ | ++	+ | ++	++ | ++
E3 (3h|6h)	+ | +	+ | ++	++ | ++	E3 (3h|6h)	+ | +	+ | +	+ | +
E4 (3h|6h)	+ | +	+ | +	+ | ++	E4 (3h|6h)	+ | +	+ | ++	+ | ++

"+" indicates less than 10% average residuals due to the use of longer than hourly of the inputs.
"++" indicates more than 10% average residuals due to the use of longer than hourly of inputs.

The results lead us to the conclusion that it is necessary to observe meteorological variables at an hourly basis to conduct process-based snow accumulation and melt simulations and related hydrological and ecological studies. While the results showed that 6-hourly meteorological inputs substantially reduced the model accuracy, temporal resolution of 3-hour resolution may provide very similar estimates of SCA and SWE as that from the 1-hr scenario at snow dominated elevations, both below and above alpine treeline.

This work will benefit agencies that are responsible for generating meteorological data sets. The results could be used as a guide to decide on optimal observation/reanalysis time steps in different settings. These results will inform modelers of the errors in their simulations because of the temporal resolution of their inputs, and how the errors may vary depending on elevation ranges and wet/dry years. Since the errors change with precipitation regimes, the analyses suggests that model errors based on a given resolution might vary temporally, and should be appropriately tracked while performing climate change impact simulations in snow dominated regions.

3.7. References

Aguado, E., and Burt, J. E. (2013). Understanding Weather and Climate, Pearson.

Beniston, M. (1997). "Variation of snow depth and duration in the Swiss Alps over the last 50 years: Links to changes in large-scale climatic forcing." Climate Change, 36, 281–300.

Beniston, M. (2012). "Is snow in the Alps receding or disappearing?" WIREs Climate Change (Wiley Interdisciplinary Reviews / Climate Change), DOI:10.1002/wcc.179.

Darmody, R. G., Thorn, C. E., Shlyter, P., and Dixon, J. C. (2004). "Relationship of vegetation distribution to soil properties in Karkevagge, swedish lapland." Arctic, Antarctic and Alpine Research, 36(1), 21-32.

Elder, K., Dozier, J., and Michaelse, J. (1991). "Snow Accumulation and Distribution in an Alpine Watershed." Water Resources Research, 27(7), 1541-155.

Frew, J. E. (1990). "The Image Processing Workbench," Ph.D, University of California: Santa Barbara, CA.

Garen, D. C., and Marks, D. (2005). "Spatially distributed energy balance snowmelt modelling in a mountainous river basin: estimation of meteorological inputs and verification of model results." Journal of Hydrology, 315, 126-153.

Grünewald, T., and Lehning, M. (2011). "Altitudinal dependency of snow amounts in two small alpine catchments : Can catchment-wide snow amounts be estimated via single snow or precipitation stations?" Annals of Glaciology, 52(58), 153-158.

Gu, R., McCutcheon, S., and Chen, C.-J. (1999). "Development of weather-dependent flow requirements for river temperature control." Environmental Management, 24(4), 529-540.

Hock, R., and Holmgren, B. (2005). "A distributed surface energy-balance model for complex topography and its application to Storglaciaren, Sweden." Journal of Glaciology, 51(172), 25-36.

Homan, J. W., Luce, C. H., McNamara, J. P., and Glenn, N. F. (2010). "Improvement of distributed snowmelt energy balance modeling with MODIS-based NDSI-derived fractional snow-covered area data." Hydrological Processes, 25, 650–660.

Howat, I. M., and Tulaczyk, S. (2005). "Climate sensitivity of spring snowpack in the Sierra Nevada." Journal of Geophysical Research, 110, F04021.

Keller, F., Goyette, S., and Beniston, M. (2005). "Sensitivity analysis of snow cover to climate change scenarios and their impact on plant habitats in alpine terrain." Climate Change, 72, 299–319.

Kormos, P. R., Marks, D., McNamara, J. P., Marshall, H. P., Winstral, A., and Flores, A. N. (2014a). "Snow distribution, melt and surface water inputs to the soil in the mountain rain–snow transition zone." Journal of Hydrology, 519, 190-204.

Kormos, P. R., Marks, D., Williams, C. J., Marshall, H. P., Aishlin, P., Chandler, D. G., and McNamara, J. P. (2014b). "Soil, Snow, Weather, and Sub-Surface Storage Data from a Mountain Catchment in the Rain–Snow Transition Zone." Earth System Science Data, 6, 165–173.

Korner, C. (1998). "A re-assessment of high elevation treeline positions and their explanation." Oecologia 115, 445-459.

Kumar, M., Marks, D., Dozier, J., Reba, M., and Winstral, A. (2013). "Evaluation of distributed hydrologic impacts of temperature-index and energy-based snow models." Advances in Water Resources, 56, 77-89.

Kumar, M., Wang, R., and Link, T. E. (2012). "Effects of more extreme precipitation regimes on maximum seasonal snow water equivalent." Geophysical Research Letters, 39(20), DOI: 10.1029/2012GL052972.

Lee, S., Klein, A. G., and Over, T. M. (2005). "A comparison of MODIS and NOHRSC snow-cover products for simulating streamflow using the Snowmelt Runoff Model." Hydrological Processes, 19, 2951–2972.

Link, T. E., and Marks, D. (1999). "Distributed simulation of snowcover mass- and energybalance in the boreal forest." Hydrological Processes, 13, 2439–52.

Liston, G. E., and Elder, K. (2006). "A Distributed Snow-Evolution Modeling System (SnowModel)." Journal of Hydrometeorology, 7(6), 1259–1276.

Little, M. A., and Hanna, J. M. (1978). "Climate characteristics of high-altitude zones." The Biology of High-Altitude Peoples, P. T. Baker, ed., Cambridge University Press.

Luce, C., Staab, B., Kramer, M., Wenger, S., Isaak, D., and McConnell, C. (2014). "Sensitivity of summer stream temperatures to climate variability in the Pacific Northwest." Water Resources Research, 50(4), 3428–3443.

Luce, C. H., Tarboton, D. G., and Cooley, K. R. (1998). "The influence of the spatial distribution of snow on basin-averaged snowmelt." Hdrological Processes, 12, 1671-1683.

Luce, C. H., Tarboton, D. G., and Cooley, K. R. (1999). "Sub-grid parameterization of snow distribution for an energy and mass balance snow cover model." Hydrological Processes, 13, 1921-1933.

Marks, D. (1988). "Climate, energy exchange, and snowmelt in Emerald Lake watershed, Sierra Nevada," Ph.D., University of California: Santa Barbara, CA.

Marks, D., Domingo, J., and Frew, J. (1999a). "Software tools for hydro-climate modeling and analysis: Image Processing Workbench, Version 2." Electronic Document, [Online] ARS Technical Bulletin 99-1. Northwest Watershed Research Center, USDA Agricultural Research Service: Boise, Idaho: Available: http://www.nwrc.ars.usda.gov/ipw.

Marks, D., Domingo, J., Susong, D., Link, T., and D.Garen. (1999b). "A spatially distributed energy balance snowmelt model for application in mountain basins." Hydrological Process 13, 1935-1959.

Marks, D., Kimball, J., Tingey, D., and Link, T. (1998). "The sensitivity of snowmelt processes to climate conditions and forest cover during rain-on-snow: a case study of the 1996 Pacific Northwest food." Hydrological Processes, 12, 1569-1587.

Marks, D., Winstral, A., Reba, M., Pomeroy, J., and Kumar, M. (2013). "An evaluation of methods for determining during-storm precipitation phase and the rain/snow transition elevation at the surface in a mountain basin." Journal of Advances in Water Resources, 55, 98-110.

Martin, E., Brun, E., and Durand, Y. (1994). "Sensitivity of the French Alps snow cover to the variation of climatic variables." Annales Geophysicae, 12(5), 469-477.

Mazurkiewicz, A. B., Callery, D. G., and McDonnell, J. J. (2008). "Assessing the controls of the snow energy balance and water available for runoff in a rain-on-snow environment." Journal of Hydrology, 354, 1-14.

Molotch, N. P., and Bales, R. C. (2005). "Scaling snow observations from the point to the grid element: Implications for observation network design." Water Resources Research, 41, W11421.

Morán-Tejeda, E., López-Moreno, J. I., and Beniston, M. (2013). "The changing roles of temperature and precipitation on snowpack variability in Switzerland as a function of altitude." Geophysical Research Letters, 40, 1-6.

Moriasi, D. N., Arnold, J. G., Liew, M. W. V., Bingner, R. L., Harmel, R. D., and Veith, T. L. (2007). "Model evaluation guidelines for systematic quantification of accuracy in watershed simulations." Transactions of the ASABE, 50(3), 885-900.

Pohl, S., and Marsh, P. (2006). "Modelling the spatial–temporal variability of spring snowmelt in an arctic catchment." Hydrol Processes, 20, 1773–1792.

Pohl, S., Marsh, P., and Liston, G. E. (2006). "Spatial-Temporal Variability in Turbulent Fluxes during Spring Snomelt." Arctic, Antarctic and Alpine Research, 38(1), 136-146.

Raleigh, M. S., and Lundquist, J. D. (2012). "Comparing and combining SWE estimates from the SNOW-17 model using PRISM and SWE reconstruction." Water Resour Manage, 48, W01506.

Reba, M. L., Marks, D., Winstral, A., Link, T. E., and Kumar, M. (2011). "Sensitivity of the snowcover energetics in a mountain basin to variations in climate." Hydrological Processes, 25(21), 3312-3321.

Rohli, R. V., and Vega, A. J. (2008). "The climate system: controls on climate." Climotology, Jones and Bartlett Publishers, 30-60.

Scherrer, S. C., and Appenzeller, C. (2004). "Trends in Swiss Alpine snow days: The role of local- and large-scale climate variability." Geophysical Research Letters, 31, L13215.

Schimel, J. P., Bilbrough, C., and Welker, J. M. (2004). "Increased snow depth affects microbial activity and nitrogen mineralization in two Arctic tundra communities." Soil Biology & Biochemistry, 36, 217-227.

Sensoy, A., Sorman, A. A., Tekeli, A. E., Sorman, A. U., and Garen, D. C. (2006). "Point-scale energy and mass balance snowpack simulations in the upper Karasu basin, Turkey." Hydrological Processes, 20, 899–922.

Seyfried, M. S., Grant, L. E., Marks, D., Winstral, A., and McNamara, J. (2009). "Simulated soil water storage effects on streamflow generation in a mountainous snowmelt environment, Idaho, USA." Hydrological Processes, 23, 858–73.

Sohrabi, M., Ryu, J., Abatzoglou, J., and Tracy, J. (2015). "Development of Soil Moisture Drought Index to Characterize Droughts." J. Hydrol. Eng., DOI: 10.1061/(ASCE)HE.1943-5584.0001213.

Sultana, R., Hsu, K. L., Li, J., and Sorooshian, S. (2014). "Evaluating the Utah Energy Balance (UEB) snow model in the Noah land-surface model." Hydrolo. Earth Syst. Sci., 18, 3553-3570.

Susong, D., Marks, D., and Garen, D. C. (1999). "Methods for developing time-series climate surfaces to drive topographically distributed energy- and water-balance models." Hydrol Proc, 13, 2003-2021.

Torp, M. (2010). "The effect of snow on plants and their interactions with herbivores," PhD, Umeå University, Umeå

Wang, R., Kumar, M., and Link, T. E. (2016). "Potential trends in snowmelt generated peak streamflow in a warming climate." Geophysical Research Letters, 43(10), 5052–5059.

Wang, R., Kumar, M., and Marks, D. (2013). "Anomalous trend in soil evaporation in a semi-arid, snow-dominated watershed." Advances in Water Resources, 57, 32-40.

Webb, B. W., Clack, P. D., and Walling, D. E. (2003). "Water–air temperature relationships in a Devon river system and the role of flow." Hydrological Processes, 17, 3069–3084.

Weill, S., Altissimo, M., Cassiani, G., Deiana, R., Marani, M., and Putti, M. (2013). "Saturated area dynamics and streamflow generation from coupled surface–subsurface simulations and field observations." Advances in Water Resources, 59, 196-208.

Winstral, A., Elder, K., and Davis, R. E. (2002). "Spatial Snow Modeling of Wind-Redistributed Snow Using Terrain-Based Parameters." Journal of Hydrometeorology, 3, 524–538.

Winstral, A., and Marks, D. (2002). "Simulating wind fields and snow redistribution using terrain-based parameters to model snow accumulation and melt over a semi-arid mountain catchment." Hydrological Processes, 16, 3585–3603.

Winstral, A., Marks, D., and Gurney, R. (2009). "An efficient method for distributing wind speeds over heterogeneous terrain." Hydrological Processes, 23, 2526–2535.

Winstral, A., Marks, D., and Gurney, R. (2013). "Simulating wind-affected snow accumulations at catchment to basin scales." Advances in Water Resources, 55, 64-79.

Winstral, A., Marks, D., and Gurney, R. (2014). "Assessing the Sensitivities of a Distributed Snow Model to Forcing Data Resolution." Journal of Hydrometeorology, 15, 1366–1383.

Chapter 4. How Fine Is A Fine Spatial Resolution for Process-Based Snow Modeling?

4.1. Abstract

Hydrological processes in mountainous settings depend on snow distribution, whose prediction accuracy is a function of model spatial scale. Although model accuracy is expected to improve with finer spatial resolution, the reduction in scale comes with modeling costs. This computational expense is still a limiting factor for many large watersheds and there exists a lack of understanding of which processes dominate snow distribution at different topographic elevations and climate conditions. Thus, the objective of this work is to unveil what physical processes lead to loss in model accuracy with regard to inputs spatial resolution under different climatic conditions and elevation ranges. The main hypothesis is that the topographic information loss at increased spatial resolutions affects the energy balance and consequently accumulation/ablation of snow. To address this objective and hypothesis, a spatially distributed snow model, iSnobal, was run with inputs distributed at 50m – our benchmark for comparison – and 100m resolutions and with aggregated inputs from the 50m model to 100m, 250m, 500m and 750m resolution for wet, average and dry years over the Upper Boise River Basin (6,963 km^2), which spans 4 elevation bands: rain dominated, rain-snow transition and snow dominated below treeline and above treeline. Residuals of simulated snow cover area (SCA) and snow water equivalent (SWE) were generally slight in the aggregated scenarios. This was due to transferring the effects of topography on meteorological variables from the 50m model to the coarser scales through aggregation. Residuals in SCA and SWE in the distributed 100m simulation were even larger than those of the aggregated 750m. Topographic features such as slope and aspect were flattened due to coarsening the topography from the 50 to 100m resolution. Therefore, net radiation was overestimated and snow drifting was modified and caused substantial SCA and SWE underestimation in the distributed 100m model relative to the 50m model. Large residuals were observed in the wet year and at the highest elevation band when and where snow mass was large. These results support that model accuracy reduces substantially with model scales coarser than 50m.

Keywords: *Spatial resolution, Physics-based snow modeling, Mountainous regions, Rain-snow transition, Alpine treeline, Model accuracy, Model evaluation*

4.2. Introduction

Accumulation and ablation of snow is critical for hydrological cycles and ecological systems in mountainous settings (Homan et al. 2010; Nitaa et al. 2014; Raleigh and Lundquist 2012). In these regions, precipitation accumulates as snow during winter and the accumulated water, then, releases during spring and early summer (Luce et al. 1998). Spatio-temporal distribution of these water releases from the snow cover is critical for hydrological studies, because spatial distribution, timing and magnitude of snow melt controls soil moisture dynamics (Kormos et al. 2014a; Liston and Elder 2006), groundwater recharge (Kormos et al. 2014b; Kumar et al. 2013) and runoff and streamflow generation (Garen and Marks 2005; Weill et al. 2013). In addition, many variables that are important for ecosystem depend on spatio-temporal distribution of snow accumulation and ablation. Spring and early summer air temperatures and soil moisture distribution, which are fundamental factors for vegetation distribution (Darmody et al. 2004; Sensoy et al. 2006; Torp 2010), are moderated by snow cover the former due to increase in albedo (Marks et al. 2013; Molotch and Bales 2005). Soil microbial activities continues even during winter (Schimel et al. 2004), because soil is insulated from very low air temperatures due to snow low thermal conductivity (Liston and Elder 2006; Torp 2010). Moreover, contribution of snow melt to discharge prevents stream temperature from following increasing trend in air temperatures in late spring and early summer (Luce et al. 2014). As a result, stream temperature, which is an important element for aquatic ecosystems, is influenced by spatio-temporal distribution of melt (Gu et al. 1999; Webb et al. 2003). Therefore, accurate estimation of spatio-temporal distribution of snow accumulation and ablation is necessary to predict hydrologic response from watersheds.

For accurate estimation of snow distribution, an appropriate model scale is required to consider heterogeneous snow distribution caused by rugged terrain and vegetation (Bloschl 1999; Luce et al. 1998; Pohl et al. 2006). Topographic features and/or vegetation changes

over small distances in mountainous settings and this causes snow distribution to be strongly heterogeneous (Winstral et al. 2014). The interaction among several factors such as elevation, slope, aspect and vegetation highly impacts distribution of meteorological variables, particularly radiation, wind and precipitation (Marks et al. 1999b; Trujillo et al. 2007). Changes in these meteorological variables over small distances results in heterogeneity in snow accumulation and ablation (Elder et al. 1991).

Heterogeneous snow accumulation is mainly due to spatial variability of precipitation and redistribution of snow (Trujillo et al. 2007), but spatially variable energy fluxes cause heterogeneous snow ablation (Pohl and Marsh 2006). At a watershed scale, snow accumulation distribution depends on distribution of precipitation, which varies based on changes in elevation (Winstral et al. 2013). Wind is responsible for re-deposition of snow during a snowfall event and redistribution of snow after the event (Liston 2004; Winstral et al. 2009). Even if precipitation pattern was uniform over a watershed, snow accumulation would be heterogeneous due to wind disparity, which is caused by terrain irregularities in mountainous settings (Elder et al. 1991; Luce et al. 1999; Winstral and Marks 2002). Snow ablation is heterogeneous because of large spatial disparities in energy fluxes. In mountainous settings, slope and aspect that vary over small distances cause spatial variation in radiation on sunny days, which has a key role in snow ablation heterogeneity (Keller et al. 2005; Pohl et al. 2006). On warm and cloudy days, spatial variation in turbulent energy caused by spatial disparity in air temperature, vapor pressure and wind speed is mainly responsible for snow ablation heterogeneity (Marks et al. 2013; Pohl and Marsh 2006).

Neglecting small scale variability of these meteorological variables and energy fluxes impacts estimation of snow cover properties, and the extent of this impact may vary in different elevation ranges and climate conditions. In rain dominated and rain-snow transition bands, where precipitation can fall either in form of rain or snow, precipitation phase can be misidentified due to neglecting spatial variability in dew point or wet-bulb temperature (Beniston 2012). This causes inaccurate estimation of snow mass and advected heat from precipitation to the snow cover. In snow dominated bands, it is critical to capture small scale variations in snow drifting and energy exchanges at the interface of air-snow (Luce et al. 1998). Small scale variation in wind-induced snow drifting is important because of large wind

spatial disparity, particularly at regions above alpine treeline where only topographic variability constrain redistribution (Deems et al. 2006; Korner 1998; Winstral et al. 2009). Estimation of the energy exchange between snow and the atmosphere can be less reliable when topography-induced spatial disparity in net radiation and turbulent energy is neglected. Spatial disparity in meteorological variables is also likely to vary between years that have different climatology. For example, in a wet year, spatial disparity in dew point temperature and energy fluxes is on an average less pronounced due to high humidity and large number of cloudy days (Rohli and Vega 2008). In contrast, in a dry year spatial variability in these variables is pronounced. These examples suggest that the effect of model scale on prediction accuracy is likely to vary across elevation bands and years with characteristically different climatology.

4.3. Background

To accurately account for heterogeneity in snow accumulation and ablation an appropriate model scale is required so that the model be able to capture process scale (natural) variability of snow accumulation and ablation (Bloschl 1999). For instance, process scale (correlation length) is small, in regions where SWE substantially changes over small distances. Therefore, in order to capture variability in SWE at process scale, the model scale needs to be finer than the process scale or the model must have a tool to consider sub-grid variability. Sub-grid variability of snow distribution is usually calculated using statistical distributions and/or empirical relationship between snow cover area and sow depth or SWE rather than considering small scale physical processes (Liston 2004; Luce and Tarboton 2004; Luce et al. 1999; Meromy et al. 2013; Nitaa et al. 2014; Niu and Yang 2007).

It is important to analyze effect of scaling on estimation of snow accumulation and ablation to identify an appropriate model scale for snow modeling. Scaling effect on prediction of snow accumulation and ablation can be evaluated using three approaches (Bloschl 1999); (1) a spectral analysis; (2) variogram analysis; and (3) analyzing changes in the average value of a snow variable, i.e. SWE, over an area given coarsening the measurement resolution or the model scale. All these three approaches lead to the same results for linear processes.

However, for non-linear processes the third approach, which is generally used, may have different results than the first two approaches (Bloschl 1999). This is due to impact of scale change on the mean value of a variable over an area in non-linear processes. A process is linear, if the process conserves mass and/or energy. For instance, average SWE of a basin calculated from measured SWE at a 1 m grid is the same as average SWE of that basin calculated from measured SWE at a 10 m grid (Bloschl 1999). However, estimation of SWE is a non-linear process, because SWE estimation relies on meteorological variables with topography-induced spatial variation, i.e. net radiation and snow drifting (Bloschl 1999; Hopkinson et al. 2010). Topographic features such as slope, aspect, sky view factor and etc. change as model scale changes. As a result, average value of SWE over a basin estimated using different model scales are not necessary the same, although physics-based snow models conserve mass and energy to estimate SWE.

Scaling impact on snow cover properties have been investigated in previous studies using the stated three approaches. Deems et al. (2006) and Trujillo et al. (2007) analyzed scaling effect on snow depth from LIDAR data at couple of Colorado catchments using variogram and spectral analyses, respectively. They reported that scale breaks (correlation length) of snow depth were ranged from 15 to 40 m. They found that scaling behavior of snow depth depends on spatial distribution of vegetation height and wind. They concluded that scaling characteristics of snow depth is controlled by spatial distribution of vegetation height in forested regions where interception is the dominant factor for snow distribution. However, in non-forested or sparse forested regions, where wind is responsible for snow redistribution, scaling characteristics of snow depth is controlled by wind. Luce et al. (1998) analyze impact of spatial resolution of inputs on snow accumulation and ablation by comparing simulation from lump and distributed models. They found that detail spatial information of snow drifting is as or more important than that of net radiation in their study watershed. Cline et al. (1998) modeled SWE spatial distribution for a short melt period after SWE peak using inputs resolutions of 30, 90, 250 and 500 m to force a coupled remote sensing/distributed energy balance snowmelt model (SNODIS) over a small watershed (1.2 km^2). They observed no significant difference between basin-averaged SWE generated from 30 to 500 m. Winstral et al. (2014) analyzed sensitivity of basin averaged SWI to the model scale and used spatial resolution of 10 to 1500 m for inputs to run a distributed physics-based snow model (iSnobal)

over a small watershed (6 km^2). They observed that simulated basin averaged SWI using 100 m resolution of the inputs was very similar to that of 10 m resolution with less than 4% biases. However, they concluded that due to small drainage area of the studied watershed, selecting the appropriate model scale for other watersheds requires further analyses related to the watershed of interest.

There is no optimum model scale for snow modeling, because in practice a grid size is selected by considering data availability, modeling costs and required resolution and/or accuracy of predictions (Bloschl 1999; Winstral et al. 2014). In distributed snow models that require distributed forcing inputs, the use of a fine model scale increases substantially modeling costs, such as runtime and storage space. This substantial increase in the modeling costs is mainly due to spatially distributing forcing inputs rather than running snow models. On the other hand using a coarse model scale neglects small scale variations, which reduces prediction accuracy. The extent of this reduction in model accuracy is unknown. It is difficult to fill this knowledge gap and generalize a scale which does not mask critical information about snow cover properties based on the results of the previous studies. Prior studies were conducted either for a short period of a snow season or small spatial extent. In addition, in these studies effect of model scale on prediction accuracy was merely evaluated based on changes in inputs resolution by aggregating inputs from a fine resolution to obtain coarse resolutions. This may result in transferring information from inputs with a fine resolution to those with coarse resolutions. Moreover, aggregating inputs does not provide any information on how much prediction accuracy reduces when topographic settings such as slope, aspect, sky view factor and etc. are changed due to coarsening DEM.

Therefore, there is a need to understand transferred and lost information in estimation of snow cover properties due to neglecting topography-induced heterogeneity of meteorological variables caused by coarsening the model spatial resolution. The objective of this work is to understand what sort of information can be lost over a watershed due to the model spatial resolution for a range of climatic and topographic conditions. Its main hypothesis is that increasing model scale affects energy balance and consequently precipitation phase and accumulation/ablation of snow because it smoothens topographical complexity. This work addresses these knowledge gaps with these specific objectives: (1) quantifying the impact of

model scale on snow model response by analyzing SCA and SWE; (2) assessing the role of annual climatology on the sensitivity of predictions accuracy to model scale; and (3) identifying the elevation range where predictions accuracy are most sensitive to model scale.

4.4. Study Area and Data

The study area is the portion of the Boise River basin (BRB) (Idaho, USA), upstream of the Lucky Peak Dam, with drainage area of 6,963 km^2 (Figure 4.1). This portion of the BRB is an important source of water that provides agricultural and urban water demands using three reservoirs, including Lucky Peak, Arrow Rock and Anderson Ranch Dams. Vegetation cover of the BRB is mainly coniferous forest (41%) and shrubland (35%) and the rest of the BRB is covered with bare rock, grass, deciduous forest, or burned/harvested forest. Elevations of the BRB range from 841 m to 3,168 m, which vary from rain to snow dominated regions. Due to this wide range of elevations, average annual precipitation that is received through the basin varies substantially from about 500 mm at low elevations to approximately 1,500 mm at high elevations.

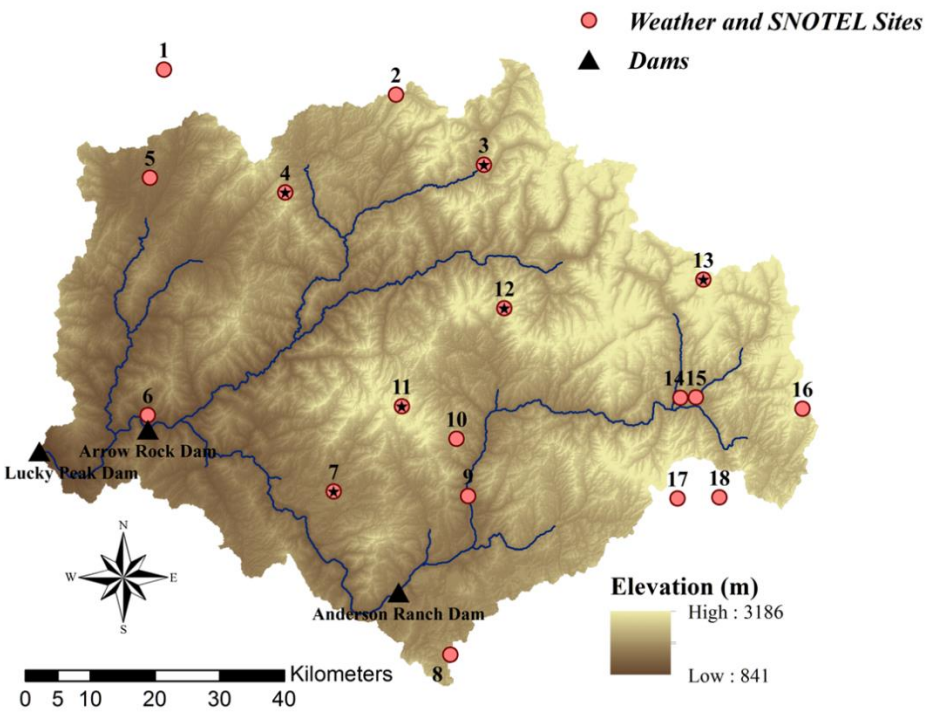

Figure 4.1. Boise River Basin and weather and SNOTEL sites. Black stars indicate SNOTEL sites with SWE measurements, which were used in the evaluation of model performance.

There are 18 weather and SNOTEL stations in or near BRB that measure hourly meteorological variables, including precipitation (p), air temperature (t), relative humidity (rh), solar radiation (sr) and wind (w) (Figure 4.1 and Table 4.1). Precipitation and temperature are measured at all the stations, whereas relative humidity, solar radiation and wind are available at 5, 6 and 9 of these stations, respectively. Ten of these 18 stations are SNOTEL sites that are operated by Natural Resources Conservation Service (NRCS) and the rest of the stations are weather stations that either operated by Bureau of Land Management (BLM) and U.S. Department of Agriculture (USDA) Forrest Service (FS; 5 stations) or Bureau of Reclamation (BR; 3 stations).

Table 4.1. Detailed information of the stations.

NO.	Station Name	Latitude (Decimal ◦)	Longitude (Decimal ◦)	Elevat-ion (m)	Variables Measured	Operated by
1	Little Anderson	44.09	-115.88	1389	p, t, rh, sr, w	BLM & FS
2	Jackson Peak	44.05	-115.44	2155	p, t, w, SWE	NRCS
3	Graham Guard STA.	43.95	-115.27	1734	p, t, w, SWE	NRCS
4	Mores Creek Summit	43.93	-115.67	1859	p, t, SWE	NRCS
5	Town Creek	43.94	-115.91	1415	p, t, rh, sr, w	BLM & FS
6	Arrowrock Dam	43.61	-115.92	998	p, t	BR
7	Prairie	43.50	-115.57	1463	p, t, SWE	NRCS
8	Camas Creek Divide	43.27	-115.35	1740	p, t, SWE	NRCS
9	South Fork Boise	43.49	-115.31	1286	p, t	BR
10	Wagontown	43.57	-115.33	1881	p, t, rh, sr, w	BLM & FS
11	Trinity Mountain	43.63	-115.44	2368	p, t, SWE	NRCS
12	Atlanta Summit	43.76	-115.24	2310	p, t, sr, w, SWE	NRCS
13	Vienna Mine	43.80	-114.85	2731	p, t, w, SWE	NRCS
14	Fleck Summit	43.62	-114.90	2164	p, t, rh, sr, w	BLM & FS
15	Big Smokey Ranger	43.62	-114.87	1706	p, t	BR
16	Dollarhide Summit	43.60	-114.67	2566	p, t, SWE	NRCS
17	Soldier Mountain Peak	43.48	-114.91	2904	p, t, rh, w	BLM & FS
18	Soldier R.S.	43.48	-114.83	1749	p, t, SWE	NRCS

Variable abbreviations: p, precipitation; t, air temperature; rh, relative humidity; sr, solar radiation; w, wind speed and direction; SWE, snow water equivalent.
Abbreviations for institutes operate the stations: BLM & FS, Bureau of Land Management and U.S. Department of Agriculture (USDA) Forrest Service, respectively; NRCS, Natural Resources Conservation Service; BR, Bureau of reclamation.

4.5. Methodology

4.5.1. Snow Model: iSnobal

Snobal is a physics-based snow model that conserves both mass and energy at a point (Marks 1988). Spatial (image) version of Snobal, iSnobal, was developed by Marks et al. (1999b) and uses the same set of equations as Snobal to calculate mass and energy flux exchanges at each grid cell. The model uses a two-layer representation of the snow cover with a 0.25 mm fixed-thickness top layer, the interface between air and snow, and the bottom layer having the rest

of the snowpack. Calculation of water exchanges, such as evaporation, condensation and sublimation, are conducted in the top layer. However, computation of energy exchanges are performed at both layers at each time step for each grid cell with the following energy balance equation (Eq. 4.1) (Eq. 3.1), (Garen and Marks 2005; Marks et al. 1999b) :

$$\Delta Q = R_n + H + L_v E + G + M \qquad \text{(Eq. 4.1)}$$

where ΔQ (W m^{-2}) is the snow cover energy that depends on changes in net radiation (R_n), sensible heat (H), latent heat ($L_v E$), conduction (G) and advection (M) energies (all units of W m^{-2}). L_v (W m^{-2} kg^{-1}) indicates specific latent heat of water and E (kg) represents mass of water that has phase change. An increase in the snow cover energy causes a decrease in the cold content, which is energy required to bring the snow cover temperature to 0 °C. Melt calculated at both layers and occurs once the cold content reaches 0 °C. Estimated melt in the model consists of both melt and rain on snow and it drains out when total liquid water content in snowpack is higher than a specified threshold. Melt that drains out is surface water input (SWI).

4.5.2. Spatial Distribution of Meteorological data

Distributed meteorological inputs such as precipitation, air temperature, vapor pressure, solar radiation, and wind speed are required to force iSnobal. Details about the spatial interpolation methodology for meteorological variables were described in our previous work (Sohrabi et al. In Preparation) and the following is a brief description about the method used. Inputs were spatially distributed using interpolation detrended elevation (vertical) and distance (horizontal) Kriging method (Garen and Marks 2005). Air temperature-elevation trends were constrained to be zero or negative, because air temperature decreases as elevation increases. However, we did not constrain relative humidity-elevation trends. The distributed relative humidity and air temperature was then used to compute dew point temperature and vapor pressure. Dew point temperatures were used to identify precipitation phase (Garen and Marks

2005). Wind speed and direction were distributed using a detrended elevation and distance based Kriging method. Wind speed of a cell, then, was adjusted using Winstral et al. (2002) algorithm. In this algorithm, topographically wind exposed and sheltered cells are identified using maximum upwind slope (s_x). At exposed cells, negative s_x, wind speed is increased due to vertical flow constriction, whereas wind speed is decreased at topographically sheltered cells, positive s_x, due to expansion of flow (Winstral and Marks 2002). Analogous to wind speeds, precipitation was first distributed using a detrended elevation and distance based Kriging method. Precipitation-elevation trends were constrained to be zero or positive, because precipitation increases with elevation (Garen and Marks 2005). Wind-induced snow drifting was, then, calculated using upwind slope break (s_b) and wind speed (Winstral et al. 2002; Winstral et al. 2013; Winstral et al. 2014). Snow is eroded at exposed cells once wind speed is high. The transported snow particles from these cells are, then, deposited at sheltered cells where wind speed is low. Solar radiation was distributed using a detrended elevation and distance based Kriging method. The distributed solar radiation was then corrected for solar angle, shading, vegetation, and albedo (Link and Marks 1999; Susong et al. 1999). Snow albedo was adjusted to consider snow aging due to dust and organic debris exposure (Garen and Marks 2005). Distributed thermal radiation was computed for clear sky based on the distributed air temperature and vapor pressure and elevation and sky view factor. The calculated thermal radiation was then adjusted given cloud cover and vegetation (Link and Marks 1999).

4.5.3. Scenarios Design

To evaluate effect of scaling on estimation of SCA and SWE, iSnobal was run for 5 different grid sizes (scale) of inputs, including 50 m (50 m (d)), 100 m (100 m (a)), 250 m (250 m (a)), 500 m (500 m (a)) and 750 m (750 m (a)). To do this, inputs were distributed at 50 m resolution and the distributed inputs were then aggregated to obtain 100 to 750 m resolutions of inputs, hereafter aggregated scenarios that are indicated as 100 m (a) to 750 m (a). Values of an input for 50-m cells that were located in a coarser grid cell were averaged to degrade resolution of that input. Aggregated scenarios used in this work are similar to those used in Winstral et al. (2014). Coarser resolutions than 750 m were not used, because Winstral et al.

(2014) identified those scales as inappropriate scales for snow modeling at a watershed scale. In addition to the aggregated scenarios, iSnobal was run using inputs that were distributed at 100 m resolution, hereafter 100 m (d) scenario. This scenario was added due to the following reasons; (a) understand magnitude of information that is transferred from the distributed inputs at 50 m resolution to those that aggregated to 100 m resolution; and (b) understand how prediction accuracy and distribution of inputs vary regarding to changes in topographic features such as slope, aspect and sky view factors due to coarsening the DEM from 50 m to 100 m resolution.

Hourly time step of inputs was used and model runs were performed for entire water years (WY), which start on October of the previous year and end in September of the current year. Each scenario was run for a wet (WY2006-359mm), average (WY2010-325mm), and dry year (WY2007-209mm) to understand sensitivity of model scale impacts on prediction accuracy to various climatic conditions (Sohrabi et al. 2015; Sohrabi et al. 2013). These years were identified from the period of 1950-2010 using four different drought indices at Boise Airport station.

4.5.4. Model Performance Evaluation and Analyses

In our previous work (Sohrabi et al. In Preparation), 50m grid predicted SWE for the wet, average and dry years was validated using measured SWE at six out of the ten SNOTEL sites located inside BRB: Prairie, Graham Guard, Mores Creek Summit, Atlanta Summit, Trinity Mountain and Vienna Mine (Figure 4.1). We observed average Nash-Sutcliffe coefficient (NSC) of 0.76 and root mean square error (RMSE)-observations standard deviation ratio (RSR) of 0.42 over all sites and years. NSC and RSR values were generally larger than 0.75 and lower than 0.5, representing very reliable estimations (Moriasi et al. 2007). In non-linear processes such as SCA and SWE estimation, an appropriate approach to understand scaling effect is to analyze changes in the mean values of these variables over an area as scale changes (Bloschl 1999). To do this, estimated daily time series of SCA and SWE from all the scenarios were divided into four elevation bands (Table 4.2). At the rain-snow transition region (E2), where precipitation can fall either as rain or snow, precipitation phase is very

sensitive to changes of dew point temperature (Beniston 2012; Marks et al. 2013). E2 includes range of elevations from 1,500 to 1,800 m in the Pacific Northwestern USA (Kormos et al. 2014a; Kormos et al. 2014b). E2 in the BRB was set to regions that have elevation from 1,400 to 1,900 m. The rain dominated (E1) and snow dominated (E3) regions are below and above E2, respectively. Alpine treeline (E4) is an imaginary line, which indicates that above this line trees cannot grow because of low air temperatures and long snow cover duration. E4 in the BRB includes regions that have elevations greater than 2,400 m (Korner 1998).

Table 4.2. Elevation Bands

Bands	***Elevation (m)***	***Description***	***% of Grid Cells***
E1	≤ 1400	Rain Dominated	16
E2	> 1400 and ≤ 1900	Rain-Snow Transition	44
E3	> 1900 and ≤ 2400	Snow Dominated	28
E4	> 2400	Alpine Treeline	12

Modeled SWE were spatially averaged over each band. SCA represents percent of the area covered with snow, which was calculated by dividing number of cells with SWE greater than 0 over total number of cells at each band. The spatially averaged snow water equivalent ($\overline{SWE}_{i,j}(t)$) and snow cover area ($SCA_{i,j}(t)$) for the *i*-th band (E1, E2, E3 and E4) with area, A_i, and the *j*-th scenario, such as 50 m (d), 100 m (d), 100 m (a), 250 m (a), 500 m (a) and 750 m (a), are computed as follows:

$$\overline{SWE}_{i,j}(t) = \frac{1}{A_i}\int_0^{A_i} SWE_{i,j}(t,a)\,da \qquad \text{(Eq. 4.2)}$$

$$with\ i = E1-E4\ and\ \ j = 100\text{m (d)}, 100\text{m (a)}, 250\text{m (a)}, 500\text{m (a)}, 750\text{m (a)}$$

$$SCA_{i,j}(t) = \frac{100}{A_i}\int_0^{A_i} SC_{i,j}(t,a)\,da \quad and \quad \begin{cases} SC_{i,j}(t,a)=1 & SWE_{i,j}(t,a)>0 \\ SC_{i,j}(t,a)=0 & SWE_{i,j}(i,x)=0 \end{cases} \qquad \text{(Eq. 4.3)}$$

where $SWE_{i,j}(t,a)$ and $SC_{i,j}(t,a)$ are the SWE and snow cover index, respectively, for each cell of area *a* at time t. The spatially averaged residual of SWE and SCA for each band, which was applied for visualizing the results, was computed as:

$$\mathrm{Res}_{i,j}(t) = SV_{i,j}(t) - SV_{i,50m}(t) \quad \text{(Eq. 4.4)}$$
$$with\ i = E1-E4\ and\ j = 100\mathrm{m\,(d)}, 100\mathrm{m\,(a)}, 250\mathrm{m\,(a)}, 500\mathrm{m\,(a)}, 750\mathrm{m\,(a)}$$

where $SV_{i,j}$ stands for $\overline{SWE}_{i,j}(t)$ and $SCA_{i,j}(t)$ for each *j*-th scenario. To present residuals in SWE in percentage, the residuals were divided by the mean of the estimated SWE from the 50 m (d) for a given snow season. Effect of scaling on the estimated snow variables for each band was quantified using mean absolute error (MAE). In our case, increase in value of MAE indicates reduction in prediction accuracy. MAE is computed as follows (Moriasi et al. 2007):

$$MAE_{i,j} = \frac{1}{T}\int^{T} \left| SV_{i,50m}(t) - SV_{i,j}(t) \right| dt \quad \text{(Eq. 4.5)}$$
$$with\ i = E1-E4\ and\ j = 100\mathrm{m\,(d)}, 100\mathrm{m\,(a)}, 250\mathrm{m\,(a)}, 500\mathrm{m\,(a)}, 750\mathrm{m\,(a)}$$

where *T* indicates the period of time that MAE is computed. MAE was calculated for the entire snow season (total MAE), accumulation (Rising Limb; RL) and ablation (Falling Limb; FL) periods at each band. RL begins as snow cover forms and terminates when SWE reaches its peak. FL begins after SWE peak occurs and continues to the time snow ablates completely.

To understand the reasons that caused discrepancies between the estimated SCA and SWE from the 50 m (d) scenario and those of the aggregated scenario, two 750 m cells were selected in E2, hereafter 750m-E2-cell, and E4, hereafter 750m-E4-cell. November 24th and October 26th, 2005 were selected for the 750m-E2-cell and 750m-E4-cell, respectively, to identify reasons that caused the differences in the estimated SCA and SWE during RL. April 27th and June 20th, 2006 were selected to identify causes for different ablation rates in the aggregated scenarios relative to that of the 50 m (d) scenario at the 750m-E4-cell.

To investigate the reasons that caused differences between the estimated SCA and SWE of the 50 m (d) and 100 m (d) scenarios, a 100 m cell was selected in E3, hereafter 100m-E3-cell. November 10th, 2005, May 20th and December 27th, 2006 were selected for the 100m-E3-cell to analyze changes in the inputs as a result of coarsening the DEM from 50 m to 100 m. To understand changes in wind-induced snow drifting due to coarsening the DEM from 50 m to 100 m, iSnobal was ran for the 100 m (d) scenario with precipitation that was distributed at 50 m and aggregated to 100 m, hereafter 100 m (d)-nodrift scenario. Addition of the 100 m (d)-nodrift scenario helps to understand how much changes in snow drifting is responsible for the differences between the estimated SCA and SWE from 50 m (d) scenario and those of the 100 m (d) scenario. The 100 m (d)-nodrift scenario was applied to run iSnobal only for the wet year, because this year had larger snow mass than the average and dry hears.

4.6. Results and Discussion

4.6.1. Scaling Effect on the Model Performance

4.6.1.1. Snow Cover Area (SCA)

Residuals in the aggregated scenarios increased with scale from negligible for the 100 m (a) scenario (less than 2.0 %) to large in the 750 m (a) scenario (up to 17.6 %; Figure 4.2). Total MAE reduced with increase in elevation from rain dominated to snow dominated above the treeline (Table 4.3). The largest MAE for RL and FL were related to the 750 m (a) scenario. As elevation increased, MAE decreased for the accumulation period (RL), but MAE increased for the ablation period (FL). Residuals in RL were generally positive, representing overestimation of SCA in the aggregated scenarios relative to the 50 m (d) scenario. In FL, residuals were positive at the beginning of the ablation periods, but they were negative after the middle of the ablation periods. The largest difference between the estimated SCA from the 50 m (d) simulation and that of the aggregated scenarios were observed in the average year. The largest total MAE was related to the average year, whereas the lowest total MAE was related to the wet year over all the aggregated scenarios and elevation bands. MAE for RL and FL were larger in the wet year than the other years, except in E3 and E4 that the dry year had the greatest MAE for RL. Neglecting spatial variability of meteorological inputs was

responsible for these residuals in the aggregated scenarios. The residuals increased as spatial resolution of the aggregated scenarios increased, because larger variability of meteorological inputs was lost as spatial resolution of inputs increased.

Residuals in the 100 m (d) scenario were even larger than those observed in the 750 m (a) scenario. Maximum residual of 48.7 % was observed in the 100 m (d), whereas residuals of the 750 m (a) did not exceed 17.6 %. Similar to the aggregated scenarios, MAE generally decreased with increasing elevation from E1 to E4 during RL, but increased during FL. Residuals were positive in E1 and E2, except in the wet year that had negative residuals in these bands, and they were negative in E3 and E4. The wet year had large residuals (up to 48.7 %) in E1 and E2, but large residuals in E3 and E4 were observed in the dry year. The large difference between estimated SCA from the 50 m (d) and the 100 m (a) simulations and that of the 100 m (d) simulation indicated the need for considering effect of topographic variability at 50 m on meteorological inputs. The effect of topographic variability at 50 m on meteorological inputs was transferred by aggregation in the 100 m (a) simulation. However, topographic variability at 50 m was completely neglected in distribution of inputs in the 100 m (d) scenario.

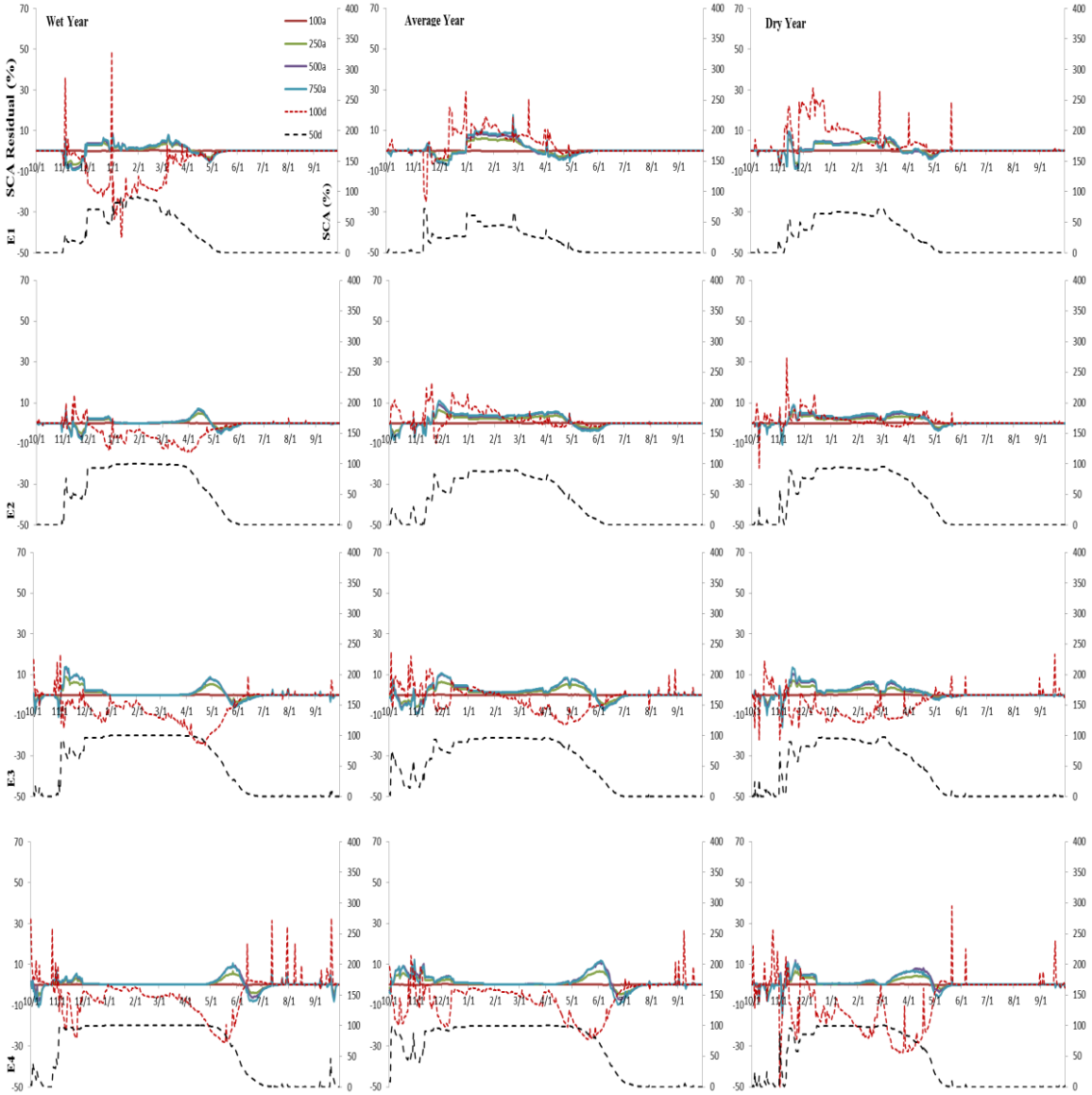

Figure 4.2. Aggregated estimated SCA over 4 elevation bands. Dotted lines show the 50 m (d) and 100 m (d) scenarios, but solid lines indicate the aggregated scenarios (from the 100 m (a) to 750 m (a)). Primary Y (left) axis shows residuals, the estimated SCA generated from all the scenarios minus that of the 50 m (d) scenario. Secondary Y (right) axis shows the estimated SCA from the 50 m (d) scenario.

Table 4.3. MAE for SCA (%) in each band.

Bands	MAE (%)	100 m (a)	250 m (a)	500 m (a)	750 m (a)	100 m (d)
E1	RL (Wet| Average| Dry)	0 | 0 | 0	3 | 4 | 3	4 | 5 | 4	4 | 6 | 4	15 | 9 | 12
	FL (Wet| Average| Dry)	0 | 0 | 0	1 | 2 | 1	2 | 2 | 2	2 | 2 | 2	3 | 4 | 2
	Total (Wet| Average| Dry)	0 | 0 | 0	2 | 3 | 2	3 | 4 | 3	3 | 4 | 3	11 | 7 | 8
E2	RL (Wet| Average| Dry)	0 | 0 | 0	1 | 2 | 2	1 | 4 | 3	1 | 4 | 3	6 | 5 | 3
	FL (Wet| Average| Dry)	0 | 0 | 0	2 | 2 | 2	3 | 3 | 3	3 | 3 | 3	5 | 1 | 1
	Total (Wet| Average| Dry)	0 | 0 | 0	1 | 2 | 2	2 | 3 | 3	2 | 4 | 3	6 | 2 | 2
E3	RL (Wet| Average| Dry)	0 | 0 | 0	1 | 2 | 3	2 | 3 | 4	2 | 4 | 4	8 | 4 | 9
	FL (Wet| Average| Dry)	0 | 0 | 0	2 | 3 | 1	3 | 4 | 2	3 | 4 | 2	10 | 7 | 4
	Total (Wet| Average| Dry)	0 | 0 | 0	2 | 2 | 2	2 | 4 | 3	2 | 4 | 3	9 | 5 | 7
E4	RL (Wet| Average| Dry)	0 | 0 | 0	1 | 1 | 1	1 | 2 | 2	1 | 2 | 2	6 | 7 | 13
	FL (Wet| Average| Dry)	0 | 0 | 0	2 | 3 | 2	3 | 4 | 4	4 | 5 | 4	11 | 13 | 18
	Total (Wet| Average| Dry)	0 | 0 | 0	1 | 2 | 2	2 | 3 | 3	2 | 3 | 3	8 | 9 | 15

4.6.1.2. Snow Water Equivalent (SWE)

Similarly to SCA, SWE residuals increased with coarsening resolution in the aggregated scenarios. The 50 m (d) and 100 m (a) simulations were similar with total MAE and residuals that were less than 0.5mm and 0.6%, respectively, but the 750 m (a) simulation indicated total MAE and residuals as large as 40.8 mm and 40%, respectively. Residuals and total MAE were low in E2 with average residual of 3.7% over all the years. Residuals and total MAE generally increased with elevation from E2 to E4 (Figure 4.3 and Table 4.4). The largest residuals were in E1 with average residual of 11.6% over all the years, whereas the largest total MAE was in E4, which was due to the larger mean SWE in E4 than E1. Residuals were negligible and generally negative during RL, except in E4 whose residuals were generally positive. However, they were large during FL and were more pronounced in E3 and E4 than those in E1 and E2. Similar to the SCA results, residuals were positive in the beginning of FL, but they turned to negative residuals after the middle of FL. Residuals were larger in the average year with average residual of 6.8% over all the elevation bands than that of the wet and dry years with average residuals of 4.9% and 4.3%, respectively. As spatial resolution increased in the aggregated scenarios, larger variability in meteorological inputs neglected and caused larger SWE residuals, particularly in years and elevation bands when and where meteorological inputs variation and snow mass was large.

Residuals for the 100 m (d) scenario were as large as 66% and thus substantially larger than those in the 750 m (a) (Figure 4.3 and Table 4.4). Residuals were larger in E1 than E2, but total MAE was slightly larger in E2 than E1. Residuals and total MAE increased with elevation from E2 to E4. Residuals were negative, indicating substantial underestimation of SWE relative to the 50 m (d) simulation, except in the average and dry years in E1 and E2 where they were positive. Large residuals and MAE were observed in the wet year with average residual of 18.8% over the elevation bands. Residuals and total MAE in the average and dry years were less pronounced (with average residual of 9% and 10.1%, respectively) relative to the wet year. Distribution of inputs at 100 m led to substantial information loss in topography-induced heterogeneity of meteorological variables as topographic features changed by coarsening the DEM from 50 to 100 m. This substantial information loss in meteorological inputs spatial variability caused underestimation of snow mass, particularly in the wet year and E4 that snow mass was large.

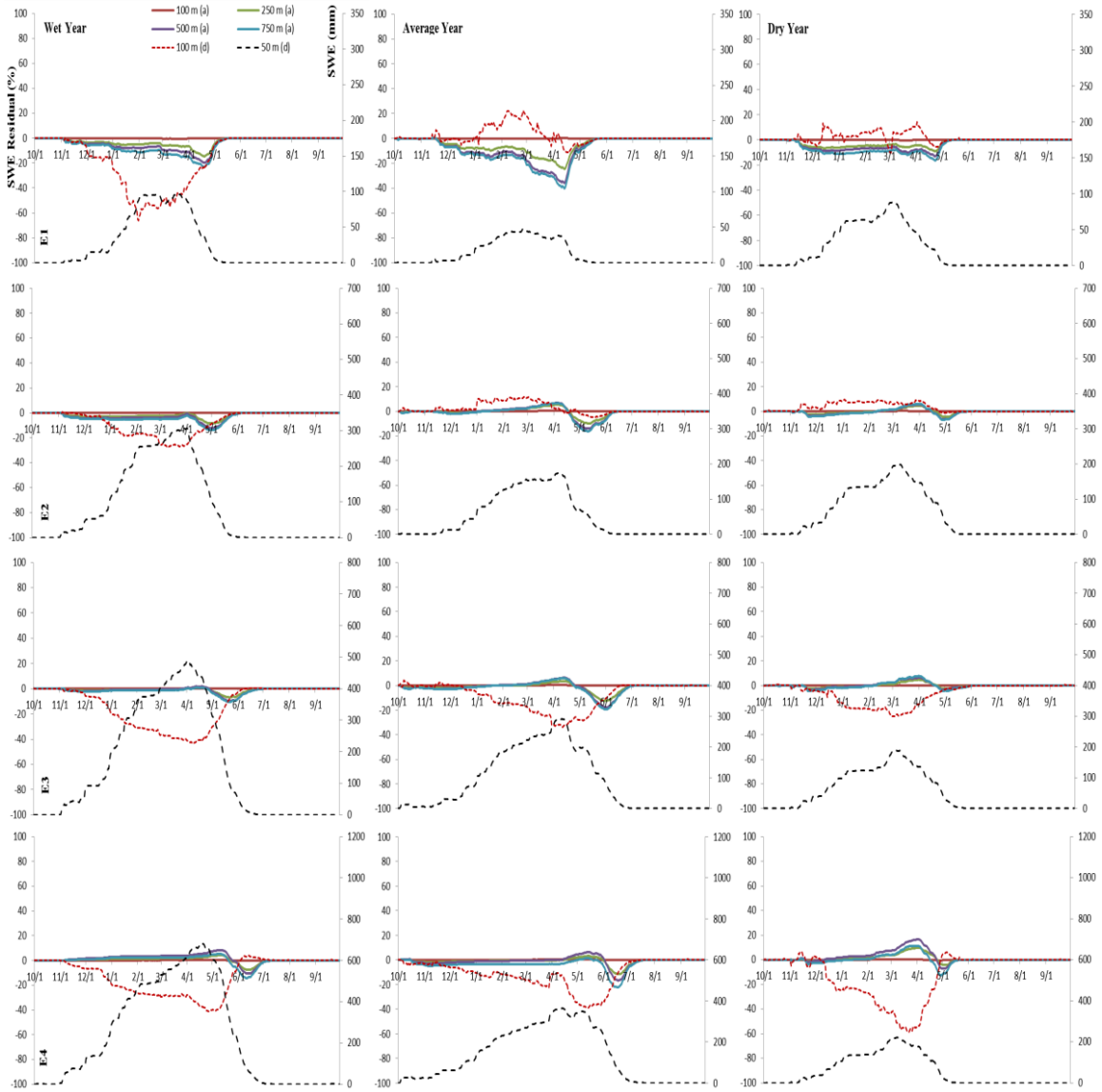

Figure 4.3. Aggregated estimated SWE over 4 elevation bands. Dotted lines show the 50 m (d) and 100 m (d) scenarios, but solid lines indicate the aggregated scenarios (from the 100 m (a) to 750 m (a)). Primary Y (left) axis shows residuals, the estimated SWE generated from all the scenarios minus that of the 50 m (d) scenario. Secondary Y (right) axis shows the estimated SWE from the 50 m (d) scenario.

Table 4.4. MAE for SWE in each band.

Bands	MAE (mm)	100 m (a)	250 m (a)	500 m (a)	750 m (a)	100 m (d)
E1	RL (Wet| Average| Dry)	0 | 0 | 0	2 | 1 | 2	3 | 2 | 3	4 | 2 | 4	14 | 2 | 2
	FL (Wet| Average| Dry)	0 | 0 | 0	3 | 3 | 2	5 | 4 | 3	6 | 5 | 4	10 | 1 | 2
	Total (Wet| Average| Dry)	0 | 0 | 0	2 | 2 | 2	3 | 3 | 3	4 | 4 | 4	13 | 2 | 2
E2	RL (Wet| Average| Dry)	0 | 0 | 0	3 | 1 | 1	5 | 1 | 1	6 | 1 | 1	17 | 3 | 4
	FL (Wet| Average| Dry)	0 | 0 | 0	5 | 4 | 2	8 | 5 | 3	9 | 6 | 3	13 | 1 | 3
	Total (Wet| Average| Dry)	0 | 0 | 0	4 | 2 | 1	6 | 2 | 2	7 | 2 | 2	16 | 3 | 4
E3	RL (Wet| Average| Dry)	0 | 0 | 0	2 | 1 | 1	2 | 2 | 1	3 | 2 | 1	46 | 12 | 9
	FL (Wet| Average| Dry)	0 | 0 | 0	5 | 6 | 2	8 | 8 | 2	8 | 9 | 3	38 | 17 | 7
	Total (Wet| Average| Dry)	0 | 0 | 0	3 | 3 | 1	4 | 4 | 2	5 | 4 | 2	43 | 13 | 8
E4	RL (Wet| Average| Dry)	0 | 0 | 0	3 | 2 | 1	7 | 2 | 2	5 | 6 | 1	48 | 17 | 15
	FL (Wet| Average| Dry)	0 | 0 | 0	8 | 6 | 4	13 | 9 | 7	14 | 10 | 6	39 | 34 | 25
	Total (Wet| Average| Dry)	0 | 0 | 0	5 | 3 | 2	9 | 5 | 4	8 | 7 | 3	45 | 23 | 19

4.6.1.3. What caused the observed discrepancies in the estimated SCA and SWE?

Homogenization of the spatial heterogeneity of energy fluxes caused the observed differences between the 50 m (d) and the aggregated scenarios. For instance, a 750 m area is composed by 225 50-m cells, each of them with a set of energy flux inputs. Thus, in the 50 m (d) scenario, 225 different sets of energy flux inputs were used to calculate the snow cover energy over a 750 m area, whereas only one energy flux is used in the 750 m (a) scenario. The use of different sets of energy flux inputs inside a 750 m area made the model capable of delineating areas that were preferable for snow accumulation, hereafter low energy 50 m cells, from those with preferable condition for snow ablation, hereafter high energy 50 m cells. These cells were neglected in the 750 m (a) scenario by using one set of energy flux inputs that were averaged over inputs of all 50 m cells inside a 750 m cell. During the accumulation periods (RL), disregarding high and low energy cells caused overestimation of SCA and underestimation of SWE in E1 to E3 and overestimation of SWE in E4 for the 750 m (a) scenario. At the beginning of the ablation periods (FL), snow ablation rate was underestimated in all elevation bands, which was indicated by the positive residuals of SCA and SWE, whereas snow ablation rate was overestimated from the middle of FL.

The differences between SCA and SWE from the 50 m (d) and 750 m (a) simulations were negligible from October 1st until November 20th, 2009 at the 750m-E2-cell. During this period at this cell, snow cover was formed at times, but it was completely ablated in a day or two because of undesirable condition for snow cover retention. On November 20th, snow cover was formed for the 50 m (d) simulation at some 50 m cells, low energy cells, inside the 750m -E2-cell, but snow was completely ablated during the course of the day for the 750 m (a) simulation at the 750m -E2-cell. This continued until November 24th and caused negative residuals in SWE for the 750 m (a) simulation. On November 24th, snow cover still did not formed at high energy 50 m cells inside the 750m -E2-cell, but formed for the 750 m (a) simulation and caused a positive residual in SCA for the 750 m (a) simulation (Figure 4.4 a). This positive residual in SCA became zero in the middle of the December when snow cover was formed at all 50 m cells within the 750m -E2-cell. However, magnitude of the negative residual (residual of 4 mm) in SWE remained almost constant for the rest of RL as snow accumulation and ablation rates were similar between estimated SWE from the 750 m (a) simulation at the 750m -E2-cell and that of the 50 m (d) simulation averaged over 50 m cells inside the 750m -E2-cell.

At the 750m -E4-cell, snow cover was formed for the 750 m (a) scenario and for the 50 m (d) scenario at all 50 m cells inside this cell, except at one 50 m cell, on October 26th, 2005 (Figure 4.4 b). This caused a negligible positive residual in SCA for the 750 m (a) simulation at the 750m -E4-cell. On this day, the difference between the estimated SWE from the 750 m (a) simulation and that of the 50 m (d) simulation averaged over all 50 m cells inside the 750m -E4-cell was a positive residual of only 0.2 mm. This positive residual continuously increased during RL and led to a positive residual of 59 mm in SWE by the time of SWE peak, which was April 26th, 2006. This was due to neglecting snow melt in the 750 m (a) simulation during RL at high energy cells, similar to the cell with zero SWE on October 26th, 2005 (Figure 4.4 b).

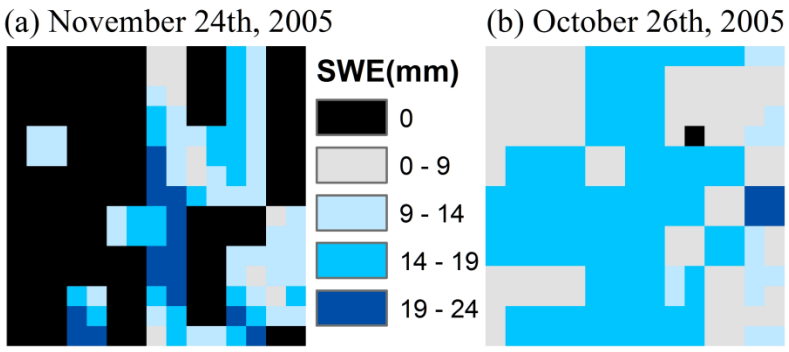

Figure 4.4. Sub-grid variability of SWE in (a) the 750m-E2-cell and (b) 750m-E4-cell.

On April 27th 2006, when ablation period was started, the positive residual of 59 mm in SWE for the 750 m (a) scenario was increased to 60.6 mm from the prior day in the 750m -E4-cell (Figure 4.5 a). On this day, the snow cover energy (ΔQ) of 17.5 W/m^2 was estimated for the 750 m (a) scenario for the 750m -E4-cell. The estimated snow cover energy ranged from 11.4 to 28.4 W/m^2 in the 50 m (d) scenario for 50 m cells inside the 750m -E4-cell with average of 20.1 W/m^2 over all the 50 m cells. As a result, SWI was estimated as large as 6 mm for the 50 m cells with average of 1.7 mm, whereas SWI of 0.1 mm was estimated for the 750 m (a) scenario for the 750 m (a)-E4-cell. This was due to neglecting energy fluxes at high energy cells. The positive residual in SWE for the 750 m (a) scenario continuously increased until snow started to melt at low energy cells. After initiation of melt at low energy cells, the positive residual decreased and eventually turned to a negative residual when snow was completely melted (zero SWE) at high energy cells. At the 750m-E4-cell, positive residual of 1.4 mm in SWE in the 750 m (a) scenario on June 19th, 2006 was turned to negative residual of 11.1 mm on June 20th. On this day, SWI of 27.5 mm was estimated for the 750 m (a) scenario, whereas averaged SWI over all the 50 m cells was 15 mm (Figure 4.5 b). Snow melt occurred only at low energy cells where the snow cover was still available and energy flux inputs of high energy cells had no contribution in reduction of SWE. However, energy flux inputs of high energy cells still had contribution in ablating snow in the 750 m (a) scenario, because energy flux inputs of all 50 m cells inside the 750m-E4-cell were aggregated to generate that of the 750 m (a) scenario. This continued to the end of FL and caused FL to be shorter in the 750 m (a) scenario than in 50 m (d) scenario.

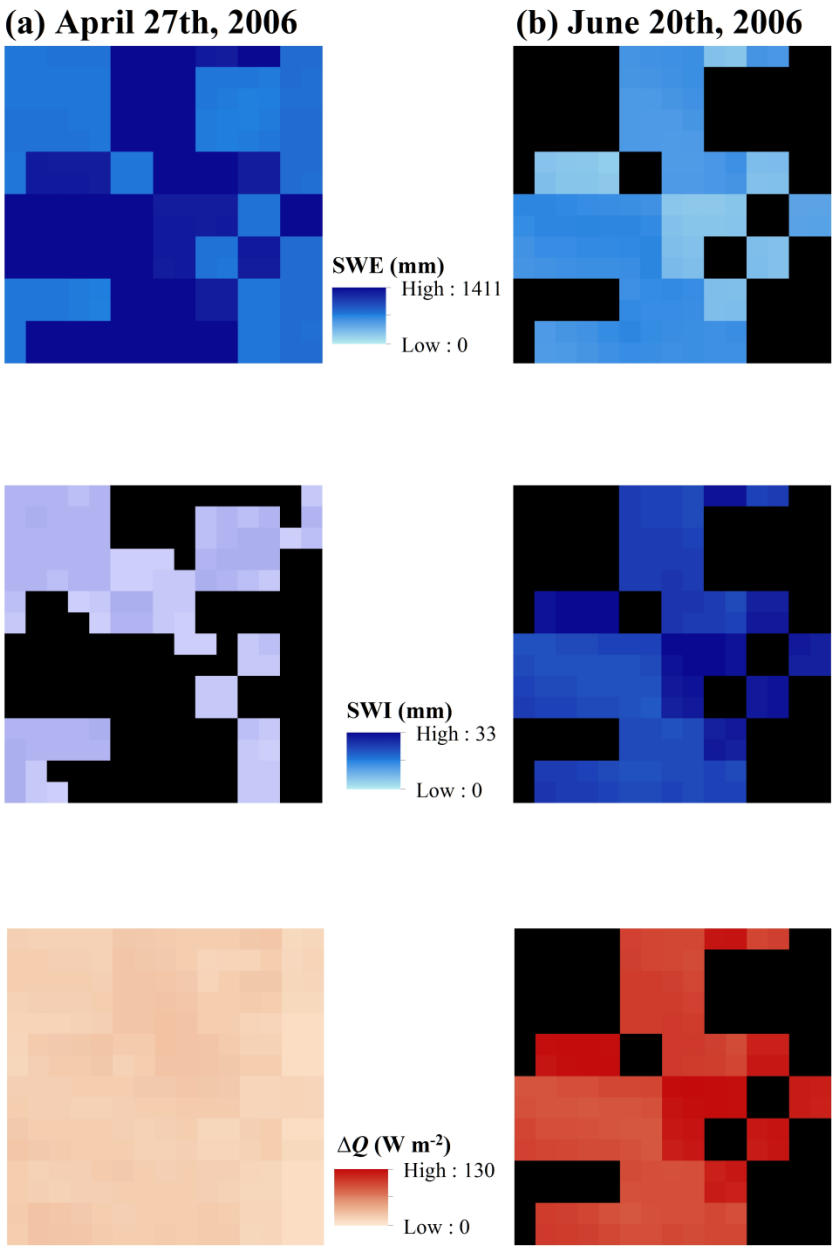

Figure 4.5. Sub-grid variability of SWE, SWEI and ΔQ in the 750m-E4-cell.

The differences between the 50 m (d) or 100 m (a) and 100 m (d) simulations were due to changes in topographic features such as slope, aspect, sky view factor and to some extent elevation. These topographic features changed, due to the coarsening the DEM from 50 m to 100 m resolution for the distributed case. For 50 m cells inside a 100 m cell, energy flux inputs were distributed using four different slopes, aspects, sky view factors and elevations. The effects of these topographic features on meteorological inputs were transferred by

aggregating the inputs to obtain 100 m resolution aggregated scenario (the 100 m (a) scenario). In the 100 m (a) simulation only variation of meteorological inputs at these four 50 m cells was lost, which had negligible impact on estimation of SCA and SWE. However, when inputs were distributed at 100 m, on top of overlooking meteorological inputs variation, variation in slope, aspect, sky view factor and elevation inside a 100 m cell were neglected.

As a result, the effects of these topographic features on meteorological inputs were lost in the 100 m (d) scenario and caused significant changes in snow cover properties prediction. Even in the 750 m (a) simulation, the effects of the topographic features on meteorological inputs were transferred through aggregation procedure. This is the reason for substantially larger residuals of SCA and SWE in the 100 m (d) simulation than that of the 750 m (a) simulations.

Difference between the estimated net radiations of the 50 m (d) and 100 m (d) scenarios was the main reason that caused the observed discrepancies between these scenarios. Changes in slope and aspect were responsible for estimating different net solar radiations in the 50 m (d) and 100 m (d). Changes in sky view factor and to some extent elevation caused the calculated thermal radiation to be different for these scenarios. Slope changes were substantially moderated in the 100 m DEM relative to the 50 m DEM. As a result, less pronounced slope breaks were observed, which in turn resulted in moderating the effect of wind-induced snow drifting. At hours that measured relative humidity had substantially different values at the observation sites, changes in elevation due to the use of different resolution of the DEM led to estimation of different relative humidity values, which cause different estimation of dew point temperatures for these scenarios. The net effect was an incorrect identification of precipitation phase or inaccurate estimation of precipitation temperature and snow density. Therefore, overlooking variation in topographic features resulted in negative residuals in SCA and SWE, except in the dry and average year in E1 and E2.

The 50 m DEM shows a ridge where the 100m-E3-cell is located with four 50m-cell having within 100m-E3-cell different slopes, aspects and elevations. This feature is not present in the 100 m DEM due to smoothing of the topography. Cell1 and cell2 inside the 100m-E3-cell (Figure 4.6 a) were southeast facing (with aspects of 99° and 113.3°, respectively), but cell3 and cell4 were northeast facing (with aspects of 48.5° and 44.5°, respectively). Cell1, cell2, cell3 and cell4 had slopes of 27.1%, 25.9%, 40.4% and 42.1% and their elevations were 2,282

m, 2,266 m, 2,278 m and 2,296 m, respectively. Sky view factor of cell1 was 0.95 and the other cells had sky view factor of 0.94. However, the 100m-E3-cell was east facing with aspect of 76.3° and slope, sky view factor and elevation of this cell was 25.6%, 0.76 and 2,281 m, respectively. As a result of these topographical changes, estimated net radiation in the 100 m (d) scenario was substantially larger than that of the 100 m (a) scenario during RL, which caused underestimation of snow accumulation in the 100 m (d) scenario. Net solar radiation of the 100 m (d) scenario was larger in the morning than that of the 100 m (a) (or 50 m (d); Figure 4.6 b). Due to this net solar radiation of the 100 m (d) was larger than that of the 100 m (a) during RL when solar angle is low and sun hour in the afternoon is short. In addition, the calculated thermal radiation in the 100 m (d) scenario was larger than that of the 100 m (a) scenario (Figure 4.6 c). During FL when sun angle is high and days are longer, net solar radiation of the 100 m (d) was lower than that of the 100 m (a) (Figure 4.6 d). This caused lower ablation rate in the 100 m (d) scenario relative to the 100 m (a) scenario. Similar to RL, the calculated thermal radiation in the 100 m (d) scenario was larger than that of the 100 m (a) scenario during FL (Figure 4.6 e).

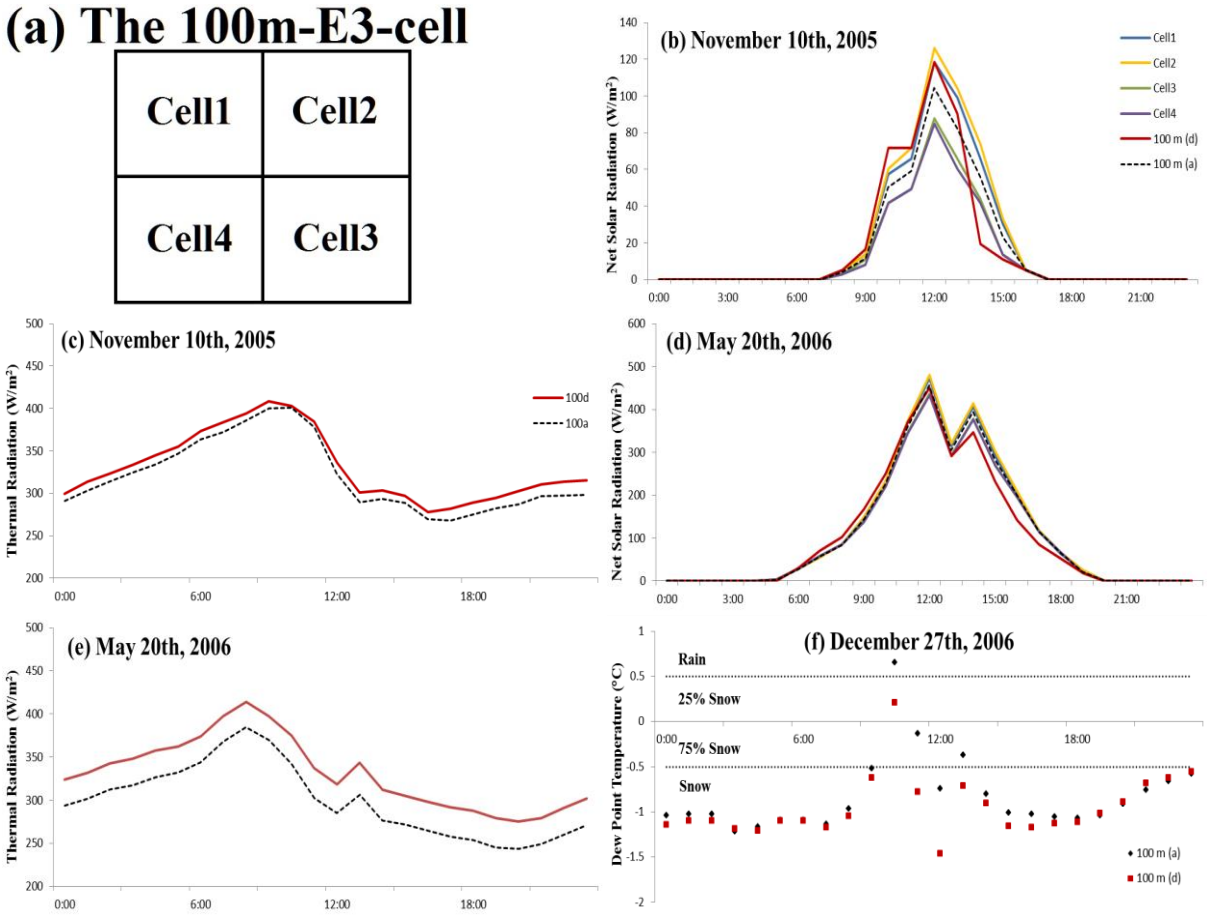

Figure 4.6. Differences in the estimated net solar and thermal radiations and dew point temperatures of the 50 m (d) or 100 m (a) scenarios and those of the 100 m (d) scenario. Figure a indicates establishment of 50 m cells inside the 100m-E3-cell. The estimated thermal radiation and dew point temperatures of the 50 m (d) and 100 m (a) were very similar.

Another reason that caused discrepancies between the 50 m (d) or 100 m (a) and 100 m (d) scenarios was inaccurate estimation of dew point temperatures. Differences in dew point temperatures of the 50 m (d) or 100 m (a) and 100 m (d) scenarios were in range of decimal degree. These small differences caused incorrect identification of precipitation phase at times when dew point temperatures fluctuated around freezing point. For instance, on December 27th, 2006 precipitation occurred during the entire day and difference between precipitation phase and temperature and snow density of the 100 m (a) and those of the 100 m (d) occurred from 10 am to 1 pm (Figure 4.6 f). At 10 am, precipitation phase was identified as a rainfall for the 100 m (a) scenario, whereas a mixed rain/snow event with 75% rain and 25% snow was estimated for the 100 m (d) scenario. Precipitation phase was estimated as snow for the

100 m (d) scenario for the rest of the day, but a mixed rain/snow event of 25% rain and 75% snow was estimated for the 100 m (a) scenario at 11 am and 1 pm. This was due to change in elevation and change in distance of grid of interest from the observation sites, which were weighting factors to distribute relative humidity.

In addition to net solar and thermal radiations, changes in wind-induced snow drifting, which is important during RL, was another reason that caused the observed discrepancies between the 50 m (d) or 100 m (a) and 100 m (d) simulations. Extent of the discrepancies in SCA and SWE estimations caused by changes in drifting varied based on vegetation and elevation (Figure 4.7). SCA and SWE estimations from the 100 m (d) scenario were very similar to those of the 100 m (d)-nodrift scenario in E2, representing negligible importance of wind-induced snow drifting in this elevation band. E2 vegetation cover was coniferous forest and in forested areas wind-induced snow drifting is negligible (Deems et al. 2006; Trujillo et al. 2007). E1 vegetation cover was mainly sagebrush and E3 vegetation cover was either sparse coniferous forest or bare rock. As a result, residuals in SCA and SWE during RL in the 100 m (d)-nodrift simulation were substantially lower than those of the 100 m (d) simulation in E1, E3 and E4. In SCA, the maximum residual during RL in E1 was reduced from 48.5% in the 100 m (d) simulation to 24.6% in the 100 m (d)-nodrift simulation with 4.8% reduction in MAE of RL. In E3 and E4, MAE of RL in SCA was reduced from 7.1% in the 100 m (d) simulation to 3.1% in the 100 m (d)-nodrift simulation. In SWE, MAE of RL in E3 and E4 was reduced from 48.3 mm in the 100 m (d) simulation to 37.2 mm in the 100 m (d)-nodrift simulation. In E1, MAE of RL in SWE in the 100 m (d)-nodrift simulation (7.7 mm) was about half of that of the 100 m (d) simulation (14.4 mm).

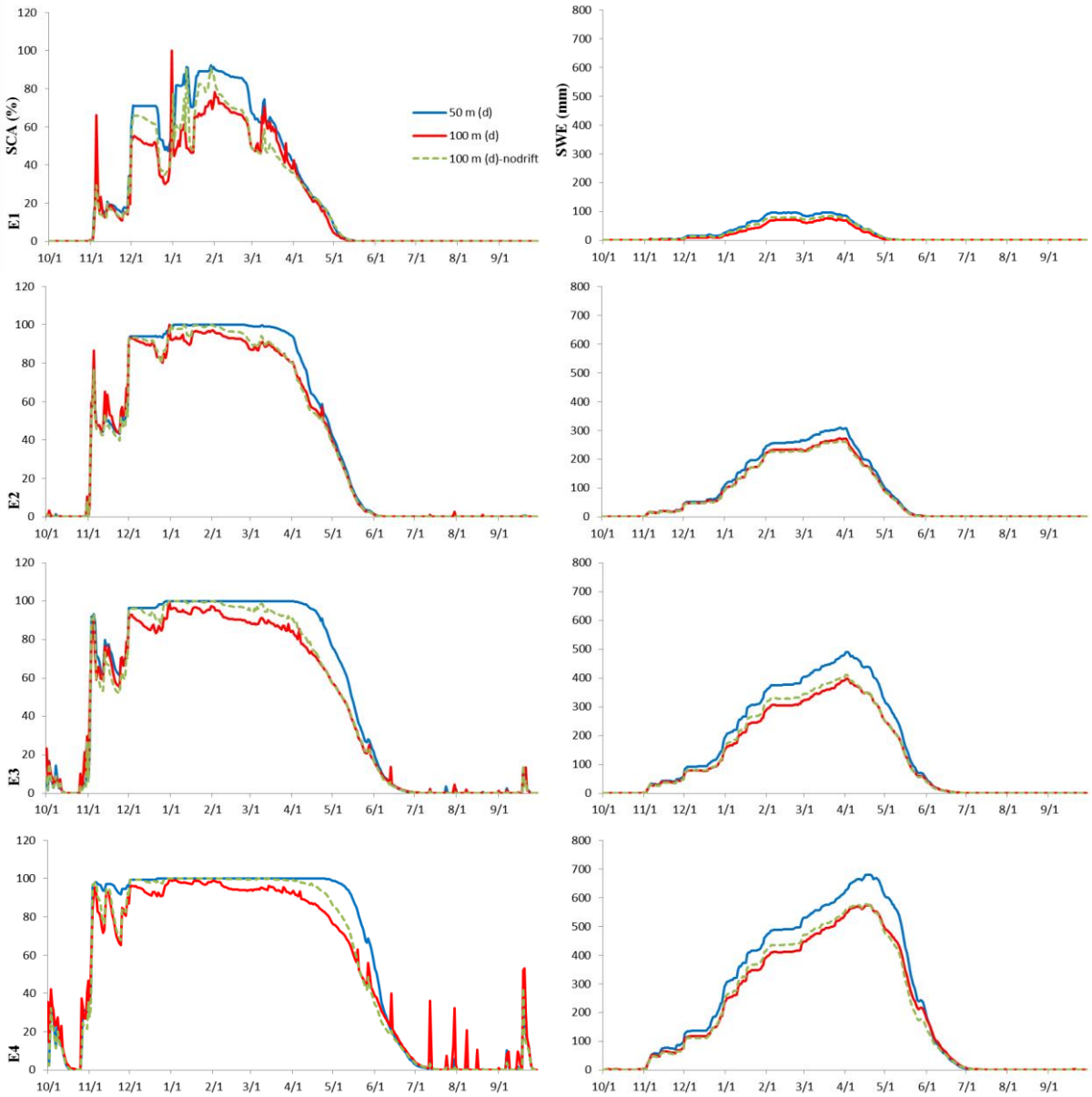

Figure 4.7. The scaling effect on the estimation of SCA and SWE once the effect of scaling on wind-induced snow drifting was remove. The left column indicates the estimated SCA and the right column shows the estimated SWE for the 50 m (d) (solid blue line), 100 m (d) (solid red line) and 100 m (d)-nodrift (dotted green line) for the wet year over all the elevation bands.

In agreement with the results of Winstral et al. (2014), our results related to the aggregated scenarios indicated negligible residuals in the 100 m (a) scenario (residuals of less than 2% in SCA and less than 0.6% in SWE) over all the years and elevation bands. Residuals increased as resolution coarsened. Negligible residuals were observed during accumulation period (RL), but residuals were large during FL, particularly for the 500 m (a) and 750 m (a). This was due

to increase in spatial variation of energy fluxes during FL as a result of an increase in sun angle (Winstral et al. 2014). Residuals in SCA and SWE were large in the low elevation band, E1, because in this band snow cover area is very sensitive to spatial variation in energy fluxes (Howat and Tulaczyk 2005; Scherrer and Appenzeller 2004). The largest differences between the estimated SCA and SWE from the 50 m (d) and that of the aggregated scenarios were observed in the average year. Because spatial variability of the energy fluxes might be larger in the average year than the wet year due to lower humidity and fewer cloudy days (Aguado and Burt 2013; Rohli and Vega 2008) and precipitation mass was larger than the dry year.

This work found substantial underestimation in SCA and SWE as model spatial resolution coarsened from 50 m (50 m (d) scenario) to 100 m (100 m (d) scenario). The underestimation in SCA and SWE was caused by overestimation of net radiation and moderating wind-induced snow drifting. Coarsening of the DEM from 50 m to 100 m resulted in flattening of slopes, aspects and elevation and changes in sky view factors (Kok and Ramli 2007; Wu et al. 2008). This led to overestimation of radiation receipt, which in turn resulted in overestimation of net radiation and consequently overestimation of snow melt during accumulation period (Chen et al. 2013; Hopkinson et al. 2010). Reduction of wind-induced snow drifting was another reason for underestimation in SCA and SWE in non-forested regions, in agreement with previous works (Luce et al. 1998; Luce et al. 1999). Wind-induced snow drifting reduced because slopes were flattened in the 100 m DEM and less slope breaks were, thus, detected relative to the 50 m DEM (Deems et al. 2006). In contrast with Luce et al. (1998), this work found that topography-induced spatial variation of net radiation is more important than spatial information of snow drifting in estimation of SCA and SWE. Luce et al. (1998) used 30 m scale and found that spatial information of snow drifting as or more important than spatial variation of net radiation in their studied watershed. Snow drifting can be as important as spatial variation in net radiation for finer than 50 m scale where slope substantially changes over small distances. SCA and SWE were overestimated in the 100 m (d) simulation relative to the 50 m (d) simulation in the average and dry years in E1 and E2. In the average and dry years, differences between recorded relative humidity at observation sites were large as spatial variation in relative humidity is larger in these years than the wet year. This accompanied by changes in interpolation weighting factors due to coarsening the DEM to 100 m caused underestimation of dew point temperatures in the 100 m (d) scenario relative to the 50 m. In

E1 and E2 where dew point temperatures fluctuate around the freezing point during RL, underestimation of dew point temperatures even in range of decimal degree can cause misidentification of precipitation phase. As a result, snow mass was overestimated in the 100 m (d) simulation relative to the 50 m (d) simulation. The largest residual in SCA and SWE in the 100 m (d) scenario was observed in E4 where precipitation mass was larger than the other elevation bands. The dry year had the largest residual in SCA. In this year, net radiation overestimation caused snow cover that was just formed completely ablated in the course of a day in the 100 m (d) simulation at about 13% of cells in E4. However, SCA of 100% was estimated in the 50 m (d) simulation during RL for this band. The largest residual in SWE was related to the wet year with average residual of 18.8%. Precipitation mass was larger in this year than the dry and average years. As a result, net radiation overestimation and moderating wind-induced snow drifting caused larger residuals in snow mass estimation in the 100 m (d) simulation in the wet year than the dry and average years.

These results on the effect of input spatial resolution on snow modeling would be similar in any other process-based models. However, the magnitude of these effects may be different in other snow models because some models cannot provide consistently good performance for various climate conditions and vegetation and topographic settings. This is because these models do not take into account density and albedo of snow and storage of liquid water within snow (Essery et al. 2013), whereas iSnobal tracks changes in these parameters during a snow season. The elevation bands that indirectly define precipitation regimes in this work may be different in other regions depending on the latitude and regional climatology (Kormos et al. 2014b; Korner 1998).

4.7. Conclusions

This investigation demonstrated that model accuracy not only depends on model scale but also on climate conditions and elevation distribution, which modulate the distribution of errors within watersheds. Our results supported our hypothesis and showed inputs of 50 m or finer resolutions are necessary because coarser resolutions lose important topography-induced spatial variation in meteorological inputs by smoothing the topography, which has altered

slope, aspect, sky view factor and to some extent elevation. However, the usage of finer than 250 m resolution inputs generated from aggregation of fine scale (50m or finer) inputs has negligible effects on prediction accuracy because information from the finer scale transfer to the aggregated model. This does not occur when data are distributed at coarser than 50m scale. Modelers select coarse resolutions to reduce modeling costs such as runtime and storage space. Whereas the distribution of inputs on a coarse scale reduces modeling costs, the usage of coarse inputs generated from aggregating fine scale inputs only slightly reduces modeling costs, because distributing inputs at a fine scale is the procedure that mainly increases modeling costs rather than running a snow model.

In mountainous settings, distribution of inputs at coarser than 50 m scales is affected by the homogenization of the heterogeneity of topographic features. This smoothing effect causes underestimation of snow cover area and snow mass because of net radiation overestimation, misidentification of precipitation phase and moderation of wind-induced snow drifting. Net radiation is overestimated in all 4 elevation bands, whereas misidentification of precipitation phase occurs in rain-dominated and rain-snow transition regions and the snow drifting effect is reduced in sparse-forested or non-forested regions like above alpine treeline. The amount of error generally increases with elevation because of two effects: (1) low elevations are rain-dominate; and (2) topographical heterogeneity increases with elevation. This suggests that finer than 50m cell should be used at all elevations in watersheds where snow-dominated elevation bands control the hydrology.

Climatic conditions modulate the error induced by scale and elevation band. Effect of misidentification of precipitation phase on SCA and SWE estimation is noticeable in average and dry years, when spatial variability of relative humidity is high. However, the effects of net radiation overestimation and snow drifting reduction on SCA and SWE estimation are substantially large in wet years because of large snow mass. Prediction of SCA is considerably impacted in dry years when accurate estimation of snow cover energy is necessary for snow cover retention due to a low number of precipitation events. In wet years, when snow mass is large, net radiation overestimation and moderation of wind-induced snow drifting cause substantial underestimation of SWE. In average years, prediction of SCA is less impacted than dry years and prediction of SWE is less affected than wet years.

4.8. References

Aguado, E., and Burt, J. E. (2013). *Understanding Weather and Climate*, Pearson.

Beniston, M. (2012). "Is snow in the Alps receding or disappearing?" *WIREs Climate Change (Wiley Interdisciplinary Reviews / Climate Change)*, DOI:10.1002/wcc.179.

Bloschl, G. (1999). "Scaling issues in snow hydrology." *Hydrological Processes*, 13, 2149-2175.

Chen, X., Su, Z., Ma, Y., Yang, K., and B.Wang. (2013). "Estimation of surface energy fluxes under complex terrain of Mt. Qomolangma over the Tibetan Plateau." *Hydrol. Earth Syst. Sci.*, 17, 1607–1618.

Cline, D., Elder, K., and Bales, R. (1998). "Scale e€ ects in a distributed snow water equivalence and snowmelt model for mountain basins." *Hydrological Processes*, 12, 1527-1536.

Darmody, R. G., Thorn, C. E., Shlyter, P., and Dixon, J. C. (2004). "Relationship of vegetation distribution to soil properties in Karkevagge, swedish lapland." *Arctic, Antarctic and Alpine Research*, 36(1), 21-32.

Deems, J. S., Fassnacht, S. R., and Elder, K. J. (2006). "Fractal Distribution of Snow Depth from Lidar Data." *Journal of Hydrometeorology*, 7(2), 285-297.

Elder, K., Dozier, J., and Michaelse, J. (1991). "Snow Accumulation and Distribution in an Alpine Watershed." *Water Resources Research*, 27(7), 1541-155.

Essery, R., Morin, S., Lejeune, Y., and Ménard, C. B. (2013). "A comparison of 1701 snow models using observations from an alpine site." Advances in Water Resources, 55, 131–148.

Garen, D. C., and Marks, D. (2005). "Spatially distributed energy balance snowmelt modelling in a mountainous river basin: estimation of meteorological inputs and verification of model results." *Journal of Hydrology*, 315, 126-153.

Gu, R., McCutcheon, S., and Chen, C.-J. (1999). "Development of weather-dependent flow requirements for river temperature control." *Environmental Management*, 24(4), 529-540.

Homan, J. W., Luce, C. H., McNamara, J. P., and Glenn, N. F. (2010). "Improvement of distributed snowmelt energy balance modeling with MODIS-based NDSI-derived fractional snow-covered area data." *Hydrological Processes*, 25, 650–660.

Hopkinson, C., Chasmer, L., Munro, S., and Demuth, M. N. (2010). "The influence of DEM resolution on simulated solar radiation-induced glacier melt." *Hydrological Processes*, 24, 775–788.

Howat, I. M., and Tulaczyk, S. (2005). "Climate sensitivity of spring snowpack in the Sierra Nevada." *Journal of Geophysical Research*, 110, F04021.

Keller, F., Goyette, S., and Beniston, M. (2005). "Sensitivity analysis of snow cover to climate change scenarios and their impact on plant habitats in alpine terrain." *Climate Change*, 72, 299–319.

Kok, C. L., and Ramli, M. F. (2007). "Scale factor and digital elevation analysis for hydrological studies." *Journal of Environmental Hydrology*, 15, 1-12.

Kormos, P. R., Marks, D., McNamara, J. P., Marshall, H. P., Winstral, A., and Flores, A. N. (2014a). "Snow distribution, melt and surface water inputs to the soil in the mountain rain–snow transition zone." *Journal of Hydrology*, 519, 190-204.

Kormos, P. R., Marks, D., Williams, C. J., Marshall, H. P., Aishlin, P., Chandler, D. G., and McNamara, J. P. (2014b). "Soil, Snow, Weather, and Sub-Surface Storage Data from a Mountain Catchment in the Rain–Snow Transition Zone." *Earth System Science Data*, 6, 165–173.

Korner, C. (1998). "A re-assessment of high elevation treeline positions and their explanation." *Oecologia* 115, 445-459.

Kumar, M., Marks, D., Dozier, J., Reba, M., and Winstral, A. (2013). "Evaluation of distributed hydrologic impacts of temperature-index and energy-based snow models." *Advances in Water Resources*, 56, 77-89.

Link, T. E., and Marks, D. (1999). "Distributed simulation of snowcover mass- and energybalance in the boreal forest." *Hydrological Processes*, 13, 2439–52.

Liston, G. E. (2004). "Representing Subgrid Snow Cover Heterogeneities in Regional and Global Models." *Journal of Climate*, 17(6), 1381-1397.

Liston, G. E., and Elder, K. (2006). "A Distributed Snow-Evolution Modeling System (SnowModel)." *Journal of Hydrometeorology*, 7(6), 1259–1276.

Luce, C., Staab, B., Kramer, M., Wenger, S., Isaak, D., and McConnell, C. (2014). "Sensitivity of summer stream temperatures to climate variability in the Pacific Northwest." *Water Resources Research*, 50(4), 3428–3443.

Luce, C. H., and Tarboton, D. G. (2004). "The application of depletion curves for parameterization of subgrid variability of snow." *Hydrological Processes*, 18, 1409–1422.

Luce, C. H., Tarboton, D. G., and Cooley, K. R. (1998). "The influence of the spatial distribution of snow on basin-averaged snowmelt." *Hdrological Processes*, 12, 1671-1683.

Luce, C. H., Tarboton, D. G., and Cooley, K. R. (1999). "Sub-grid parameterization of snow distribution for an energy and mass balance snow cover model." *Hydrological Processes*, 13, 1921-1933.

Marks, D. (1988). "Climate, energy exchange, and snowmelt in Emerald Lake watershed, Sierra Nevada," Ph.D., University of California: Santa Barbara, CA.

Marks, D., Domingo, J., Susong, D., Link, T., and D.Garen. (1999). "A spatially distributed energy balance snowmelt model for application in mountain basins." *Hydrological Process* 13, 1935-1959.

Marks, D., Winstral, A., Reba, M., Pomeroy, J., and Kumar, M. (2013). "An evaluation of methods for determining during-storm precipitation phase and the rain/snow transition elevation at the surface in a mountain basin." *Journal of Advances in Water Resources*, 55, 98-110.

Meromy, L., Molotch, N. P., Link, T. E., Fassnacht, S. R., and Rice, R. (2013). "Subgrid variability of snow water equivalent at operational snow stations in the western USA." *Hydrological Processes*, 27, 2383–2400.

Molotch, N. P., and Bales, R. C. (2005). "Scaling snow observations from the point to the grid element: Implications for observation network design." *Water Resources Research*, 41, W11421.

Moriasi, D. N., Arnold, J. G., Liew, M. W. V., Bingner, R. L., Harmel, R. D., and Veith, T. L. (2007). "Model evaluation guidelines for systematic quantification of accuracy in watershed simulations." *Transactions of the ASABE*, 50(3), 885-900.

Nitaa, T., Yoshimura, K., Takata, K., O'ishi, R., Sueyoshi, T., Kanae, S., Oki, T., Abe-OuchI, A., and Liston, G. E. (2014). "Representing Variability in Subgrid Snow Cover and Snow Depth in a Global Land Model: Offline Validation." *Journal of Climate*, DOI: 10.1175/JCLI-D-13-00310.1.

Niu, G.-Y., and Yang, Z.-L. (2007). "An observation-based formulation of snow cover fraction and its evaluation over large North American river basins." *Journal of Geophysical Research*, 112, D21101.

Pohl, S., and Marsh, P. (2006). "Modelling the spatial–temporal variability of spring snowmelt in an arctic catchment." *Hydrol Processes*, 20, 1773–1792.

Pohl, S., Marsh, P., and Liston, G. E. (2006). "Spatial-Temporal Variability in Turbulent Fluxes during Spring Snomelt." *Arctic, Antarctic and Alpine Research*, 38(1), 136-146.

Raleigh, M. S., and Lundquist, J. D. (2012). "Comparing and combining SWE estimates from the SNOW-17 model using PRISM and SWE reconstruction." *Water Resour Manage*, 48, W01506.

Rohli, R. V., and Vega, A. J. (2008). "The climate system: controls on climate." Climotology, Jones and Bartlett Publishers, 30-60.

Scherrer, S. C., and Appenzeller, C. (2004). "Trends in Swiss Alpine snow days: The role of local- and large-scale climate variability." *Geophysical Research Letters*, 31, L13215.

Schimel, J. P., Bilbrough, C., and Welker, J. M. (2004). "Increased snow depth affects microbial activity and nitrogen mineralization in two Arctic tundra communities." *Soil Biology & Biochemistry*, 36, 217-227.

Sensoy, A., Sorman, A. A., Tekeli, A. E., Sorman, A. U., and Garen, D. C. (2006). "Point-scale energy and mass balance snowpack simulations in the upper Karasu basin, Turkey." *Hydrological Processes*, 20, 899–922.

Sohrabi, M., Ryu, J., Abatzoglou, J., and Tracy, J. (2015). "Development of Soil Moisture Drought Index to Characterize Droughts." *J. Hydrol. Eng.*, DOI: 10.1061/(ASCE)HE.1943-5584.0001213.

Sohrabi, M. M., Benjankar, R., Tonina, D., Kumar, M., Marks, D., and Kormos, P. (In Preparation). "Role of temporal resolution of meteorological inputs on process-based snow modeling."

Sohrabi, M. M., Ryu, J., Abatzoglou, J., and Tracy, J. (2013). "Climate extreme and its linkage to regional drought over Idaho." *Natural Hazards*, 65(1), 653-681.

Susong, D., Marks, D., and Garen, D. C. (1999). "Methods for developing time-series climate surfaces to drive topographically distributed energy- and water-balance models." *Hydrol Proc*, 13, 2003-2021.

Torp, M. (2010). "The effect of snow on plants and their interactions with herbivores," PhD, Umeå University, Umeå

Trujillo, E., Ramı´rez, J. A., and Elder, K. J. (2007). "Topographic, meteorologic, and canopy controls on the scaling characteristics of the spatial distribution of snow depth fields." *Water Resources Research*, 43, W07409.

Webb, B. W., Clack, P. D., and Walling, D. E. (2003). "Water–air temperature relationships in a Devon river system and the role of flow." *Hydrological Processes*, 17, 3069–3084.

Weill, S., Altissimo, M., Cassiani, G., Deiana, R., Marani, M., and Putti, M. (2013). "Saturated area dynamics and streamflow generation from coupled surface–subsurface simulations and field observations." *Advances in Water Resources*, 59, 196-208.

Winstral, A., Elder, K., and Davis, R. E. (2002). "Spatial Snow Modeling of Wind-Redistributed Snow Using Terrain-Based Parameters." *Journal of Hydrometeorology*, 3, 524–538.

Winstral, A., and Marks, D. (2002). "Simulating wind fields and snow redistribution using terrain-based parameters to model snow accumulation and melt over a semi-arid mountain catchment." *Hydrological Processes*, 16, 3585–3603.

Winstral, A., Marks, D., and Gurney, R. (2009). "An efficient method for distributing wind speeds over heterogeneous terrain." *Hydrological Processes*, 23, 2526–2535.

Winstral, A., Marks, D., and Gurney, R. (2013). "Simulating wind-affected snow accumulations at catchment to basin scales." *Advances in Water Resources*, 55, 64-79.

Winstral, A., Marks, D., and Gurney, R. (2014). "Assessing the Sensitivities of a Distributed Snow Model to Forcing Data Resolution." *Journal of Hydrometeorology*, 15, 1366–1383.

Wu, S., Li, J., and Huang, G. H. (2008). "A study on DEM-derived primary topographic attributes for hydrologic applications: Sensitivity to elevation data resolution." *Applied Geography*, 28(3), 210-223.

Chapter 5. Reflection of Estimated Surface Water Input Inaccuracy Caused By Inputs Resolution on Streamflow and Stream Temperature Predictions Given Groundwater Role in A Mountainous Watershed

5.1. Abstract

Water management, from energy production to aquatic habitat quality assessment, uses integrated hydrological modeling to predict water quantity, temperature and timing. Although model prediction accuracy depends on spatial and temporal resolutions of meteorological inputs, few works have assessed the impact of these resolutions on predicted hydrological responses, particularly in large mountainous watersheds and under different climate conditions. This work main objective is to quantify the role of spatial and temporal resolutions of meteorological inputs on predicted quantity, timing and temperature of streamflow given the watershed area and climate conditions. To address this objective, a physics-based snow model, iSnobal, was run with hourly inputs distributed at 50 and 100m resolutions and with aggregated inputs from the 50m resolution to 100m, 250m, 500m and 750m resolution for wet, average and dry years. ISnobal was also run with 3-hourly and 6-hourly inputs aggregated from hourly inputs. Estimated SWI from these scenarios were used to run Penn State Integrated Hydrology Model and the Stream Water Temperature Model to estimate streamflow and stream temperature at Anderson Ranch Dam (2,490 km^2). The results indicated that inputs spatial resolution was more important than temporal resolution in streamflow estimations. Coarse inputs spatial resolutions aggregated from 50m resolution had negligible effects on streamflow estimations. However, inputs distributed at 100m resolution showed the largest inaccuracy in streamflow predictions, which reduced as watershed area increased. In watersheds larger than 800 km^2, all spatial and temporal resolution scenarios indicated similar streamflow estimations due to the groundwater buffering effect. However, in watersheds smaller than 300 km^2, using coarse spatial and temporal resolutions of inputs caused inaccurate streamflow estimations, whose magnitude depended strongly on climate conditions and the watershed surface cover, which impact the groundwater buffering effect. Our results show that only fine temporal hourly and spatial (50m) provide consistent

streamflow modeling performance among climatic conditions. All the inputs spatial and temporal resolutions investigated in this work are sufficient input scales to provide streamflow estimations for stream temperature modeling.

Keywords: *Integrated hydrologic modeling, Watershed scale, Surface water input, streamflow, stream temperature, spatial and temporal resolution*

5.2. Introduction

Discharge is one of the most important hydrologic variables because it indicates changes in hydrological, geological and climatological cycles over a watershed (Choo et al. 2015; Dingman and Bjerklie 2006). Accurate discharge estimations are necessary for flood forecasting, water resource planning and management, reservoir operation, river restoration and ecological studies (Smith and Pavelsky 2008; Smith et al. 2014). Availability of discharge estimations can also improve the prediction accuracy of stream water temperature (Luce et al. 2014; Piccolroaz et al. 2016; Vliet et al. 2011), which is of high importance in ecological studies, restoration of rivers and aquatic habitats. Stream water temperature plays an important role in aquatic ecosystems and is a critical cue for organism behavior (Isaak et al. 2012; Jobling 1997; Rice et al. 1983; Rieman et al. 2007), fish metabolism (Forseth and Jonsson 1994; Isaak et al. 2015; Mesa et al. 2013; Railsback and Rose 1999) and growth rates (Brett 1979; Crozier et al. 2010; Xu et al. 2010). These indicate the value of accurate daily discharge and stream temperature estimates for dam and water resource managers, ecologists, economists and decision makers.

Hydrologic models are sensitive to the distribution of precipitation data (Ajami et al. 2004; Wang et al. 2015) and this sensitivity varies from one watershed to another as catchments respond differently to a precipitation event (Choo et al. 2015; Segond et al. 2007; Viglione et al. 2010b). Accurate discharge estimations for watersheds with complex topography and rugged terrain, which causes a pronounced precipitation spatial disparity, depend strongly on accuracy and detailed spatial information of precipitation (Ahl et al. 2008; Viglione et al.

2010a). Several previous studies showed that the use of detailed spatial information of precipitation increases discharge prediction accuracy in such watersheds (Ajami et al. 2004; Haddeland et al. 2002; Lobligeois et al. 2014; Smith et al. 2004). Boyle et al. (2001) concluded that detailed spatial information of precipitation improves estimation of peak rather than base flow.

In addition to the detailed spatial information of precipitation, the distribution, timing and magnitude of surface water input (SWI), which is combination of snow melt, rain on snow and rain on bare ground, are necessary for hydrologic modeling in mountainous watersheds (Ahl et al. 2008; Kormos et al. 2014; Liston and Elder 2006; Weill et al. 2013). In such watersheds, precipitation is accumulated as snow in winter and the accumulated water is released in spring and early summer. In these watersheds, not only precipitation, but also snow accumulation and ablation are highly heterogeneous due to changes of elevation, slope, aspect and vegetation over small distances (Elder et al. 1991; Marks et al. 2013; Trujillo et al. 2012; Winstral et al. 2013). This adds more complexity to hydrologic modeling of mountainous watersheds, where accurate estimations of snow accumulation and ablation are required for modeling in addition to the hydro-meteorological and geological processes that are calculated for rain dominated watersheds (Chen et al. 2016; Piccolroaz et al. 2016; Toffolon and Piccolroaz 2015; Winstral et al. 2014).

Our previous works showed the dependence of accurate snow cover area (SCA) and snow water equivalent (SWE) estimations on spatial and temporal resolutions of meteorological inputs (Sohrabi et al. In Preparation-a; Sohrabi et al. In Preparation-b). Changes in SCA and SWE caused by different spatial and temporal scenarios are expected to be reflected in the distribution, timing and magnitude of SWI, which is the source of water for streamflow. Comparing estimated streamflow and stream temperatures generated from estimated SWI from these scenarios to those of the observed is a reliable quantitative metric to evaluate accuracy of the SWI estimations (Luce et al. 1998). To do this, an integrated hydrological modeling framework is required, in which snow, streamflow and stream temperature models are coupled.

The advances in numerical modeling and the computational power of computers have increased the application of integrated hydrologic modeling frameworks, which helps to link

changes in meteorological variables with physical hydrologic processes (Merenlender and Matella 2013; Null et al. 2010). In such frameworks, the use of fine spatial and temporal resolutions of meteorological inputs substantially increases modeling costs such as runtime and storage space, especially in large watersheds. While, coarse-resolution of inputs reduces modeling costs, it comes at the in expense of prediction accuracy, whose reduction is not well known. There are still knowledge gaps on the effect of inputs resolution on integrated hydrologic modeling in mountainous watershed, as previous works merely addressed the impact of precipitation resolution on streamflow modeling over rain-dominated watersheds (Ajami et al. 2004; Boyle et al. 2001; Haddeland et al. 2002; Viglione et al. 2010a; Viglione et al. 2010b). Because precipitation occurred mainly in the form of rain in their studied watershed it was not necessary to use an integrated hydrologic modeling framework for these works. Therefore, there is still a need to understand and quantify the reduction in prediction accuracy due to inputs resolution in integrated hydrologic modeling in mountainous watersheds, particularly (a) in large mountainous watersheds, where hydrological characteristics vary from rain dominated to snow dominated (Winstral et al. 2014); (b) under different climate conditions such as wet, average and dry years, when catchments respond differently to a melt event (Rosenberg et al. 2013); and (c) in watersheds with different drainage area and geology (surface cover) where the contribution of hydrological processes such as runoff and groundwater to streamflow generation varies (Frisbee et al. 2011; Miller et al. 2016; Orlova and Branfireun 2014) and this may change the dependency of streamflow estimations to SWI.

To fill these knowledge gaps and understand the appropriate resolution of inputs in an integrated hydrologic modeling framework in mountainous watersheds, this work addresses these specific objectives: (1) quantifying the effect of the observed inaccuracy in SCA and SWE caused by the use of different spatial and temporal scenarios on streamflow and stream temperatures estimations for various climatic conditions. As a result, these inaccuracies can be described in terms of their influence on estimation of peak flows and summer's high stream temperatures in wet, average and dry years; and (2) quantifying the effect of inaccuracy in SWI on streamflow, groundwater level and stream temperature estimations with regard to climate conditions and the watershed size. The main hypotheses of this work are: (a) groundwater dominated systems that are less impacted by inaccuracy in surface water input

(SWI) because of the temporary storage of water in the ground; and (b) the larger the system the less depends on SWI due to groundwater buffering and the buffering effect of groundwater is a function of climate conditions and the watershed surface cover.

5.3. Study Area

The upper section of the South Fork of the Boise River (SFB), with drainage area of 2490 km^2 at Anderson Ranch Dam closure point, was selected for the integrated hydrological modeling (Figure 5.1). This watershed is not regulated and has a wide range of elevations, from rain dominated (1,174 m) to snow dominated above alpine (3,100 m). This helps to evaluate the effect of the observed inaccuracy in SCA and SWE in all the elevation bands regarding the estimation of streamflow and stream temperature. Streamflow is measured at the dam and at Featherville. Stream temperature is also measured at Featherville.

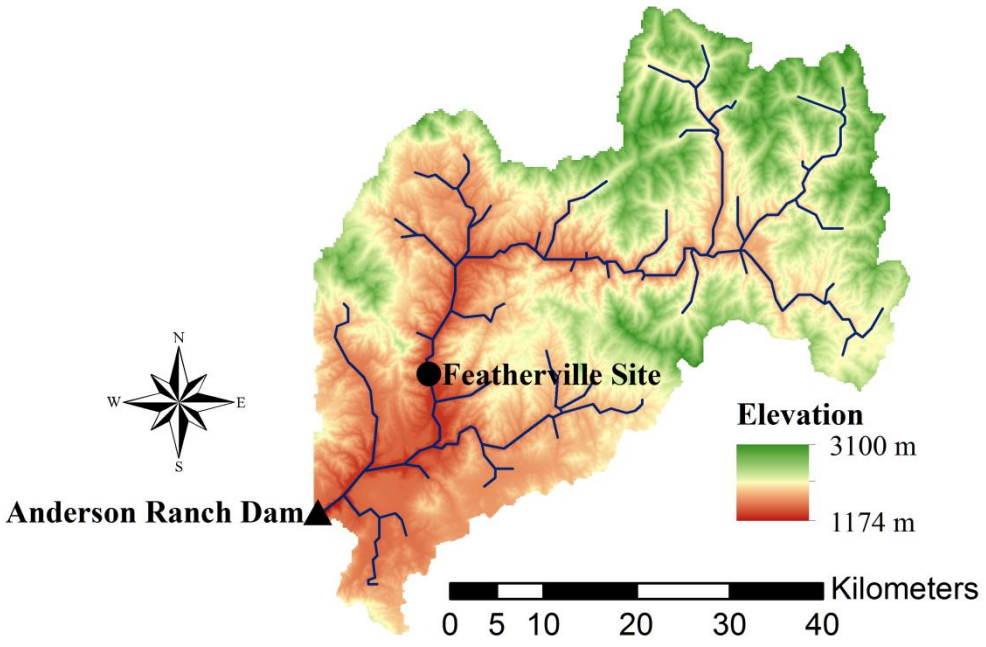

Figure 5.1. River network and DEM of the study area.

5.4. Method

To route runoff from the watershed to tributary confluences and estimate daily mean streamflow, a process-based snow model, iSnobal, was coupled with the Penn State Integrated Hydrology Model (PIHM; Figure 5.2). To do this distributed SWI generated from iSnobal was used instead of precipitation and the temperature index snowmelt tool in PIHM was switched off in the source code. Daily mean streamflow estimations were then fed along with daily mean air temperatures to a stream water temperature model, SWTM, to estimate daily mean stream temperatures.

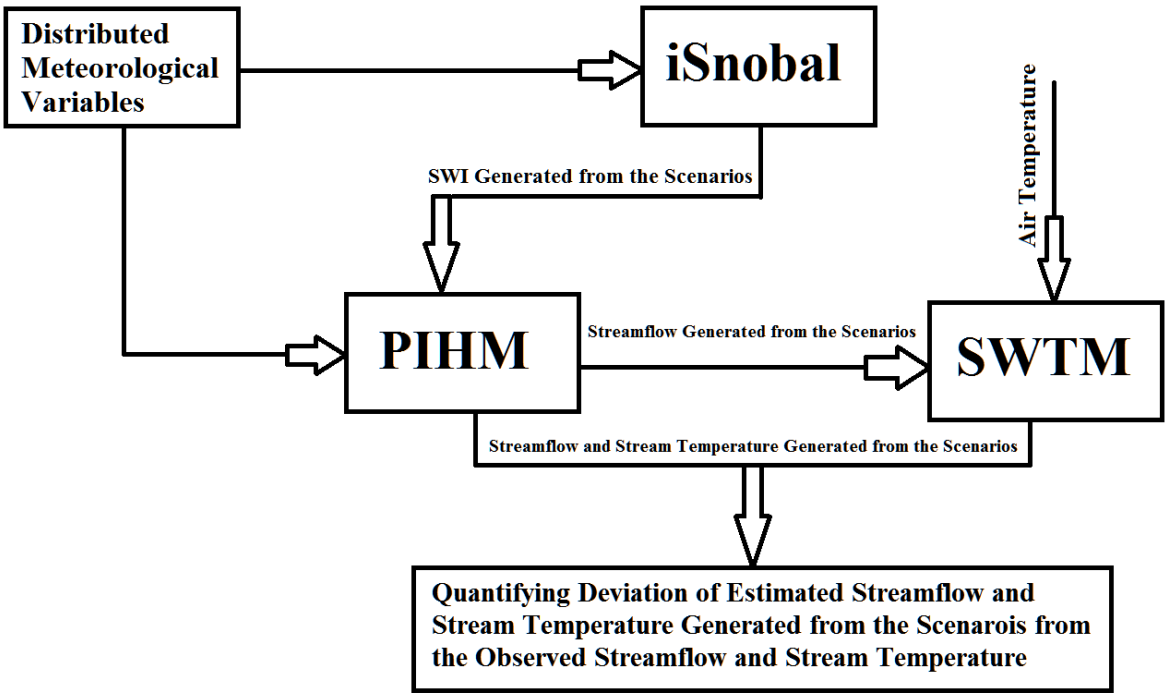

Figure 5.2. Diagram of the integrated hydrologic modeling framework.

5.4.1. Snow Model, iSnobal, and Spatial and Temporal Scenarios

ISnobal is a physics-based and spatially distributed snow model (Marks et al. 1999). The model requires distributed meteorological inputs including air temperature, precipitation, solar

and thermal radiations, vapor pressure and wind speed to calculate mass and energy flux exchanges at each grid cell. To understand the role of temporal and spatial resolution of the meteorological inputs on SCA and SWE estimations, iSnobal was run using: (a) hourly (scenario 1h), 3-hourly (scenario 3h) and 6-hourly (scenario 3h) meteorological inputs; and (b) six different model scales. Two out of six spatial scenarios were obtained by distributing meteorological inputs at 50 m (scenario 50 m (d)) and 100 m (scenario 100 m (d)) resolutions. In four out of six spatial scenarios, meteorological inputs were aggregated from the 50 m (d) scenario to obtain 100 m (scenario 100 m (a)), 250 m (scenario 250 m (a)), 500 m (scenario 500 m (a)) and 750 m (scenario 750 m (a)) resolution of inputs. Hourly time step was used in the spatial scenarios and aggregated meteorological inputs at 100 m resolution (100 m (a) scenario) were used in the temporal scenarios. Thus, 1h and 100 m (a) scenarios are the same. These scenarios were run for three water years (wy), including a wet (wy2006), average (wy2010), and dry year (wy2007) in order to understand the impact of time step of inputs and model scale on prediction accuracy for various climatic conditions.

In our previous work (Sohrabi et al. In Preparation-a), the 50m grid predicted SWE for the wet, average and dry years was validated using measured SWE at six SNOTEL sites located inside the Boise River Basin (BRB). The average Nash-Sutcliffe coefficient (NSC) of 0.76 and the root mean square error (RMSE)-observations standard deviation ratio (RSR) of 0.42 were observed over all sites and years. NSC and RSR values were generally larger than 0.75 and lower than 0.5, representing very reliable estimations (Moriasi et al. 2007).

5.4.2. Penn State Integrated Hydrology Model (PIHM)

PIHM was developed to estimate hydrological state variables and hydrological processes (Kumar 2009). The hydrological state variables include soil moisture of unsaturated zone, groundwater level and stream depths and hydrological processes consist of evapotranspiration, surface and subsurface flow and streamflow. PIHM has been used to estimate these hydrological state variables and hydrological processes over several watersheds, including the Young Womans Creek and the Little Juniata River in Pennsylvania (Yu et al. 2013), the Lysina watershed in Czech Republic (Yu et al. 2014) and the Reynolds

Creek Experimental Watershed in Idaho (Chen et al. 2016; Kumar et al. 2013). In the latter watershed, coupled iSnobal and PIHM were used and evaluated.

PIHM is a semi-distributed hydrology model that employs the D8 algorithm for routing and watershed identification (Tarboton 1997). It uses the finite volume method to solve partial differential equations of the hydrological state variables on a constrained unstructured mesh, which is called the semi-discrete finite volume method (Kumar et al. 2009; Yu et al. 2013). Streamflow within the channel routing and surface flow over ground are predicted with a one-dimensional (1-D) and 2-D diffusive wave approximation of Saint Venant equations, respectively. The Richard's equation (Richards 1931) is employed to compute subsurface flow. The subsurface domain is composed of unsaturated and saturated soil layers. The unsaturated layer thickness is assumed to be 0.5 meters and the saturated layer depth is defined by the user. Unsaturated zone has only vertical flow, a 1D flow, whereas groundwater flow is 2-D (vertical and along maximum slope). The Van Genuchten (1980) equation is used to define soil water storage in the subsurface layers. Potential evapotranspiration is calculated using the Penman-Monteith approach (Monteith 1965). Actual evapotranspiration is computed using the Noah-LSM approach, which is based on potential evapotranspiration, vegetation fraction, maximum canopy capacity, canopy resistance, field capacity and wilting point (Yu et al. 2013).

5.4.2.1. PIHM Inputs

River elements and mesh were generated in an integrated GIS framework, PIHMgis (Kumar et al. 2010). The algorithm for mesh generation provides restriction options such as minimum angle and maximum area of cells. This allows generation of large cells at homogenous areas and small cells at locations with significant contribution in streamflow simulation (i.e. close to river elements).

PIHM inputs are air temperature, relative humidity, solar net radiation, wind speed, vapor pressure and SWI of which their spatial distribution over BRB were quantified (Sohrabi et al. In Preparation-a; Sohrabi et al. In Preparation-b). The gridded data of these variables inside a mesh cell were averaged to generate one time series for each input for each mesh cell. The

same sets of data for air temperature, relative humidity, solar net radiation, wind speed and vapor pressure, which are needed for evapotranspiration calculation in PIHM, were used for all the scenarios. Therefore, differences in the streamflow estimations between the scenarios were only due to using different SWI inputs.

Estimation of SWI is a non-linear process, because SWI estimation relies on meteorological variables with topography-induced spatial variation, i.e. net radiation and snow drifting (Bloschl 1999; Hopkinson et al. 2010). Therefore, the mean values of estimated SWI over an area varies as the spatial and temporal resolutions of meteorological inputs change (Bloschl 1999). Sensitivity of estimated streamflow from the scenarios to size of mesh cells were tested by using 3 sets of meshes, which were: (a) 592 mesh cells that had the largest and averaged mesh cell had areas of 8.9 km^2 and 4.2 km^2, respectively (Figure 5.3) (b) 880 mesh cells that had the largest and averaged mesh cell areas of 5.6 km^2 and 2.8 km^2, respectively; and (c) 1453 mesh cells that had the largest and averaged mesh cell areas of 2.4 km^2 and 1.7 km^2, respectively. Estimated streamflow from the scenarios were insensitive to the size of the mesh cells as similar streamflow in terms of NSC and RSR was estimated using 592, 880 and 1452 mesh cells. Therefore, the 592-cell mesh with 152 river elements was selected to reduce runtime.

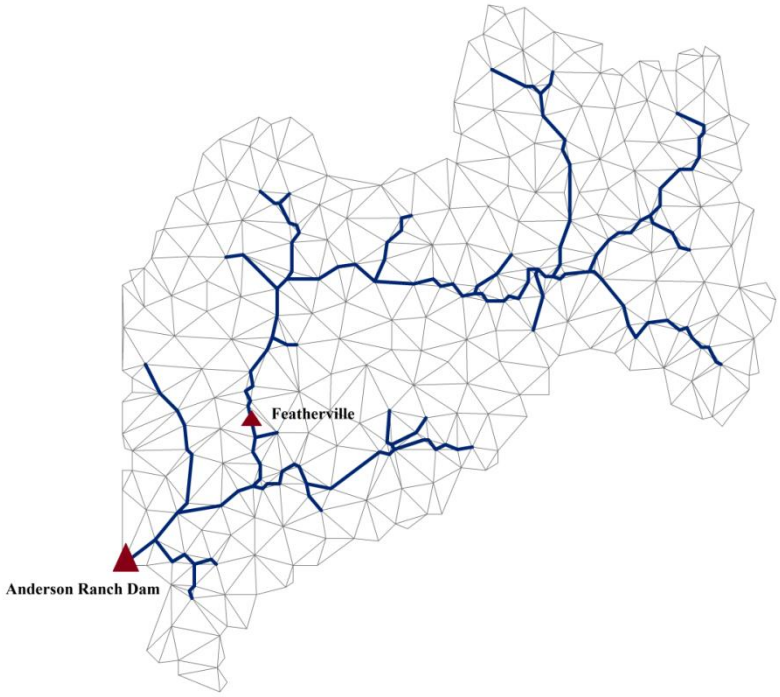

Figure 5.3. River elements and mesh cells generated for upstream of Anderson Ranch Dam.

The groundwater initial level and its distribution are very important, because they control the timing and magnitude of groundwater contribution to streamflow. The Kumar et al. (2013) approach was used to identify groundwater initial condition over the watershed due to the unavailability of groundwater measurements in the watershed. The PIHM groundwater model was run for ten years with SWI value of zero and fully saturated groundwater condition. The purpose of this approach is to estimate the groundwater level for a condition that streamflow is merely generated by groundwater and the basin is not fed by SWI for a long time, similar to the condition of the watershed from peak streamflow in early summer through October.

5.4.3. Stream Water Temperature Model (SWTM)

The Stream Water Temperature Model (SWTM) is a piecewise statistical model that accounts for both linear and non-linear relationships between dependent and independent variables (Sohrabi et al. In Review). The model uses daily air temperatures as a meteorological driver

and daily discharges as a hydrological driver to estimate stream temperatures at a daily resolution. Air temperature is a surrogate for heat flux exchanges (Mohseni et al. 1998; Neumann et al. 2003; Webb et al. 2003). Discharge is a proper proxy for snowmelt and rain, which have notable influences on stream temperature (Gu et al. 1999; Hockey et al. 1982; Webb et al. 2003). Because the heat capacity of water is very large and larger than that of the air, stream temperature does not respond to heat exchanges as quickly as air temperature (Ahmadi-Nedushan et al. 2007; Webb et al. 2003). SWTM accounts for thermal inertia by considering the stream water temperature of the previous time step. SWTM divides the data series temporally into three groups: days T_a <1°C (group 1), days in the October to May period that T_a >1°C (group 2), and the June-Sept period (group 3). A linear model is applied for the data in group 2 and 3, whereas a non-linear model is used for the data in group 1. SWTM fits these models using the Bayesian methods (Gelman and Hill 2007; Lunn et al. 2000) and applies Markov Chain Monte Carlo (MCMC) to infer posterior distributions (Campbell et al. 1999; Tierney 1994). SWTM was tested over the Boise River Basin (BRB) and 8 different climatic regions of the USA. A statistical stream temperature model, SWTM, was used, because the objective was to understand effect of differences in estimated streamflow caused by changes in estimated SWI from the scenarios on stream temperature estimation at a point. However, physics-based stream temperature models, which carry over heat exchanges between the river and its surroundings, are useful tools to evaluate the effects of thermal pollution, presence of a reservoir and deforestation on stream temperature (Benyahya et al. 2007; Piccolroaz et al. 2016).

5.4.4. Calibration and Validation of the Integrated Hydrologic Modeling Framework:

PIHM was calibrated for the 50 m (d) scenario for wy2006, the wet year, and validated for wy2007 and wy2010, the dry and average years, respectively. The calibrated parameters were then used to generate streamflow for the other scenarios. PIHM was not calibrated for the other scenarios, because the parameters of these models could be estimated differently to compensate for the inaccuracies in SWI. Calibration of SWTM was conducted using observed daily mean air temperatures and estimated streamflow from the 50 m (d) simulation for wy2006 at Featherville. The calibrated parameters were then used to run SWTM using the

observed daily mean air temperatures and estimated streamflow generated from the other scenarios at Featherville. Streamflow and stream temperatures estimated from these scenarios were compared with those of the observed to evaluate the effects of the observed residuals in SCA and SWE on prediction accuracy of streamflow and stream temperature. The Nash-Sutcliffe coefficient (NSC) and the root mean square error (RMSE)-observations standard deviation ratio (RSR) were used to evaluate the performance of the modeling framework against the observed streamflow and stream temperature.

Estimated streamflow from the 50 m (d) scenario matched that of the observed reasonably well with a NSC of 0.93 and 0.72 and a RSR of 0.24 and 0.57 over the calibration and validation periods, respectively, at Anderson Ranch Dam and Featherville. Estimated stream temperatures from the 50 m (d) scenario also captured that of the observed reasonably well with a NSC of 0.93 and 0.91 and a RSR of 0.27 and 0.30 over the calibration and validation periods, respectively, at Featherville. Comparisons between the measured and predicted streamflow and stream temperatures from the 50 m (d) scenario were at par with other reported studies (Moriasi et al. 2007; Moriasi et al. 2015; Vliet et al. 2011; Yu et al. 2013; Yu et al. 2014).

5.4.5. Watershed Scale Analysis

The study watershed was divided into several sub-watersheds to investigate the role of drainage area size on streamflow estimations for each scenario. Estimated SWI from the 50 m (d), 100 m (d) and 6h scenarios were accumulated for the October through July period, which was the snow accumulation and ablation season. The accumulated SWI from these scenarios were then averaged over the drainage area at each sub-basin closure point, indicated by the solid circle in Figure 5.4. At each point, Δ accumulated SWI were divided by averaged accumulated SWI of the 50 m (d) scenario related to that point to present changes in Δ accumulated SWI in percent. The percentage of differences between the accumulated SWI of the 50 m (d) scenario with the 100 m (d) (Δ accumulated SWI of the 100 m (d)) and 6h (Δ accumulated SWI of the 6h) scenarios were analyzed with regard to changes in the drainage area at these points. In a similar fashion, estimated accumulated streamflow from the 50 m (d)

and 100 m (d) scenarios were compared and anlyzed at these points. Observed streamflow was unavailable at these points. Thus, the 50 m (d) simulation was used as the benchmark because the estimated SWE and streamflow from the 50 m (d) simulation well matched those of the observed in terms of NSC and RSR values and capturing peak flows.

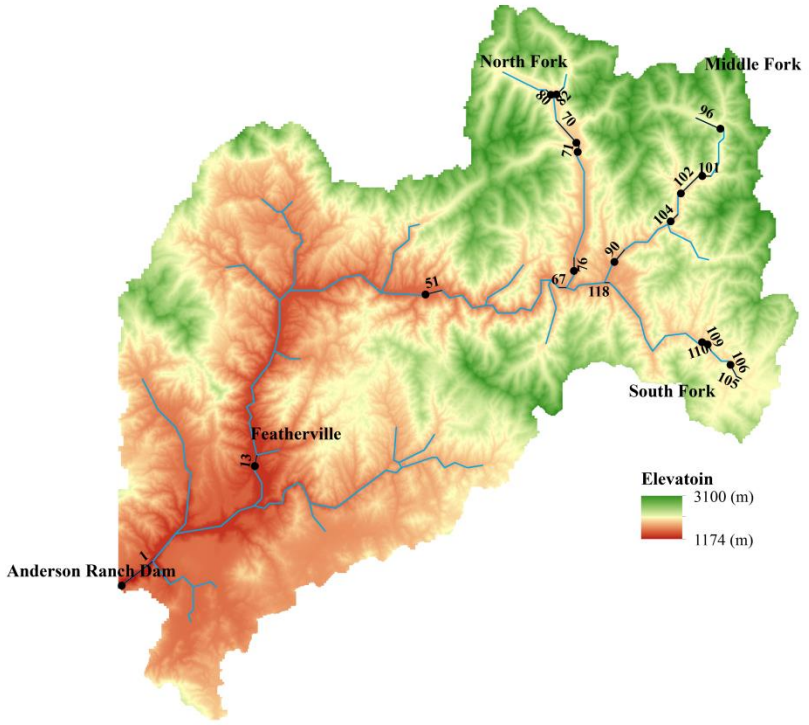

Figure 5.4. Drainage area of the black filled circles were selected to calculate difference between accumulated SWI from the 50 m (d) during the highest peak flow and that of the 100 m (d) and 6h scenario.

5.5. Results and Discussion

5.5.1. Analysis of Streamflow Estimated From the Scenarios

The 50 m (d) simulation indicated accurate streamflow estimations in terms of NSC and RSR (Table 5.1). The differences between NSC and RSR from the 50 m (d) simulation and those of the other scenarios were generally negligible, except in the dry year. The largest difference

was observed between the estimated streamflow from the 50 m (d) simulation and that of the 100m (d) simulation in terms of NSC, RSR and capturing peak flows.

Table 5.1. NSC and RSR at the Anderson Ranch Dam, without parentheses, and at the Featherville, in parentheses, for the estimated streamflow from all the scenarios.

	Wet Year (wy2006)		Average Year (wy2010)		Dry Year (wy2007)	
Scenarios	NSC	RSR	NSC	RSR	NSC	RSR
50 m (d)	0.94 (0.92)	0.23 (0.26)	0.76 (0.81)	0.49 (0.44)	0.64 (0.66)	0.65 (0.68)
3h	0.94 (0.92)	0.25 (0.27)	0.74 (0.79)	0.51 (0.46)	0.54 (0.41)	0.74 (0.74)
6h	0.92 (0.91)	0.29 (0.29)	0.74 (0.78)	0.51 (0.46)	0.36 (0.28)	0.77 (0.78)
100 m (d)	0.93 (0.91)	0.26 (0.30)	0.74 (0.74)	0.51 (0.50)	0.32 (0.28)	0.71 (0.77)
100 m (a)	0.94 (0.92)	0.23 (0.27)	0.75 (0.8)	0.49 (0.45)	0.61 (0.48)	0.71 (0.77)
250 m (a)	0.94 (0.92)	0.23 (0.26)	0.73 (0.76)	0.52 (0.48)	0.49 (0.47)	0.74 (0.78)
500 m (a)	0.94 (0.92)	0.24 (0.27)	0.71 (0.75)	0.54 (0.50)	0.49 (0.36)	0.74 (0.78)
750 m (a)	0.94 (0.92)	0.23 (0.26)	0.68 (0.72)	0.57 (0.53)	0.60 (0.50)	0.69 (0.73)

The estimated streamflow from the 50 m (d) simulation captured the observed streamflow peaks during the wet year (the calibration period; Figure 5.5). However, in the 100 m (d) simulation, streamflow was overestimated April's peak flows, but underestimated the late spring and early summer's peak flows. Smoothing topographic features such as slope and aspect in the 100 m DEM relative to 50 m DEM caused net radiation overestimation during winter or snow accumulation period. This caused SWI overestimation in the 100 m (d) simulation relative to the 50 m (d) simulation during winter, which was mainly stored in the ground rather than generating streamflow (Figure 5.5). Due to this, the groundwater level was higher in the 100 m (d) simulation relative to the 50 m (d) simulation by the time streamflow started to rise (the beginning of April). As a result, during April, when SWI from the 100 m (d) simulation was slightly lower relative to the 50 m (d) simulation, groundwater compensated for the difference in SWI and also caused streamflow overestimations in the 100 m (d) simulation. This caused large reduction in the difference between the groundwater level estimations from these two scenarios. In contrast, the late spring and early summer's peak

flows were underestimated, because of lower groundwater contributions and lower SWI in the 100 m (d) simulation relative to the 50 m (d) simulation (Figure 5.5). During May, the estimated snow mass, SWE, in the 100 m (d) simulation was lower relative to the 50 m (d) simulation, as in the 100 m (d) simulation large portions of the snow mass was melted during the winter. This caused SWI from the 100 m (d) simulation to be lower than that of the 50 m (d) simulation during May. This difference in the estimated SWI was negated to some extent with the larger groundwater level of the 100 m (d) simulation due to SWI overestimations during the winter relative to the 50 m (d) simulation. Groundwater level difference of the two scenarios became zero in mid-May, as all the extra water storage in the 100 m (d) simulation due to SWI overestimation during winter was turned to streamflow. From mid-May to early June, SWI from the 50 m (d) simulation was larger relative to the 100 m (d) simulation and generated larger streamflow that captured the highest and last peaks. However these two peaks were underestimated in the 100 m (d) simulation. As a result, differences between NSC and RSR of the 50 m (d) simulation and those of the 100m (d) simulation were as large as 0.1 during peak flows. This is consistent with the Boyle et al. (2001) study that found the spatial resolution of precipitation input has a larger effect on simulation of peak flows than base flow.

The inaccuracy in estimated peak flows in the 100 m (d) simulation due to lost meteorological information requires changing the parameters related to water retention and groundwater, which means providing a different watershed response. This indicates that the 100 m (d) scenario is unreliable for presenting physical hydrologic processes because changes in the timing and magnitude of estimated SWI in this scenario changes how the system works. The use of estimated SWI from the 100 m (d) scenario changes the system toward increasing water retention.

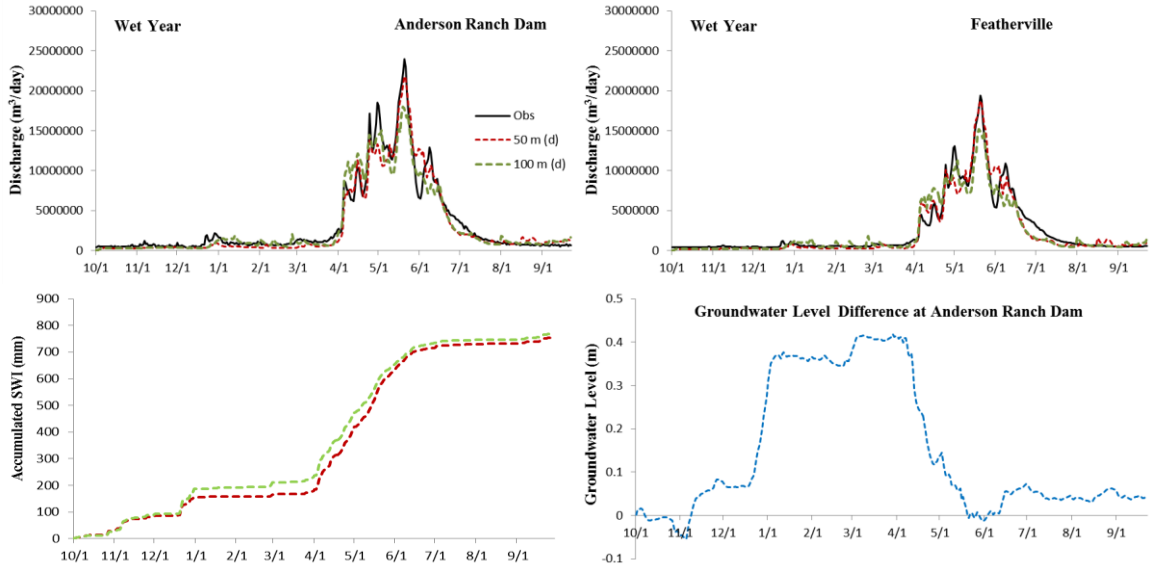

Figure 5.5. Visual comparison between the estimated streamflow from the 50 m (d) and 100 m (d) and that of observed in the wet year (calibration period) at Anderson Ranch Dam and Featherville (top figures). Differences between the averaged estimated SWI (bottom left figure) and groundwater level (bottom right figure) from the 50 m (d) and 100 m (d) simulations in the wet year over the Anderson Ranch Dam. Note that positive values in groundwater level difference indicate larger groundwater level in the 100 m (d) simulation relative to the 50 m (d) simulation.

In the average year, difference between estimated streamflow from the 50 m (d) and the 100 m (d) simulations were negligible in terms of NSC, RSR and capturing peak flows (Figure 5.6; Table 5.1). In this year, the difference between the estimated SWI of these scenarios was low. This low difference in the estimated SWI was also buffered by temporarily storing water in the ground and releasing it later, which caused negligible differences between the estimated streamflow from these scenarios.

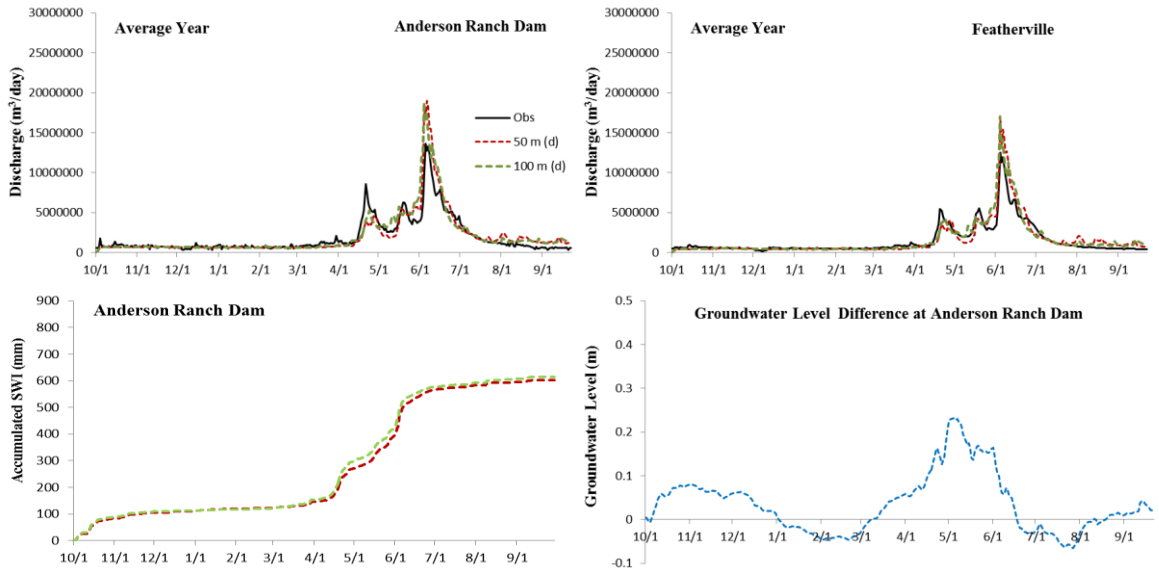

Figure 5.6. Visual comparison between the estimated streamflow from the 50 m (d) and 100 m (d) and that of observed in the average year at Anderson Ranch Dam and Featherville (top figures). Differences between the averaged estimated SWI (bottom left figure) and groundwater level (bottom right figure) from the 50 m (d) and 100 m (d) simulations in the average year over the Anderson Ranch Dam. Note that positive values in groundwater level difference indicate larger groundwater level in the 100 m (d) simulation relative to the 50 m (d) simulation.

Differences between NSC and RSR values of the 50 m (d) simulation and those of the 100 m (d) were larger in the dry year relative to the wet and average years. Similar but with much less pronounced magnitude to the wet year, SWI from the 100 m (d) simulation was larger than that of the 50 m (d) simulation during winter in the dry year. In contrast to the wet year, during spring the SWI from the 100 m (d) simulation was still larger than that of the 50 m (d) simulation in the dry year. Therefore, differences between the estimated SWI from these scenarios were not buffered by storing water in the ground and releasing it later as happened in the wet year. The largest difference between estimated streamflow from these scenarios was during the period between April and May, when the 100 m (d) simulation overestimated streamflow and caused low NSC and high RSR in this scenario. This streamflow overestimation in the 100 m (d) simulation was due to on average larger SWI of this scenario at the Anderson Ranch Dam watershed relative to that of the 50 m (d) (Figure 5.7). This was caused by underestimation of the sublimation in the 100 m (d) simulation in comparison to that of the 50 m (d). Underestimation of the net solar radiation in the 100 m (d) simulation during the melt period, which is a primary energy input for the energy balance, was responsible for underestimation of sublimation. Net solar radiation underestimation was due

to flattening slopes and aspects as a result of coarsening the DEM from 50 m to 100 m. The magnitude of the underestimation of sublimation was much more pronounced in the dry year than the wet year, which was due to shallow snowpack and a large number of sunny days in the dry year.

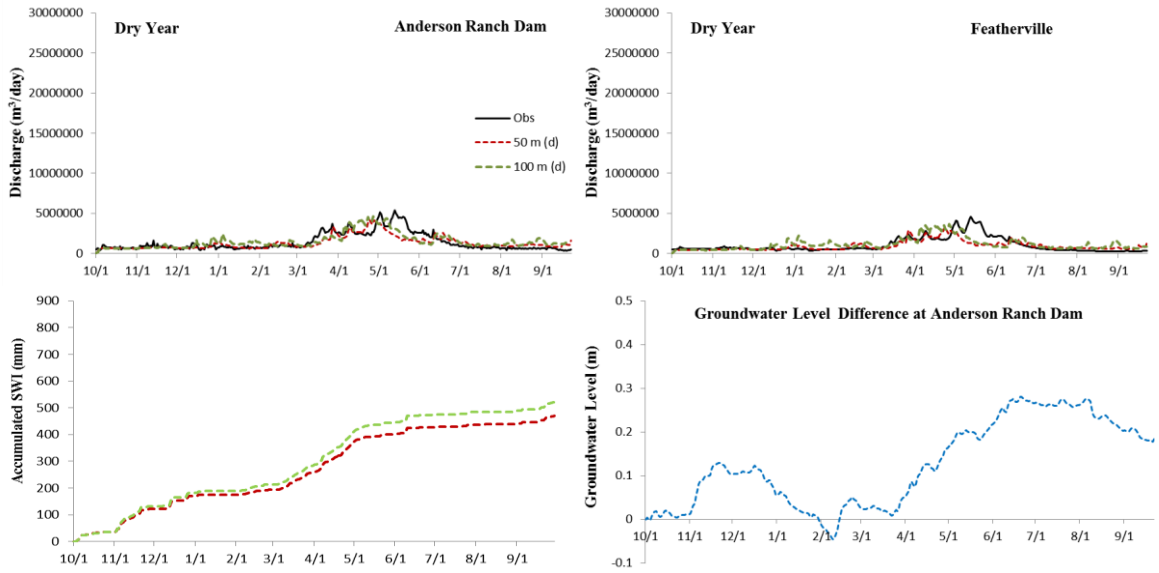

Figure 5.7. Visual comparison between the estimated streamflow from the 50 m (d) and 100 m (d) and that of observed in the dry year at Anderson Ranch Dam and Featherville (top figures). Differences between the averaged estimated SWI (bottom left figure) and groundwater level (bottom right figure) from the 50 m (d) and 100 m (d) simulations in the dry year over the Anderson Ranch Dam. Note that positive values in groundwater level difference indicate larger groundwater level in the 100 m (d) simulation relative to the 50 m (d) simulation.

Differences between NSC and RSR of the 50 m (d) simulation and those of the other scenarios were larger at Featherville than at Anderson Ranch Dam. This was due to the larger drainage area of Anderson Ranch Dam relative to that of Featherville. Reduction in watershed size increases the sensitivity of streamflow estimation to SWI time series as reduction in watershed drainage area decreases watersheds' water retention and groundwater storage (Frisbee et al. 2011; Miller et al. 2016; Orlova and Branfireun 2014). In addition, the differences between SWI from the scenarios were on average lower in a large watershed than a small watershed, which is discussed in section 5.5.3.

5.5.2. Analysis of Stream Temperatures Estimated From the Scenarios

A negligible difference was observed between the estimated stream water temperature from the 50 m (d) and that of the other scenarios (Table 5.2). The lowest NSC (0.89) and largest RSR (0.33) were observed in the average year (Figure 5.8). All the scenarios had the same NSC and RSR values for the estimated stream temperatures, indicating that all the scenarios provided streamflow estimations with sufficient accuracy for stream temperature modeling. Air temperature, which is a proxy for heat flux exchanges, is the primary predictor of stream temperature (Ahmadi-Nedushan et al. 2007; Mohseni et al. 1998) and streamflow moderates stream temperature estimations in order to consider the effect of snow melt on stream temperature (Gu et al. 1999; Hockey et al. 1982; Webb et al. 2003). Therefore, differences between estimated stream temperatures from the scenarios will be negligible unless differences between estimated streamflow from the scenarios are substantially large.

Table 5.2. NSC and RSR for estimated stream temperature from all the scenarios.

	Wet Year	Average year	Dry Year
NSC	0.93	0.89	0.92
RSR	0.27	0.33	0.27

Note that all the scenarios had the same NSC and RSR values.

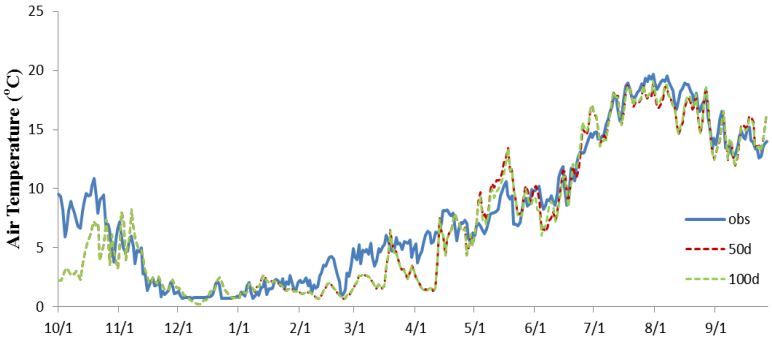

Figure 5.8. Estimated stream water temperature from the 50 m (d) and 100 m (d) simulations for the average year at Featherville.

5.5.3. Watershed Scale Analysis

Differences in Δ accumulated SWI of the 100 m (d) and 6h scenarios decreased with increasing watershed area (Figure 5.9). Percentage of Δ accumulated SWI was large in the 100 m (d) simulation, but negligible in the 6h simulation. The difference between estimated SWE from the 50 m (d) scenario and that of the 100 m (d) simulation was substantially larger than that between the 50 m (d) and the 6h scenarios (Sohrabi et al. In Preparation-a; Sohrabi et al. In Preparation-b). As a result, Δ accumulated SWI of the 100 m (d) scenario was substantially larger (as large as 205 mm) than that of the 6h scenario (less than 36.5 mm) over all the watersheds.

The largest reduction of Δ accumulated SWI of the 100 m (d) with the increase in the drainage size was related to the wet year. In this year, the difference between the SWE of the 50 m (d) simulation and that of the 100 m (d) was substantially larger due to larger snow mass of the wet than the other years. Therefore, the net radiation overestimation and snow drifting moderation due to smoothing slopes and aspects that caused by using the 100 m DEM had larger reflection on SWE estimation and consequently SWI estimation in the wet year than the other years.

The reduction of Δ accumulated SWI of the 100 m (d) was larger as watershed area increased in the North and Middle Forks than that of the South Fork. In the North, Middle and South Forks Δ accumulated SWI of the 100 m (d) decreased by about 5%, 9% and 3% from the headwaters to the outlets of these tributaries, respectively. This was due to the different ranges of elevation in the North, Middle and South Forks. The largest difference between estimated SWE from the 50 m (d) scenario and that of the 100 m (d) scenario was observed in snow dominated areas above treeline (elevations > 2400 m) (Sohrabi et al. In Preparation-a; Sohrabi et al. In Preparation-b). In addition, the difference between estimated SWE from the 50 m (d) scenario and that of the 100 m (d) simulation decreased as the elevation decreased. 48% of the North and Middle forks have elevations higher than 2400 m, whereas less than 1% of the South Fork has elevations above 2400 m. As a result, Δ accumulated SWI of the 100 m (d) at the headwaters of the North and Middle Forks were large. As watershed areas in the North and Middle Forks increased, the elevation range substantially widened, consequently causing a large reduction in Δ accumulated SWI of the 100 m (d) scenario.

At the confluence of North, Middle and South Fork tributaries (point 67 in Figure 5.4), where the main stem begins, to the Anderson Ranch Dam Δ accumulated SWI of the 100 m (d) and 6h scenarios slightly changed as watershed area increased. This indicates that on average the main stem received similar SWI from these scenarios. This caused negligible differences between estimated streamflow from the 50 m (d) and that of the 100 m (d) and 6h in terms of NSC and RSR at the Anderson Ranch Dam and Featherville. In the wet and dry years, Δ accumulated SWI of the 100 m (d) was about 13% in the main stem. This difference caused underestimation and overestimation of streamflow in the 100 m (d) simulation during peak flows in the wet and dry years, respectively, at the Anderson Ranch Dam and Featherville.

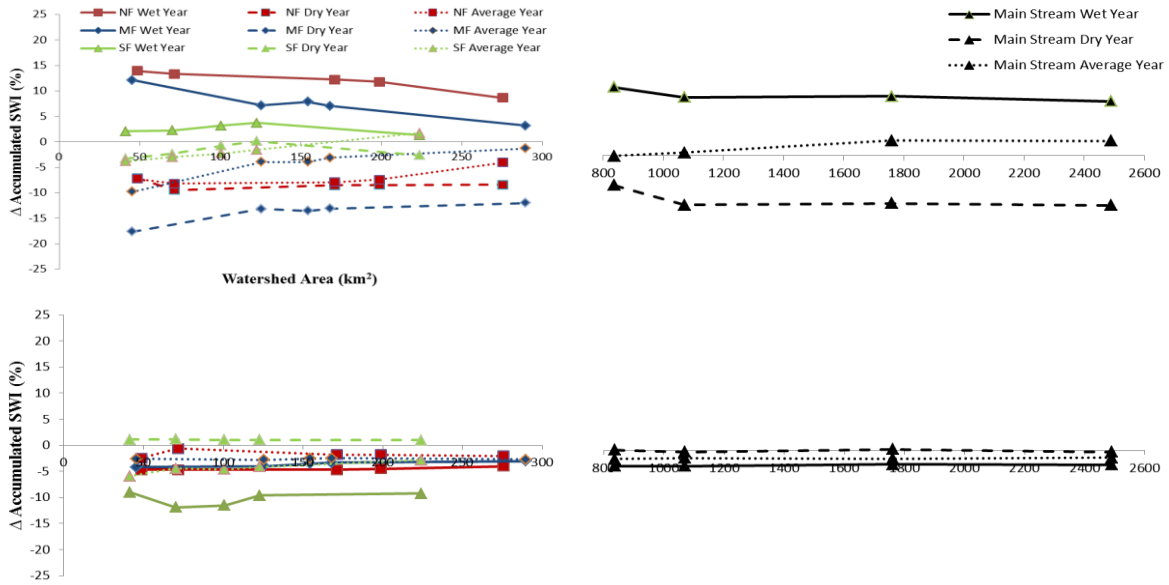

Figure 5.9. Changes of Δ accumulated SWI with regard to watershed area. Difference between accumulated SWI of the 50 m (d) scenario and that of the 100 m (d) scenario (Δ accumulated SWI of the 100m (d)) is indicated in the top row. Difference between accumulated SWI of the 50 m (d) scenario and that of the 6h scenario (Δ accumulated SWI of the 6h) is indicated in the bottom row. Note that NF, MF and SF stand for North Fork, Middle Fork and South Fork tributaries.

Percentage of Δ accumulated streamflow of the 100 m (d) generally decreased as watershed area increased (Figure 5.10). As watershed size increased, water storage increased and runoff contributions to streamflow generations decreased (Figure and Figure). As a result, the buffering effect of groundwater increased with increasing watershed size, which reduced the sensitivity of streamflow generation to SWI time series (Rosenberg et al. 2013).

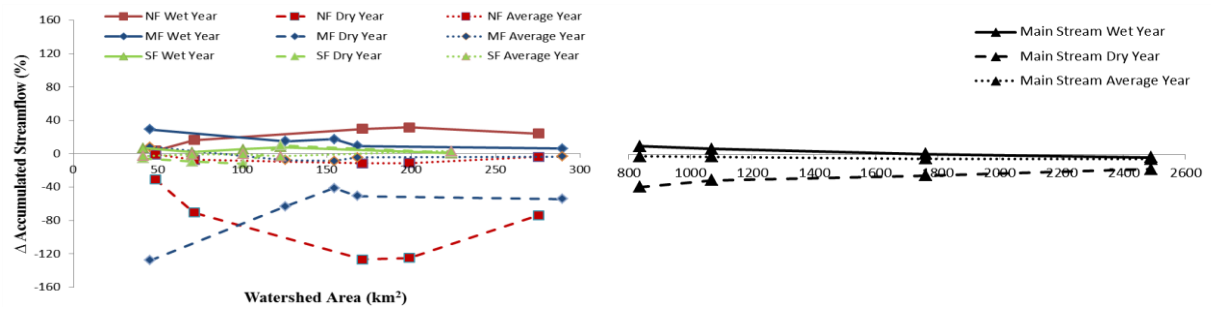

Figure 5.10. Changes in Δ accumulated streamflow of the 100 m (d) with regard to increase in watershed area. Note that NF, MF and SF stand for North Fork, Middle Fork and South Fork tributaries.

In the North Fork, Δ accumulated streamflow of the 100 m (d) increased, whereas Δ accumulated SWI decreased as watershed area increased from the headwater (point 80) to point 71, which was located before the outlet. This was due to surface cover of this basin, which was more than 86% rock. Impermeability of the rock caused the differences in SWI of these two scenarios turned to runoff and immediately contributed to streamflow rather than storing in the ground and releasing later and gradually (Figure 5.11 and Figure 5.12). From the point 71 to the outlet of the North Fork (point 76) watershed area increased by about 77 km^2 and rock surface cover reduced by about 20%. As a results, the differences in SWI of these scenarios was buffered by storing in the ground and releasing later and gradually, which caused reduction in Δ accumulated streamflow of the 100 m (d).

The largest reduction in Δ accumulated streamflow of the 100 m (d) as watershed area increased was related to the Middle Fork, where the largest reduction in Δ accumulated SWI was observed. In the Middle Fork, watershed area increased from 45 to 261 km^2 and percent of rock reduced from 50% to 33% from the headwater (point 96) to the outlet (point 90), respectively. Reduction of Δ accumulated SWI and the groundwater buffering effect caused a synergy that led to the large reduction in Δ accumulated streamflow (average reduction of 33% over all the years).

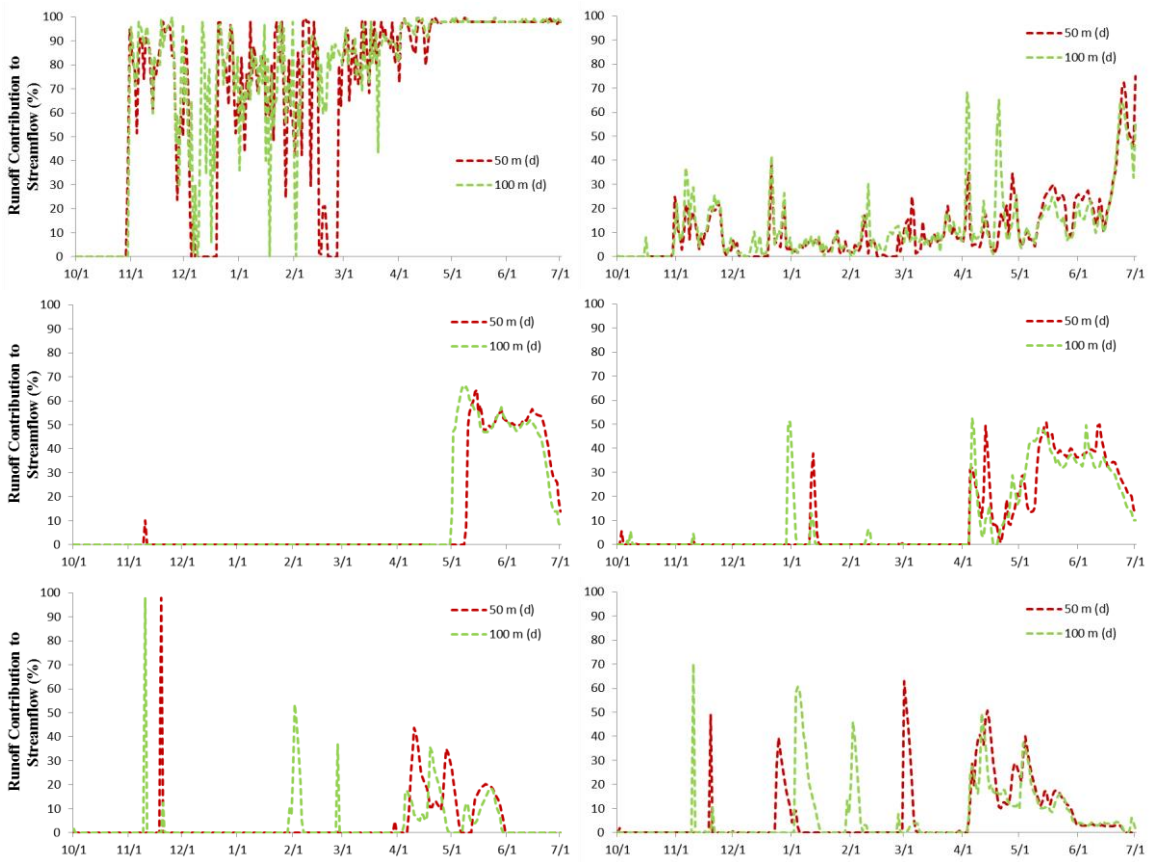

Figure 5.11. Runoff contribution to streamflow generation from the 50 m (d) and 100 m (d) simulations in the wet year at the headwaters (left column) and outlets (right column) of the North (top row), Middle (middle row) and South Forks (bottom row).

Percentage of Δ accumulated streamflow of the 100 m (d) was negligible in the South Fork, where Δ accumulated SWI percentage was low due to the elevation range of this fork. Runoff contribution for streamflow generation was low in this fork (Figure 5.11 and Figure 5.12) as the basin had permeable surface cover (0% rock), which caused increase in the groundwater buffering effect.

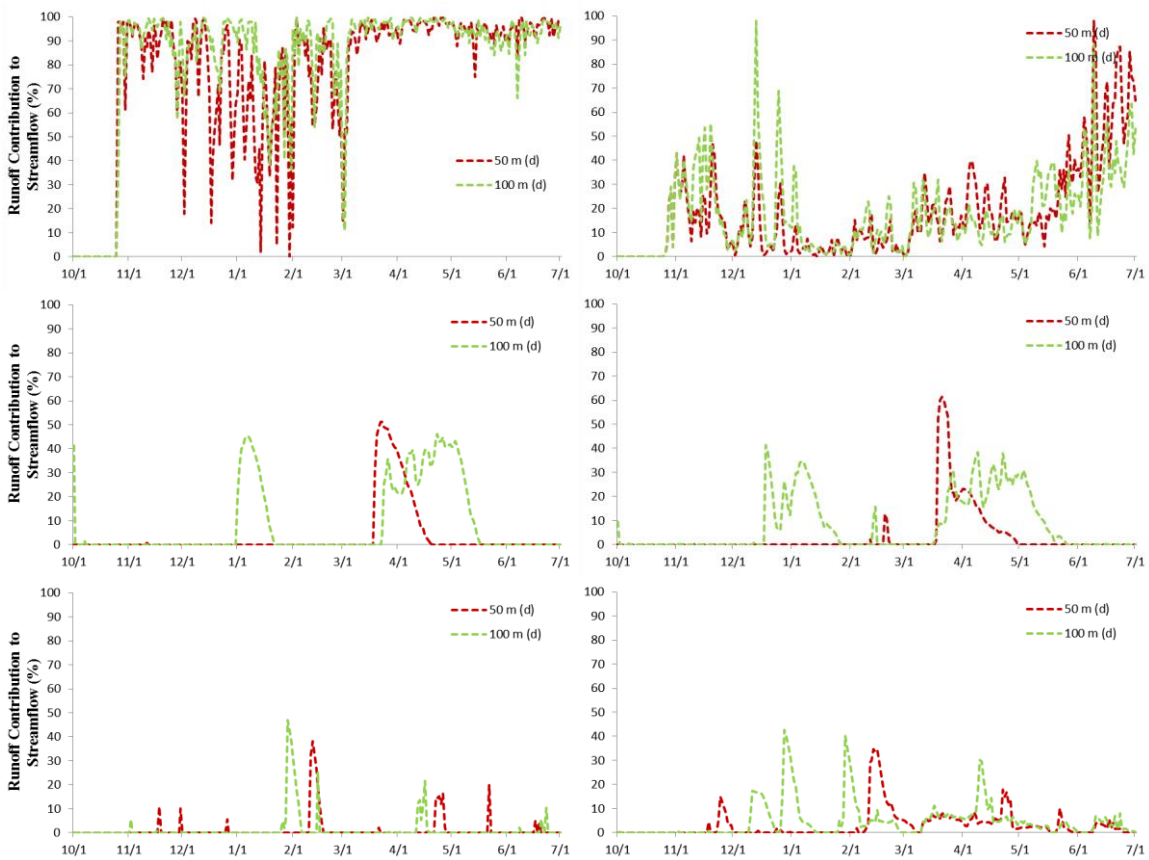

Figure 5.12. Runoff contribution to streamflow generation from the 50 m (d) and 100 m (d) simulations in the dry year at the headwaters (left column) and outlets (right column) of the North (top row), Middle (middle row) and South Forks (bottom row).

Percentage of Δ accumulated streamflow of the 100 m (d) was negligible in the main stem except in the dry year when Δ accumulated streamflow was about 26%. This indicates that SWI estimations from both the 50 m (d) and the 100 m scenarios provide similar streamflow estimation in watersheds with drainage area larger than 800 km^2. Changes in Δ accumulated streamflow from confluence of the North, Middle and South Forks tributaries (point 67) to the Anderson Ranch Dam (point 1) were negligible. This was in agreement with changes in Δ accumulated SWI of the 100 m (d) in the main stem from point 67 to point 1.

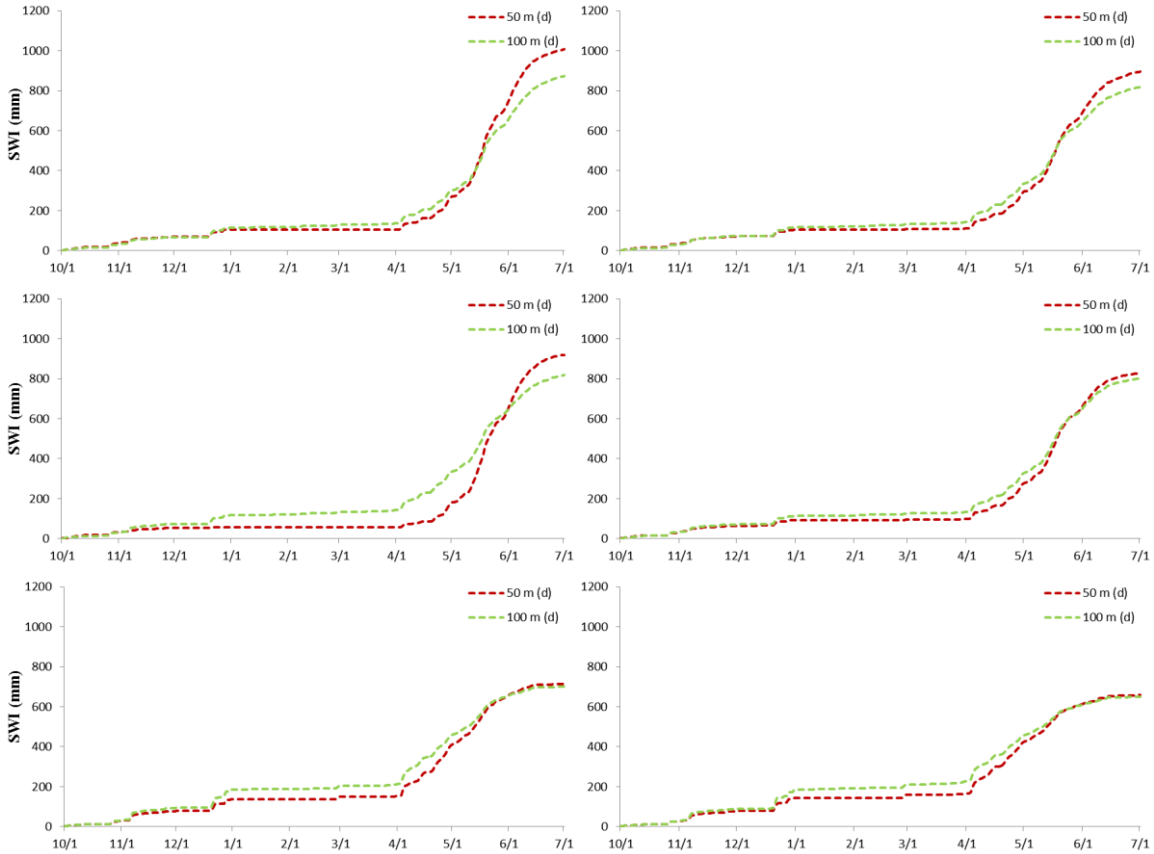

Figure 5.13. Estimated SWI from the 50 m (d) and 100 m (d) simulations in the wet year at the headwaters (left column) and outlets (right column) of the North (top row), Middle (middle row) and South Forks (bottom row).

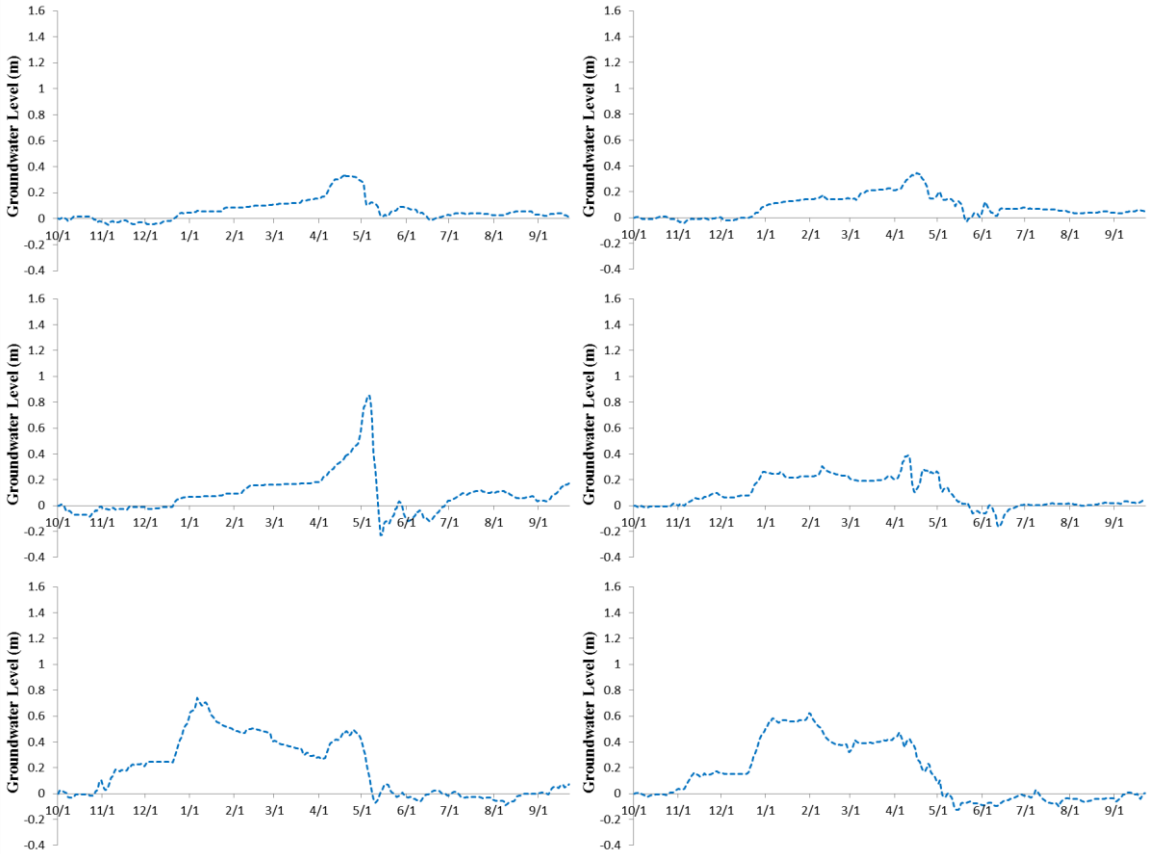

Figure 5.14. Groundwater level difference between and streamflow the 50 m (d) and 100 m (d) simulations in the wet year at the headwaters (left column) and outlets (right column) of the North (top row), Middle (middle row) and South Forks (bottom row).

Although Δ accumulated SWI percentage of the 100 m (d) was generally larger in the wet year than the dry year, Δ accumulated streamflow percentage was larger in the dry year. In the wet year, SWI overestimation in the 100 m (d) during winter stored in the ground and mainly released during spring when the 50 m (d) simulation had larger SWI than the 100 m (d) simulation (Figure 5.13 and Figure 5.14). The role groundwater buffering effect was different in the dry year than the wet year, because the 100 m (d) simulation had larger SWI than the 50 m (d) simulation over the entire season (Figure 5.15 and Figure 5.16). The average year had lowest Δ accumulated streamflow percentage of the 100 m (d), which is consistent with observed low Δ accumulated SWI percentage.

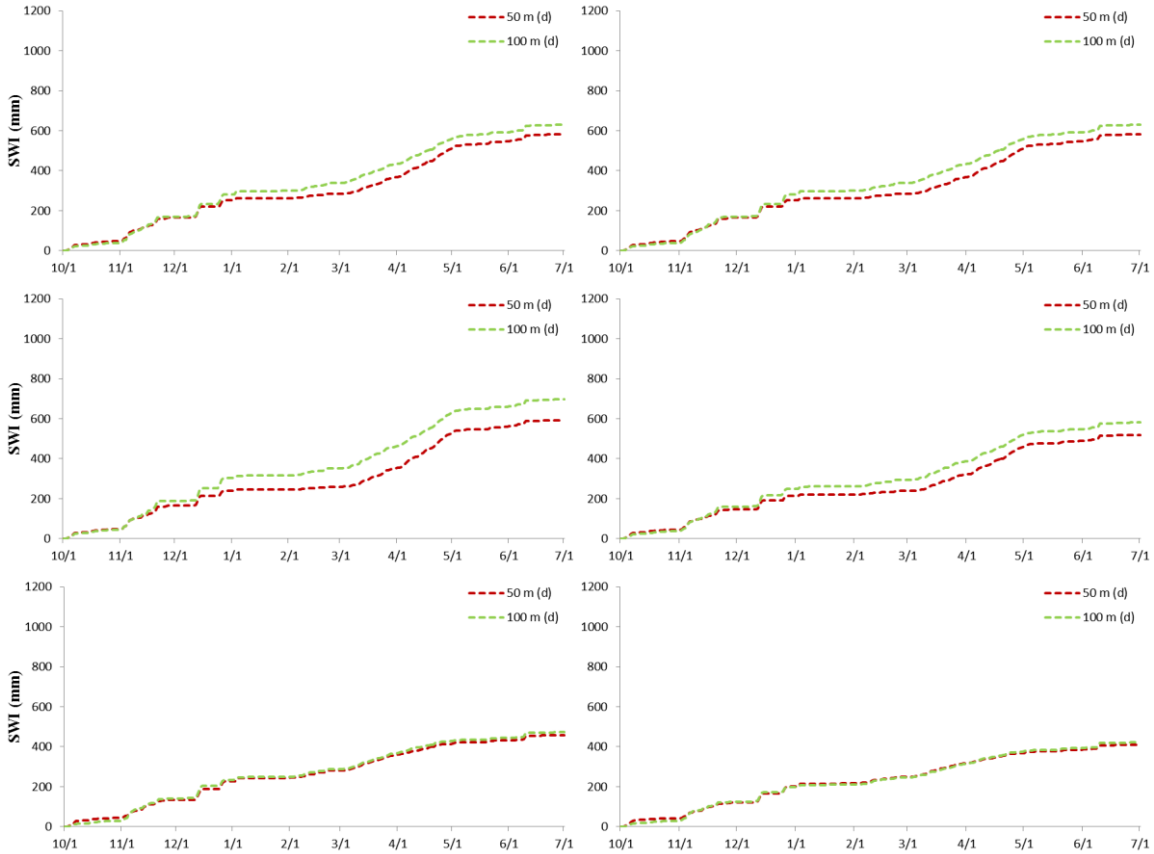

Figure 5.15. Estimated SWI from the 50 m (d) and 100 m (d) simulations in the dry year at the headwaters (left column) and outlets (right column) of the North (top row), Middle (middle row) and South Forks (bottom row).

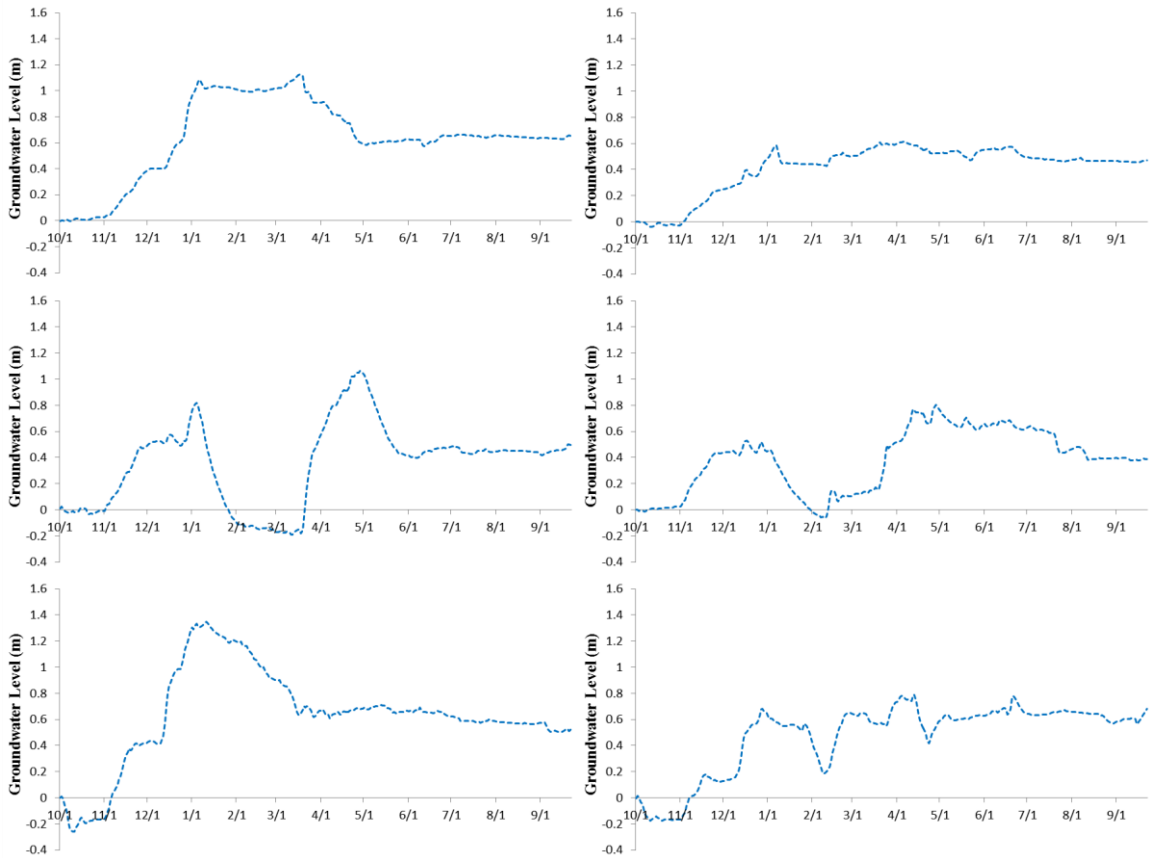

Figure 5.16. Groundwater level difference between and streamflow the 50 m (d) and 100 m (d) simulations in the wet year at the headwaters (left column) and outlets (right column) of the North (top row), Middle (middle row) and South Forks (bottom row).

The results indicate that in small mountainous watersheds, particularly watersheds with drainage area less than 100 km^2, accurate and detailed information of SWI is important. This is due to two main reasons: (a) neglecting topography-induced heterogeneity in meteorological variables causes on average large SWI prediction inaccuracy over small watersheds; and (b) streamlow estimation of such watersheds are highly sensitive to SWI time series as water retention and groundwater storage is (Frisbee et al. 2011; Miller et al. 2016; Orlova and Branfireun 2014). In contrast, in large watersheds that have drainage area larger than 800 km^2, SWI estimations even from the 100 m (d) scenario can generate accurate streamflow estimations. This is due to: (a) difference between estimated SWI from the 50 m (d) and that of the 100 m (d) scenarios is on average negligible over large watersheds; and (b) streamflow generation is less sensitive to SWI time series due to the groundwater buffering

effect. The results also indicate that the buffering effect of groundwater increase as watershed area increases and changes with climate conditions.

Therefore, the effects of inaccurate SWI estimations on streamflow estimations are moderated to a great degree in large groundwater-dominated basins and in cases that calibration and validation periods of hydrologic models have a similar climate condition. This indicates that there is a need to measure the groundwater level and soil moisture to constrain the process-based hydrological modeling. With these measurements the estimations of the following hydrological processes can be validated: (a) the groundwater recharge and depletion curve; (b) the base flow contribution to the streamflow generation; (c) the runoff generation response to a melt event; and (d) the interaction between groundwater and surface water.

5.6. Conclusions

This investigation shows that spatial and temporal resolution of meteorological inputs affect prediction accuracy of integrated hydrologic modeling framework, in which snow, streamflow and stream temperature model are coupled. The effects of inputs resolution on prediction accuracy depend strongly on climate condition and watershed size and surface cover in mountainous watersheds.

The effect of spatial resolution of inputs on streamflow estimation was much more pronounced than that of temporal resolution which confirms that 6 hour temporal resolution is sufficient in most applications. Similarly coarser resolution generated from aggregated inputs from 50 m resolution had negligible effects on stream flows as the effect of topographic features was transferred by aggregation. Conversely distributing inputs at coarser than 50m deteriorated the accuracy of the model because it caused surface water input (SWI) overestimation during winter and SWI underestimation during spring and early summer. Overestimation of SWI due to inputs spatial resolution during winter was mostly buffered by storing water in the ground, which led to small impact on base flow estimation. Then, underestimated SWI during spring and early summer was compensated by the stored water in the ground to some extent, which led to larger effect on peak flow than base flow estimations. This buffering effect of groundwater depends strongly on climate conditions, the watershed

area and surface cover. This suggests that comparison of the predicted and observed stream discharges to quantify performance of hydrological modeling is effective only if different climatic years are used.

Impact of spatial and for a lesser impact temporal resolutions of inputs on stream flow prediction accuracy decreased as watershed area increased. In large watersheds, larger than 800 km^2, SWI estimations from all resolution scenarios investigated in this study had similar streamflow estimations. However, in small watersheds, smaller than 300 km^2, SWI estimation using coarse spatial and temporal resolutions of inputs resulted in inaccurate streamflow estimations, particularly in wet and dry years and watersheds with impermeable surface cover. Groundwater level and soil moisture measurements should be added to constrain process-based hydrological modeling, as streamflow may not be adequate for validating hydrological modeling.

The effect of spatial and temporal resolution of inputs on stream temperatures estimations was negligible. Estimated stream temperatures from all the spatial and temporal resolution scenarios had the same accuracy of fit and errors in comparison to the observed stream temperatures. This indicates that 100 m spatial and 6 hourly temporal resolutions of inputs are sufficient input scales to provide streamflow estimations for stream temperature modeling.

5.7. References

Ahl, R. S., Woods, S. W., and Zuuring, H. R. (2008). "Hydrologic calibration and validation of SWAT in a snow-dominated Rocky Mountain watershed, Montana, USA." *Journal of the American Water Resources Association*, 44(6), 1411-1430.

Ahmadi-Nedushan, B., St-Hilaire, A., Ouarda, T. B. M. J., Bilodeau, L., Robichaud, E., Thiemonge, N., and Bobee, B. (2007). "Predicting river water temperatures using stochastic models: case study of the Moisie River (Qu´ebec, Canada)." *Hydrological Processes*, 21, 21–34.

Ajami, N. K., Gupta, H., Wagener, T., and Sorooshian, S. (2004). "Calibration of a semi-distributed hydrologic model for streamflow estimation along a river system." *Journal of Hydrology*, 298, 112–135.

Benyahya, L., Caissie, D., St-Hilaire, A., Ouarda, T. B. M. J., and Bobée, B. (2007). "A Review of Statistical Water Temperature Models." *Canadian Water Resources Journal*, 32(3), 179–19.

Bloschl, G. (1999). "Scaling issues in snow hydrology." *Hydrological Processes*, 13, 2149-2175.

Boyle, D. P., Gupta, H. V., Sorooshian, S., Koren, V., Zhang, Z., and Smith, M. (2001). "Toward improved streamflow forecasts: Value of semidistributed modeling." *Water Resources Research*, 37(11), 2749-2759.

Brett, J. R. (1979). "Environmental factors and growth." *Fish Physiology*, VIII, 599-675.

Campbell, E. P., Fox, D. R., and Bates, B. C. (1999). "A Bayesian approach to parameter estimation and pooling in nonlinear flood event models " *Water Resources Research*, 35(1), 211-220.

Chen, X., Kumar, M., Wang, R., Winstral, A., and Marks, D. (2016). "Assessment of the timing of daily peak streamflow during the melt season in a snow-dominated watershed." *Journal of Hydrometeorology*, 17, 2225–2244.

Choo, T. H., Hong, S. H., Yoon, H. C., Yun, G. S., and Chae, S. K. (2015). "The estimation of discharge in unsteady flow conditions, showing a characteristic loop form." *Environmental Earth Sciences*, 73, 4451–4460.

Crozier, L. G., Zabel, R. W., Hockersmith, E. E., and Achord, S. (2010). "Interacting effects of density and temperature on body size in multiple populations of Chinook salmon." *Journal of Animal Ecology*, 79, 342-349.

Dingman, S. L., and Bjerklie, D. M. (2006). *Estimation of River Discharge. Encyclopedia of Hydrological Sciences. 5:61*.

.

Elder, K., Dozier, J., and Michaelse, J. (1991). "Snow Accumulation and Distribution in an Alpine Watershed." *Water Resources Research*, 27(7), 1541-155.

Forseth, T., and Jonsson, B. (1994). "The growth and food ration of piscivorous brown trout." *Functional Ecology*, 8, 171-177.

Frisbee, M. D., Phillips, F. M., Campbell, A. R., Liu, F., and Sanchez, S. A. (2011). "Streamflow generation in a large, alpine watershed in the southern Rocky Mountains of Colorado: Is streamflow generation simply the aggregation of hillslope runoff responses?" *Water Resources Research*, 47, W06512.

Gelman, A., and Hill, J. (2007). *Data Analysis Using Regression and Multilevel/Hierarchical Models*, Cambridge University Press.

Genuchten, M. T. V. (1980). "A closed-form equation for predicting the hydraulic conductivity of unsaturated soils." *Soil Science Society of America Journal*, 44, 892-898.

Gu, R., McCutcheon, S., and Chen, C.-J. (1999). "Development of weather-dependent flow requirements for river temperature control." *Environmental Management*, 24(4), 529-540.

Haddeland, I., Matheussen, B. V., and Lettenmaier, D. P. (2002). "Influence of spatial resolution on simulated streamflow in a macroscale hydrologic model." *Water Resources Research*, 38(7), 1124.

Hockey, J. B., Owens, I. F., and Tapper, N. J. (1982). "Empirical and theoretical models to isolate the effect of discharge on summer water temperature in the Hurunui River." *Journal of Hydrology*, 21(1), 1-12.

Hopkinson, C., Chasmer, L., Munro, S., and Demuth, M. N. (2010). "The influence of DEM resolution on simulated solar radiation-induced glacier melt." *Hydrological Processes*, 24, 775–788.

Isaak, D. J., Wollrab, S., Horan, D., and Chandler, G. (2012). "Climate change effects on stream and river temperatures across the northwest U.S. from 1980–2009 and implications for salmonid fishes." *Climate Change*, 113(2), 499-524.

Isaak, D. J., Young, M. K., Nagel, D. E., Horan, D. L., and Groce, M. C. (2015). "The cold-water climate shield: Delineating refugia for preserving salmonoid fishes through the 21st century." *Global Change Biology*, 21, 2540–2553.

Jobling, M. (1997). "Temperature and growth: modulation of growth rate via temperature change." Global Warming: Implications for Freshwater and Marine Fish, Cambridge University Press, 225-253.

Kormos, P. R., Marks, D., McNamara, J. P., Marshall, H. P., Winstral, A., and Flores, A. N. (2014). "Snow distribution, melt and surface water inputs to the soil in the mountain rain–snow transition zone." *Journal of Hydrology*, 519, 190-204.

Kumar, M. (2009). "Toward a hydrologic modeling system." *Doctor of Philosophy Dissertation in Civil Engineering, The Pennsylvania State University, 274*.

Kumar, M., Bhatt, G., and Duffy, C. J. (2010). "An object-oriented shared data model for GIS and distributed hydrologic models." *International Journal of Geographical Information Science* 24(7), 1061–79.

Kumar, M., Duffy, C., and Salvage, K. M. (2009). "A Second-Order Accurate, Finite Volume–Based, Integrated Hydrologic Modeling (FIHM) Framework for Simulation of Surface and Subsurface Flow." *Vadose Zone Journal*, DOI:10.2136/vzj2009.0014.

Kumar, M., Marks, D., Dozier, J., Reba, M., and Winstral, A. (2013). "Evaluation of distributed hydrologic impacts of temperature-index and energy-based snow models." *Advances in Water Resources*, 56, 77-89.

Liston, G. E., and Elder, K. (2006). "A Distributed Snow-Evolution Modeling System (SnowModel)." *Journal of Hydrometeorology*, 7(6), 1259–1276.

Lobligeois, F., Andréassian, V., Perrin, C., Tabary, P., and Loumagne, C. (2014). "When does higher spatial resolution rainfall information improve streamflow simulation? An evaluation using 3620 flood events." *Hydrol. Earth Syst. Sci.*, 18, 575–594.

Luce, C., Staab, B., Kramer, M., Wenger, S., Isaak, D., and McConnell, C. (2014). "Sensitivity of summer stream temperatures to climate variability in the Pacific Northwest." *Water Resources Research*, 50(4), 3428–3443.

Luce, C. H., Tarboton, D. G., and Cooley, K. R. (1998). "The influence of the spatial distribution of snow on basin-averaged snowmelt." *Hdrological Processes*, 12, 1671-1683.

Lunn, D. J., Thomas, A., Best, N., and Spiegelhalter, D. (2000). "WinBUGS-A Bayesian modelling framework: Concepts, structure, and extensibility." *Statatistical Computation*, 10(4), 325–337.

Marks, D., Domingo, J., Susong, D., Link, T., and D.Garen. (1999). "A spatially distributed energy balance snowmelt model for application in mountain basins." *Hydrological Process* 13, 1935-1959.

Marks, D., Winstral, A., Reba, M., Pomeroy, J., and Kumar, M. (2013). "An evaluation of methods for determining during-storm precipitation phase and the rain/snow transition elevation at the surface in a mountain basin." *Journal of Advances in Water Resources*, 55, 98-110.

Merenlender, A. M., and Matella, M. K. (2013). "Maintaining and restoring hydrologic habitat connectivity in mediterranean streams: an integrated modeling framework." *Hydrobiologia*, 719(1), 509-525.

Mesa, M. G., Weiland, L. K., Christiansen, H. E., and Sauter, S. T. (2013). "Development and Evaluation of a Bioenergetics Model for Bull Trout." *Transactions Of The American Fisheries Society*, 142, 41-49.

Miller, M. P., Tesoriero, A. J., Capel, P. D., Pellerin, B. A., Hyer, K. E., and Burns, D. A. (2016). "Quantifying watershed-scale groundwater loading and instream fate of nitrate using high-frequency water quality data." *Water Resources Research*, 52, 330–347.

Mohseni, O., Stefan, H. G., and Erickson, T. R. (1998). "A nonlinear regression model for weekly stream temperatures." *Water Resources Research*, 34(10), 2685–2692.

Monteith, J. L. (1965). "Evaporation and Environment." *Symposia of the Society for Experimental Biology*, 19, 205–224.

Moriasi, D. N., Arnold, J. G., Liew, M. W. V., Bingner, R. L., Harmel, R. D., and Veith, T. L. (2007). "Model evaluation guidelines for systematic quantification of accuracy in watershed simulations." *Transactions of the ASABE*, 50(3), 885-900.

Moriasi, D. N., Gitau, M. W., Pai, N., and Daggupati, P. (2015). "Hydrologic and water quality models: performance measures and evaluation criteria." *Transactions of the ASABE*, 58(6), 1763-1785.

Neumann, D. W., Rajagopalan, B., and Zagona, E. A. (2003). "Regression Model for Daily Maximum Stream Temperature." *Journal of Environmental Engineering*, 129(7), 667-674.

Null, S. E., Deas, M. L., and Lund, J. R. (2010). "Flow and water temperature simulation for habitat restoration in the Shasta River, California." *River Research and Applications*, 26, 663-681.

Orlova, J., and Branfireun, B. A. (2014). "Surface Water and Groundwater Contributions to Streamflow in the James Bay Lowland, Canada." *Arctic, Antarctic, and Alpine Research*, 46(1), 236-250.

Piccolroaz, S., Calamita, E., Majone, B., Gallice, A., Siviglia, A., and Toffolon, M. (2016). "Prediction of river water temperature: a comparison between a new family of hybrid models and statistical approaches." *Hydrological Processes*, DOI: 10.1002/hyp.10913.

Railsback, S. F., and Rose, K. A. (1999). "Bioenergetics Modeling of Stream Trout Growth: Temperature and Food Consumption Effects." *Transactions Of The American Fisheries Society*, 128, 241-256.

Rice, J. A., Breck, J. E., Bartell, S. M., and Kitchell, J. F. (1983). "Evaluating the constraints of temperature, activity, and consumption on growth of Largemouth Bass." *Environmental Biology of Fishes*, 9(3/4), 263-275.

Richards, L. A. (1931). "Capillary conduction of liquids in porous mediums." *Physics* 1, 318 – 333.

Rieman, B. E., Isaak, D. J., Adams, S., Horan, D., Nagel, D., Luce, C., and Myers, D. (2007). "Anticipated climate warming effects on bull trout habitats and populations across the Interior Columbia River Basin." *Transactions of the American Fisheries Society*, 136, 1552–1565.

Rosenberg, E. A., Clark, E. A., Steinemann, A. C., and Lettenmaier, D. P. (2013). "On the contribution of groundwater storage to interannual streamflow anomalies in the Colorado River basin." *Hydrol. Earth Syst. Sci.*, 17, 1475-1491.

Segond, M.-L., Wheater, H. S., and Onof, C. (2007). "The significance of spatial rainfall representation for flood runoff estimation: A numerical evaluation based on the Lee catchment, UK." *Journal of Hydrology*, 347, 116– 131.

Smith, L. C., and Pavelsky, T. M. (2008). "Estimation of river discharge, propagation speed, and hydraulic geometry from space: Lena River, Siberia." *Water Resources Research*, 44 W03427.

Smith, M. B., Koren, V. I., Zhang, Z., Reed, S. M., Pan, J.-J., and Moreda, F. (2004). "Runoff response to spatial variability in precipitation: an analysis of observed data." *Journal of Hydrology*, 298 267-286.

Smith, T., Marshall, L., and McGlynn, B. (2014). "Calibrating hydrologic models in flow-corrected time." *Water Resources Research*, 50, 748–753.

Sohrabi, M. M., Benjankar, R., Tonina, D., Kumar, M., Marks, D., and Kormos, P. (In Preparation-a). "Role of temporal resolution of meteorological inputs on process-based snow modeling."

Sohrabi, M. M., Benjankar, R., Tonina, D., Luce, C., Kumar, M., Marks, D., and Kormos, P. (In Preparation-b). "How fine is a fine spatial resolution for process-based snow modeling?"

Sohrabi, M. M., Benjankar, R., Tonina, D., Wenger, S. J., and Isaak, D. J. (In Review). "Estimation of Daily Stream Water Temperatures with a Bayesian Regression Approach." *Hydrological Process*.

Tarboton, D. G. (1997). "A new method for the determination of flow directions and upslope areas in grid digital elevation models." *Water Resources Research* 33(2), 309-319.

Tierney, L. (1994). "Markov Chains for exploring posterior distributions." *The Annals Of Statistics*, 22(4), 1701-1728.

Toffolon, M., and Piccolroaz, S. (2015). "A hybrid model for river water temperature as a function of air temperature and discharge." *Environmental Research Letters*, 10, 114011.

Trujillo, E., Molotch, N. P., Goulden, M. L., Kelly, A. E., and Bales, R. C. (2012). "Elevation-dependent influence of snow accumulation on forest greening." *Nature Geoscience*, 5(10), 705-709.

Viglione, A., Chirico, G. B., Komma, J., Woods, R., Borga, M., and Blöschl, G. (2010a). "Quantifying space-time dynamics of flood event types." *Journal of Hydrology*, 394, 213–229.

Viglione, A., Chirico, G. B., Woods, R., and Blöschl, G. (2010b). "Generalised synthesis of space–time variability in flood response: An analytical framework." *Journal of Hydrology*, 394, 198–212.

Vliet, M. T. H. V., Ludwig, F., Zwolsman, J. J. G., Weedon, G. P., and Kabat, P. (2011). "Global river temperatures and sensitivity to atmospheric warming and changes in river flow." *Water Resources Research*, 47, W02544.

Wang, Y., He, B., and Takase, K. (2015). "Effects of temporal resolution on hydrological model parameters and its impact on prediction of river discharge." *Hydrological Sciences Journal*, 54(5), 886-900.

Webb, B. W., Clack, P. D., and Walling, D. E. (2003). "Water–air temperature relationships in a Devon river system and the role of flow." *Hydrological Processes*, 17, 3069–3084.

Weill, S., Altissimo, M., Cassiani, G., Deiana, R., Marani, M., and Putti, M. (2013). "Saturated area dynamics and streamflow generation from coupled surface–subsurface simulations and field observations." *Advances in Water Resources*, 59, 196-208.

Winstral, A., Marks, D., and Gurney, R. (2013). "Simulating wind-affected snow accumulations at catchment to basin scales." *Advances in Water Resources*, 55, 64-79.

Winstral, A., Marks, D., and Gurney, R. (2014). "Assessing the Sensitivities of a Distributed Snow Model to Forcing Data Resolution." *Journal of Hydrometeorology*, 15, 1366–1383.

Xu, C., Letcher, B. H., and Nislow, K. H. (2010). "Context-specific influence of water temperature on brook trout growth rates in the field." *Freshwater Biology*, 55, 2253-2264.

Yu, X., Bhatt, G., Duffy, C., and Shi, Y. (2013). "Parameterization for distributed watershed modeling using national data and evolutionary algorithm." *Computers &Geosciences*, 58, 80-90.

Yu, X., Lamačová, A., Duffy, C., Krám, P., Hruška, J., White, T., and Bhatt, G. (2014). "Modelling long-term water yield effects of forest management in a Norway spruce forest." *Hydrological Sciences Journal*, 60(2), 174-191.